

USAAVRADCOM-TR-81-D-47



12

SPUR GEAR LASER SURFACE HARDENING MM&T PROGRAM

W. Altergott, P. Patel
BELL HELICOPTER TEXTRON
P.O. Box 482
Fort Worth, Tex. 76101

March 1982

Final Report for Period March 1979 - May 1981

Approved for public release;
distribution unlimited.

DTIC
ELECTE
MAY 21 1982
S H

Prepared for

COPY APPLIED TECHNOLOGY LABORATORY
U. S. ARMY RESEARCH AND TECHNOLOGY LABORATORIES (AVRADCOM)
Fort Belvoir, Va. 23604

Best Available Copy

82 05 21 031

APPLIED TECHNOLOGY LABORATORY POSITION STATEMENT

This research was conducted by Bell Helicopter Textron under Contract DAAK51-79-C-0010. The work was performed under technical management of Mr. Richard F. Mulliken of the Propulsion Technical Area, Aeronautical Technology Division.

It was anticipated that surface hardening of gears by laser would result in significantly lower manufacturing costs than those resulting from conventional carburizing.

The results of this program demonstrate a number of problems which must be solved in order to render surface hardening by laser, a satisfactory method for manufacture of helicopter gears. These include back tempering, non-uniform heating of tooth flanks and surface melting of tooth flanks. A solution of these problems is indicated.

Appropriate technical personnel of this Division have reviewed this report and concur with the conclusions.

DISCLAIMERS

The findings in this report are not to be construed as an official Department of the Army position unless so designated by other authorized documents.

When Government drawings, specifications, or other data are used for any purpose other than in connection with a definitely related Government procurement operation, the United States Government thereby incurs no responsibility nor any obligation whatsoever; and the fact that the Government may have formulated, furnished, or in any way supplied the said drawings, specifications, or other data is not to be regarded by implication or otherwise as in any manner licensing the holder or any other person or corporation, or conveying any rights or permission, to manufacture, use, or sell any patented invention that may in any way be related thereto.

Trade names cited in this report do not constitute an official endorsement or approval of the use of such commercial hardware or software.

DISPOSITION INSTRUCTIONS

Destroy this report when no longer needed. Do not return it to the originator.

Unclassified

SECURITY CLASSIFICATION OF THIS PAGE (When Data Entered)

REPORT DOCUMENTATION PAGE		READ INSTRUCTIONS BEFORE COMPLETING FORM
1. REPORT NUMBER USAAVRADCOM TR 81-D-47	2. GOVT ACCESSION NO. AD-A114670	3. RECIPIENT'S CATALOG NUMBER
4. TITLE (and Subtitle) SPUR GEAR LASER SURFACE HARDENING MM&T PROGRAM	5. TYPE OF REPORT & PERIOD COVERED FINAL REPORT MARCH 1979 - MAY 1981	
7. AUTHOR(s) W. Altercott, IIT Research Institute P. Patel, Bell Helicopter Textron	8. CONTRACT OR GRANT NUMBER(s) DAAK51-79-C-0010	
9. PERFORMING ORGANIZATION NAME AND ADDRESS Bell Helicopter Textron P.O. Box 482 Fort Worth, Texas 76101	10. PROGRAM ELEMENT PROJECT, TASK AREA & WORK UNIT NUMBERS 1807199 1497 044	
11. CONTROLLING OFFICE NAME AND ADDRESS Applied Technology Laboratory, U.S. Army Research and Technology Laboratories (AVRADCOM), Fort Eustis, Virginia 23604	12. REPORT DATE March 1982	
14. MONITORING AGENCY NAME & ADDRESS (if different from Controlling Office)	13. NUMBER OF PAGES 120	
	15. SECURITY CLASS. (of this report) Unclassified	
16. DISTRIBUTION STATEMENT (of this Report) Approved for public release; distribution unlimited.		
17. DISTRIBUTION STATEMENT (of the abstract entered in Block 20, if different from Report)		
18. SUPPLEMENTARY NOTES		
19. KEY WORDS (Continue on reverse side if necessary and identify by block number) Gears - Accessory Drive, Gears - Aircraft Quality, Surface Hardening, Case Hardening, Laser, Laser-Heat Treating, Laser-Surface Hardening, Laser-Case Hardening, Laser-Beam Splitting, Laser-Beam Integration, Multi-Beam Laser, Steel-D6AC, Steel 300M, Impact Strength D6AC		
20. ABSTRACT (Continue on reverse side if necessary and identify by block number) The purpose of this program was to surface harden spur gear specimens using laser and compare their tooth pitting life and tooth bending strength with that of carburized AMS 6265 gears. The intent was to replace aircraft quality accessory drive carburized AMS 6265 gears with laser hardened gears and achieve significant cost savings. Preliminary work was conducted using 300M. Subsequently, 300M was replaced with D6AC because it failed to meet the requirement of Rc 60 minimum surface hardness after a 300° temper.		

DTIC
ELECTE
MAY 21 1982

Unclassified

SECURITY CLASSIFICATION OF THIS PAGE (When Data Entered)

Unclassified

SECURITY CLASSIFICATION OF THIS PAGE (When Data Entered)

Laser exposure curves were developed for both 300M and D6AC using flat disc type specimens. A unique system for splitting a laser beam into four beams and integrating the individual beams and directing these at the root and adjoining tooth flanks of a tooth gap was developed. The main problems encountered were tempering of a previously hardened tooth flank, incomplete coverage from end face to end face and laser power and spatial drifts.

The report presents a detailed description of the multi-beam laser heat treating station, metallurgical properties of D6AC, findings of the laser heat treating experiments, conclusions and recommendations for overcoming problems encountered.

Unclassified

SECURITY CLASSIFICATION OF THIS PAGE (When Data Entered)

PREFACE

This report contains the results of a program to surface harden spur gear specimens using laser and compare their performance with that of carburized AMS 6265 gears. The program was terminated during Phase II due to technical difficulties. Overcoming these difficulties would have required a major modification to the program at considerable additional cost. This program was conducted by Bell Helicopter Textron (BHT) for the Applied Technology Laboratory (ATL), U. S. Army Research and Technology Laboratories (AVRADCOM), Fort Eustis, Virginia, from March 1979 to May 1981 under contract DAAK51-79-C-0010. Illinois Institute of Technology Research Institute (IITRI) was a subcontractor for BHT for all laser related efforts of this program.

ATL technical direction was provided by Richard Mulliken. The program was conducted under the technical direction of C. E. Braddock, Project Engineer, of the BHT Transmission Design Group. Technical direction at IITRI was provided by Dr. F. Seaman, Manager, IITRI Laser Center. Technical assistance was provided by W. A. Thomas, R. Battles, G. Cope, and P. Patel of BHT Engineering and W. Altergott and S. Ream of IITRI.



Accession For	
Project or	
Report	
Number	
Date	
Author	
Title	
Subject	
Availability Codes	
Scale and/or	
Other Special	

A

TABLE OF CONTENTS

	<u>Page</u>
PREFACE.....	3
List of Illustrations.....	7
List of Tables.....	10
1. INTRODUCTION.....	12
2. PROGRAM OBJECTIVES.....	13
2.1 PHASE I - OPTIMIZATION OF SELECTED PROCESSES....	13
2.2 PHASE II - APPLICATION OF LASER HARDENING TO....	13
GEARS	
2.3 PHASE III - PILOT PRODUCTION CAPABILITY.....	13
3. GEAR GEOMETRY AND REQUIREMENTS.....	14
3.1 GEAR GEOMETRY.....	14
3.2 CASE DEPTH AND METALLURGICAL REQUIREMENTS.....	14
4. REVIEW OF BASIC LASER HEAT TREATMENT TECHNOLOGY.....	16
4.1 FACTORS AFFECTING BEAM ABSORPTION AND METAL.....	17
INTERACTION	
4.1.1 Absorptive Coatings.....	17
4.1.2 Beam Power Density/Exposure Time.....	17
4.1.3 Other Factors.....	18
4.2 METALLURGICAL CONSIDERATIONS OF LASER HARDENING.....	19
5. SPECIAL REQUIREMENTS IN LASER HARDENING OF SPUR GEARS.....	24
5.1 BEAM DIRECTION.....	26
5.1.1 Tooth Tip Requirements.....	27
5.1.2 Root Requirements.....	28
5.2 DUPLEX HEATING.....	28
6. SELECTION OF GEAR STEEL.....	31
6.1 300M VS D6AC.....	31
6.2 METALLURGICAL PROPERTIES OF D6AC.....	35
6.3 PRE-LASER HARDENING HEAT TREATMENT.....	42
7. SYSTEMS ENGINEERING AND OPERATION.....	43
7.1 BEAM TRANSMISSION.....	45
7.2 WORK STATION ENCLOSURE.....	49
7.3 OPTICAL DESIGN.....	50
7.3.1 Beam Shaping Methodology.....	50
7.3.2 Optical Fabrication and Specifications....	53
7.4 OPTICAL PACKAGE FOR GEAR HEAT TREATMENT.....	58
7.5 CALORIMETER/SHUTTER DETAILS.....	61
7.5.1 Calorimeter Aspects.....	61
7.5.2 Exposure Time Control.....	64
7.6 WORKPIECE POSITIONING.....	65

TABLE OF CONTENTS (Concluded)

	<u>Page</u>
7.7 TREATING SEQUENCE.....	67
7.8 BEAM POWER CONTROL DURING RUNS.....	68
7.8.1 Spatial Drift Correction.....	68
7.8.2 Correction for Total Power Variation.....	68
7.8.3 Independent Power Drift in Individual....	69
Legs	
7.8.4 Summary of Corrective Action and Impact..	70
8. RESULTS AND DISCUSSION.....	71
8.1 LASER-GEAR STEEL INTERACTION.....	71
8.2 EFFECTS OF ABSORPTIVE COATINGS.....	76
8.3 EVALUATION OF QUENCHING MODES.....	79
8.4 EFFECTS OF BEAM PARAMETERS ON HARDENING.....	80
OF GEAR TEETH	
8.5 PROTOTYPE PRODUCTION TRIALS.....	85
8.5.1 Test Gear No. 1.....	86
8.5.2 Test Gear No. 2.....	89
8.5.3 Discussion.....	98
9. CONCLUSIONS.....	99
10. RECOMMENDATIONS.....	101
11. REFERENCES.....	103
APPENDIX A: ENGINEERING DRAWING OF SPUR GEAR.....	105
APPENDIX B: DGAC RAW MATERIAL EVALUATION RESULTS..	107
APPENDIX C: SUMMARY OF CHARACTERISTICS OF IITRI... LASER FACILITY	111
APPENDIX D: COMPARATIVE COST ANALYSIS.....	112

LIST OF ILLUSTRATIONS

<u>Figure</u>	<u>Page</u>
1. Effects of initial microstructure on..... laser hardening response	23
2. Details of the as-hobbed spur gear..... configuration	24
3. Laser hardening of gear teeth: Root-Flank-..... Flank-Root (RFFR) technique	25
4. Laser hardening of gear teeth: Flank-Root-Flank.. (FRF) technique	25
5. Geometric heat dissipation considerations..... during laser heat treatment	29
6. Laser hardened case profile for 300M before..... and after temper	33
7. Laser hardened case profile for D6AC before..... and after temper	34
8. Charpy V-Notch impact test specimen configuration.	35
9. Charpy V-Notch impact strength of D6AC at two..... core hardness levels	37
10. Compact tension fracture toughness test..... specimen configuration	38
11. Failed D6AC fracture toughness (compact..... tension) specimen	39
12. K _g fracture toughness of laser hardened D6AC..... compared against that of carburized AMS 6265	41
13. Layout of the IITRI laser facility.....	44
14. Overview of gear heat treatment tooling.....	45
15. Laser beam (crescent mode) profiles obtained..... with acrylic plates showing stability of the beam with respect to time	47
16. Beam integration schemes.....	51
17. Beam division and integration scheme..... used in this program	54

LIST OF ILLUSTRATIONS (Continued)

<u>Figure</u>	<u>Page</u>
18. Laser heating of a tooth gap using the FRF..... technique employed in this program	55
19. Tooling for locating mirror facets for the..... convex beam integrator	56
20. Optics arrangement used in the program.....	59
21. Location of calorimeter meters, work..... positioner and microprocessor	62
22. Close-up of gear on the workpiece..... positioner and simulated beams	66
23. Laser exposure versus visual case depth for..... 300M at two different power levels using flat disc specimens.	72
24. Laser exposure versus visual case depth for..... D6AC specimens at two different core hardness levels using flat disc specimens.	73
25. Surface hardness of D6AC - comparison of laser.... hardening, water quench and oil quench	75
26. Photomicrograph showing laser hardened case in.... D6AC and the case/core transition	76
27. Effect of coating type and thickness on laser..... hardened case depth of D6AC	78
28. Final gas jet configuration.....	80
29. Test gear 1 laser hardened case profile.....	87
30. Close-up of test gear 1.	87
31. Root and flank location and terminology used..... during evaluation of test gears 1 and 2	88
32. Test gear 2 - 0° tooth.....	93
33. Test gear 2 - 120° tooth.....	93

LIST OF ILLUSTRATIONS (Concluded)

<u>Figure</u>	<u>Page</u>
34. Test gear 2 - 240° tooth.....	94
35. Test gear 2 laser hardened case profile.....	95
B-1. Jominy hardenability curve for 5.25-inch-..... diameter bar of D6AC	109
B-2. Jominy hardenability curve for 7.0-inch-..... diameter bar of D6AC	110
D-1. Gear configuration A.....	113
D-2. Gear configuration B.....	114
D-3. Gear configuration C.....	115
D-4. Gear configuration D.....	116

LIST OF TABLES

<u>Table</u>	<u>Page</u>
1. Spur gear data.....	14
2. Chemical analysis of 300M.....	32
3. Chemical analysis of D6AC.....	32
4. Longitudinal Charpy V-Notch impact strength..... of D6AC at two different hardness levels from two different heats and bar sizes	36
5. Kq fracture toughness of D6AC after laser..... hardening at the crack tip	40
6. Pre-laser hardening heat treat cycles used..... for 300M and D6AC	42
7. Residual stress analysis of laser hardened..... D6AC specimen	74
8. Laser exposure at which surface melting was..... first observed in 300M specimens	74
9. Results of absorptive coating assessment.....	77
10. Temperature measurement tests.....	81
11. Parameter series results.....	83
12. Parameter series analysis.....	84
13. Laser hardening parameters used in prototype..... production trials	86
14. Visual case depths - Test gear 1.....	90
15. Microhardness test results - Test gear 1.....	91
16. Laser hardened case depth comparison (Visual..... measurement vs Rc 50 measurement)-Test gear 1	92
17. Maximum case depth at pitch diameter - Test gear 2	92
18. Visual case depths - Test gear 2.....	96

LIST OF TABLES (Concluded)

<u>Table</u>	<u>Page</u>
19. Microhardness test results - Test gear 2.....	97
B-1. D6AC chemical analysis.....	107
B-2. D6AC Macrostructure tests.....	107
B-3. D6AC Grain size determination.....	108
B-4. D6AC microcleanliness rating.....	107
D-1. Case hardening cost estimates..... Gear configuration: A	118
D-2. Case hardening cost estimates..... Gear configuration: B	118
D-3. Case hardening cost estimates..... Gear configuration: C	119
D-4. Case hardening cost estimates..... Gear configuration: D	119
D-5. Case hardening cost estimates..... Carburizing vs laser hardening	120

1. INTRODUCTION

The decade of the 70's saw the eventual implementation of high-power laser technology on a commercial scale. One of the more promising applications for large infrared (IR) lasers was found to be the selective surface hardening of steels and cast irons. During the latter half of the decade, a substantial data base relating to the response of various hardenable ferrous alloys to laser radiation was developed. The Illinois Institute Technology Research Institute (IITRI) Laser Center has been and still is contributing to the development of this technology^{1,2}.

The emphasis in this program was placed upon the application of the laser hardening process to gear teeth. Lasers have shown great promise in the selective rapid heating of the surfaces followed by a rapid cooling of the heated material as a result of the heat sink formed by the unheated substrate. Laser heating is controllable and precise enough to provide consistent case depths on gears. Furthermore, laser hardening is cost effective compared to the commonly used case hardening process of carburizing since the latter is time consuming and both labor and energy intensive.

Two of the primary objectives of the program were to develop a laser hardening technique to case harden a basic spur gear configuration as a means of reducing gear manufacturing costs and to compare the performance of laser hardened gears with that of carburized AMS 6265 (AISI 9310) gears. Surface transformation hardening of a spur gear using laser requires a compound pattern of energy to provide tooth-tip to tooth-tip coverage and optimization of the impingement angle of the beams. An unusual and effective system of generating four laser beams from a single beam and directing these beams at the tooth flanks and root was developed in this program. The program was terminated in May 1981 at the request of Applied Technology Laboratory due to technical difficulties encountered and the expense required for system modification to overcome the problems.

¹F. D. Seaman and D. S. Ganamuthy, "Using the Industrial Laser to Surface Harden and Alloy," Metal Progress, August 1975.

²L. Bonello and M. A. H. Howes, "Some Factors Affecting the Laser Heat Treating Process," Paper presented at Heat Treatment '79 Conference in Birmingham, England, May 1979.

2. PROGRAM OBJECTIVES

The purpose of this program was to demonstrate that aircraft quality accessory drive spur gears with laser hardened gear teeth represent cost and energy savings without loss of performance when compared to spur gears with carburized gear teeth.

The program was divided into three phases with specific objectives as described below.

2.1 PHASE I - OPTIMIZATION OF SELECTED PROCESS

The objective of this phase was to refine existing laser transformation hardening technology to accommodate a basic spur gear configuration. Flat disc-type specimens and gear specimens were required to be fabricated and laser hardened. The heat treatment process parameters and subsequent mechanical and metallurgical properties of the gear steel selected were to be evaluated.

2.2 PHASE II - APPLICATION OF LASER HARDENING TO GEARS

The objective of this phase was the application of the selected laser hardening process from Phase I to spur gears and the definition of the technique involved therein. Process evaluation was required through single-tooth bending tests and tooth pitting tests on spur gears hardened using the newly developed technique.

2.3 PHASE III - PILOT PRODUCTION CAPABILITY

The objective of this phase was to provide a capability for pilot production of aircraft quality accessory spur gears.

3. GEAR GEOMETRY AND REQUIREMENTS

3.1 GEAR GEOMETRY

The spur gear configuration selected for this program is typical of accessory drive gears used at Bell Helicopter Textron (BHT) and is detailed in Appendix A. For conducting preliminary laser hardening tests using a gear geometry, BHT manufactured some spur gear specimens with hobbled gear teeth. These hobbled gear specimens were subjected to the same heat treatment prior to laser hardening as required by the drawing shown in Appendix A. Important gear teeth requirements of these preliminary gear specimens and those of the finished gear (Appendix A) are summarized in Table 1 for convenience.

TABLE 1. SPUR GEAR DATA

Characteristic	Preliminary Gear Specimen (As Hobbed)	Finished Gear (Appendix A)
Type of Gear	Involute Spur	Involute Spur
Number of Teeth	40	40
Diametral Pitch	10	10
Pressure Angle	20°	20°
Root Diameter, inch	3.740/3.720	3.728/3.722
Outside Diameter, inch	4.200/4.195	4.200/4.198
Circular Tooth Thickness, inch	.154/.151	.1521/.1501
Tip Modification Slope (nominal), inch	None	-.0014
Root Fillet Radius (minimum), inch	.050	.052

3.2 CASE DEPTH AND METALLURGICAL REQUIREMENTS

The case depth and other metallurgical requirements of the spur gears for this program are detailed in the specimen drawing in Appendix A. The key requirements are summarized below.

- a. Heat treat prior to laser hardening: Normalize, harden and temper to a hardness of Rc 36-42.
- b. Laser harden the gear teeth to an effective case depth (Rc 50 depth) of .026-.034. Measure the case depth after 300°F temper and prior to finish grind operation.

- c. Stock removal after laser hardening:
 - (i) .006 inch maximum per side from the flanks and roots of gear teeth
 - (ii) .010 inch maximum per side from other areas.
- d. Finished case hardness to be R15N 90.0 - 91.5 when measured in the root of gear teeth.

4. REVIEW OF BASIC LASER HEAT TREATMENT TECHNOLOGY

This section deals with the heat treatment technology base that supported the system and process activities throughout the program. In order to appreciate adapting the laser hardening process to a complex geometry such as the test spur gear, it is first instructive to review the basic mechanism of laser heat treatment and factors affecting the results.

A patch of laser "heat" (the 10.6 μm wavelength of a CO_2 laser is far infrared, and as such can be considered as pure heat energy), if it has sufficient intensity, can rapidly heat the surface of a ferrous metal into the austenite region without affecting the cold metal below. At a given beam power and beam size, the depth of this austenitic zone increases proportionally to the square root of the exposure time. Upon termination of laser exposure, the surface heat is rapidly drawn away by conduction into the unheated base metal (convective and radiative loss from the surface also occurs). Generally, the severity of this conductive quench is sufficient to achieve almost 100 percent martensite transformation and a very high hardness, depending upon the carbon content of the steel.

Of course, alloy content, initial microstructure, and beam parameters affect the total metallurgical response, but it is not incorrect to compare the laser quench severity to that of a brine or cold water quench. Further, the 7 percent volume expansion entailed in the martensitic transformation at the near surface implies that compressive residual stresses should exist in material that has been transformed in this manner. The merits of the laser hardening process are as follows:

1. Minimal workpiece distortion due to minimal heat input and because the unaffected base metal serves to resist deformation.
2. Rapid production rates.
3. No quenchant required.
4. Usually 100 percent martensite hardness by virtue of the severity of the self-quench mechanism.
5. Enhanced fatigue performance due to the compressive residual stress pattern in the surface.
6. Selective and/or precision heat treatment of complex shapes.

It should be noted that the above statements are generic in nature and are not absolute rules. To see how the many process variables affect the metallurgical response of an alloy, the following descriptions of the critical factors are presented.

4.1 FACTORS AFFECTING BEAM ABSORPTION AND METAL INTERACTION

The relatively long 10.6 μm output wavelength of the CO_2 laser is not readily absorbed by metallic materials. For instance, polished copper is over 95 percent reflective to this wavelength and, as such, is widely used for high power laser reflective optics. A base steel surface can be up to 80 percent reflective. Fortunately, there are many factors that govern beam absorptivity, and many of them can be exploited to enhance it.

4.1.1 Absorptive Coatings

One of the factors that can be modified to enhance absorptivity is the condition of the surface. It is common practice to apply a surface coating that is highly absorptive at 10.6 μm . The three most common coatings are graphite powder, spray paint incorporating silicate filler material, and manganese or zinc phosphate. Of these, the phosphates are the best absorbers, but are also the most costly and time consuming to apply. Graphite is the poorest absorber and is harder to apply than spray paint. It has been IITRI's experience that flat black Krylon brand spray paint is the most applicable to the manufacturing environment. It has adequate absorptive capabilities and is very easy to apply; most important, the response of a steel coated in this way has been found to be relatively insensitive to the paint thickness. This is demonstrated later in this report.

4.1.2 Beam Power Density/Exposure Time

Beam power density is defined as the total beam power divided by the area over which it impinges on a surface. With regard to laser heat treatment, power density is in effect the heat flux imposed on the surface.

Since power density is the rate at which heat is delivered into the surface, high power densities (30-40 kW/in.^2 or 4.65-6.2 kW/cm^2) result in a very rapid surface temperature build-up. Insufficient time is available for heat to diffuse from the near surface into the underlying metal. This surface concentration of heat assures the rapid, precise formation of a hardened case. At the same time, the continued introduction

of heat to the surface for an excessive period of time permits the surface to reach the melting point while the austenitizing isotherm is moving deeper into the part. The time for melting is relatively short (fractions of a second), and so the distance that the austenitizing isotherm can extend into the part is also limited. For this reason, depth of the hardened case is limited, in laser heat treatment, by the start of surface melting. Process development activity attempts to optimize the balance between depth and melting for a specific steel, coating, power density, etc. Along these lines, surface melting is avoided at high power densities by employing short exposure times (or faster scan rates). This high power density/short exposure time regime is characterized by generally shallow case depth (e.g., .020-.030 inch) and high surface hardness.²

On the other hand, lower power densities (5 to 15 kW/in.² or .77-2.32 kW/cm²) allow deeper case depths by virtue of the fact that the surface temperature is not rising as rapidly as with higher power densities. More time is available for heat diffusion deeper into the part. Thus, the austenitic zone can be driven deeper without surface melting. As is expected, sufficient metallurgical response at lower power densities requires longer exposure times (or slower scan rates). The low power density/long exposure time regime is characterized by deep case depths (e.g., .040-.060 inch) and slower extraction of heat from the case. As a consequence of slower cooling rates, surface hardness of "slow-deep" cases may be lower than "fast-shallow" cases.

4.1.3 Other Factors

The resistivity of a metal also relates directly to absorptivity because beam radiation interacts with electrons in the metal. Investigators have stated that the absorptivity at 10.6 μ m is directly proportional to the square root of resistivity of the metal.³ Resistivity increases with temperature. Thus, the hotter the workpiece is, the more absorbing it is. This implies that it is very important to control workpiece temperature during laser cycling in order to promote process reproducibility.

Beam impingement angle on the work surface also affects beam absorption. Shallow impingement angles result in greater reflectivity. A normal (90°) angle is considered optimal, but this is not always possible on complex geometries such as spur gears. Typically, 45° is accepted as a minimum practical angle for effective coupling. The angular nature of gears places a premium on management of the impingement angle.

³Y. Arata, H. Maruno and I. Miyamoto, "Heat Flow in Laser Hardening," International Institute of Welding (London) Document IV-241-78, April, 1978.

Surface roughness and cleanliness have also been cited as factors affecting absorption.⁴ An insulator, such as oxide layer on steel, is a good IR coupler. Greater roughness also promotes absorption but, like resistivity, should not be considered as a primary variable. Gears have uniform finish which must be maintained when processing is changed in pre-laser operations.

In designing a laser process for the test gears, all of the above factors were kept under consideration.

4.2 METALLURGICAL CONSIDERATIONS OF LASER HARDENING

The most important metallurgical consideration during laser heat treatment is the characteristically short austenitizing cycle (typically 0.010-1.0 sec). Observations of color photographs suggest that the austenitizing temperature during laser cycling is usually in excess of 2000°F, but even this high temperature cannot always overcome the fundamental lack of time at temperature. This short cycle time has the following ramifications:

1. Dissolution of coarse structures (e.g., coarse pearlite and blocky ferrite) may not result in a totally homogeneous austenite. This points to the need for a uniform microstructure before laser hardening.
2. Complex carbides in highly alloyed steels may not have sufficient time for dissolution. Thus, the resulting hardness level may reflect a lower carbon content than is actually contained in the steel.
3. Grain coarsening is minimized by the characteristically short laser treatment cycle even though the laser austenitizing temperature is high. This is a positive factor in establishing high strength and good fatigue resistance in steels.

⁴B. Sanders and V. Gregson, "Optical Reflectivity of Some Metals Using a Transversely Excited CO₂ Laser," paper presented at the Electro-Optics Design Conf., 1973, New York.

4. Proeutectoid grain boundary constituents (i.e., ferrite in hypoeutectoid steels or cementite in hypereutectoid steels) commonly found in hot-rolled, forged, or normalized steels may not totally dissolve. Thus, even in the hardened zone after laser cycling, these constituents can still often be seen surrounding prior austenitic grains. Again, a uniform martensitic structure prior to laser hardening eliminates this problem.
5. The extremely severe quench can promote retained austenite, especially in high carbon or high alloy steels. Retained austenite necessitates a subzero treatment after laser treatment.²
6. Martensitic structures can be obtained even in commonly nonhardenable steels such as 1018. The carbon-rich austenite surrounding the dissolved or partially dissolved pearlite colony that characterizes nonhardenable steels can quench out to high carbon martensite. The resulting structure will consist of ferrite but will also have some martensite. This phenomenon dramatically illustrates the rapidity of the laser austenitizing cycle.
7. Finally, the upper critical temperature (Ac_3) is very high in laser cycling due to the rapid heating rates (typically 10^3 to 10^5 °F/s).

As indicated in the above list, initial microstructure of the ferrous alloy is a major factor to consider for laser heat treatment. Besides its effect on austenite homogeneity, structure is also a major factor controlling the case depth and hardness gradient between the hardened zone and the unaffected base metal.

Figure 1 depicts the hardness profiles of two medium carbon steel samples that are compositionally identical and have been subjected to identical laser heat treat cycles. The only difference is that prior to laser hardening, one piece was fully annealed to obtain a coarse pearlitic/blocky ferrite structure (B), while the other piece was quenched and tempered to obtain a dispersion of fine spheroidal carbides in a martensitic matrix (A). There are three points illustrated in Figure 1 that depict the effect of initial structure.

First, the transition from full martensite hardness to the core hardness is more gradual in the coarse structure (B) than in the fine structure (A), exaggerated here for the sake of clarity. This is due to the distinct thermal gradient that exists in the austenitic zone during laser treatment, the surface being much hotter than the "bottom" of the heated zone. Laser heat cycling is rapid, so that high temperature is needed to obtain uniform austenitization. With an annealed structure (B), the lower temperature of the "bottom" of the austenitic zone is not high enough for uniform carbon distribution in the coarse structure within the exposure time. Hence, we see the gradual transition down to the core hardness representing the nonuniform dissolution of the pearlite/ferrite structure of steel B. Coarser structures have longer diffusion paths in which to achieve uniform austenitization. Higher carbon and alloy steels also tend to lean this way. On the other hand, the fine carbide dispersoids in a quenched and tempered structure more readily dissolve at lower temperatures, at the given exposure time.

The quenched and tempered sample with its finer structure has a shorter diffusion path to achieve uniform austenitization. As a result, the hardness gradient is steeper between the case and core in steel A, Figure 1. Higher rates of heat input (i.e., high beam power density) tend to localize heat near the surface and promote this behavior. From a fatigue standpoint, more basic information is necessary in order to assess the trade-offs between these two different hardness gradients and core structures. The lowered surface hardness resulting from low power density/long exposure time heat cycles should also be assessed for its effect on fatigue properties.²

The second major difference between the two dissimilar core structures is the resulting case depth. It is common practice in industry to define case depths in terms of some minimum hardness value. Due to the response difference between the two structures, quenched and tempered structure will usually yield a deeper case depth than an annealed structure exposed to the same beam parameters. This is shown in Figure 1. It should be noted that surface hardness is usually the same for both structures because the extremely high surface temperature promotes homogeneous austenitization in the surface region.

The third factor to notice in Figure 1 is the drop in hardness just before the core hardness is reached. The width of this zone is usually so small that an ordinary microhardness traverse will not detect it. Nevertheless, a zone must exist corresponding to an area of the structure that "saw" only subcritical treating (or lower range intercritical heating). The core structure would be expected to be somewhat softened here, particularly in the quenched and tempered structure. However, a strong temper-resistant steel (e.g., higher carbon

or molybdenum content) would be expected to show less softening here.

The final metallurgical consideration that enters into a procedure development such as that carried out in this program is that of hardenability. The depth of penetration of heat dictates the depth of the hardened zone. Heat penetration is substantially identical in a plain carbon and low alloy steel (assuming similar initial structures and identical carbon contents). Classical hardenability theory dictates that increased carbon and alloy contents impart to a steel an ability to harden to a greater depth. However, steel hardness is a function of carbon content alone. Thus, a thin sample of 1045 steel brine-quenched through its section to a 100 percent martensite structure would be as hard as a sample of 4145 that had been similarly treated. The controlling factor is quench severity.

The laser self-quench is always severe. Further, the section thickness being quenched (i.e., the austenitic zone) is very thin. Hence, alloy content has no bearing on laser hardenability. Alloy content, however, affects the rate of dissolution of carbides in austenite and the extent of softening of the surface and subcritical zone. (Of course, stringent core property requirements in a relatively heavy section may necessitate alloy additions). In contrast to this, other surface hardening processes, such as flame or induction methods, do require an alloy-induced hardenability. Thus, the laser (and electron beam) hardening processes become significantly more attractive when the critical status of vital alloy metals is considered.

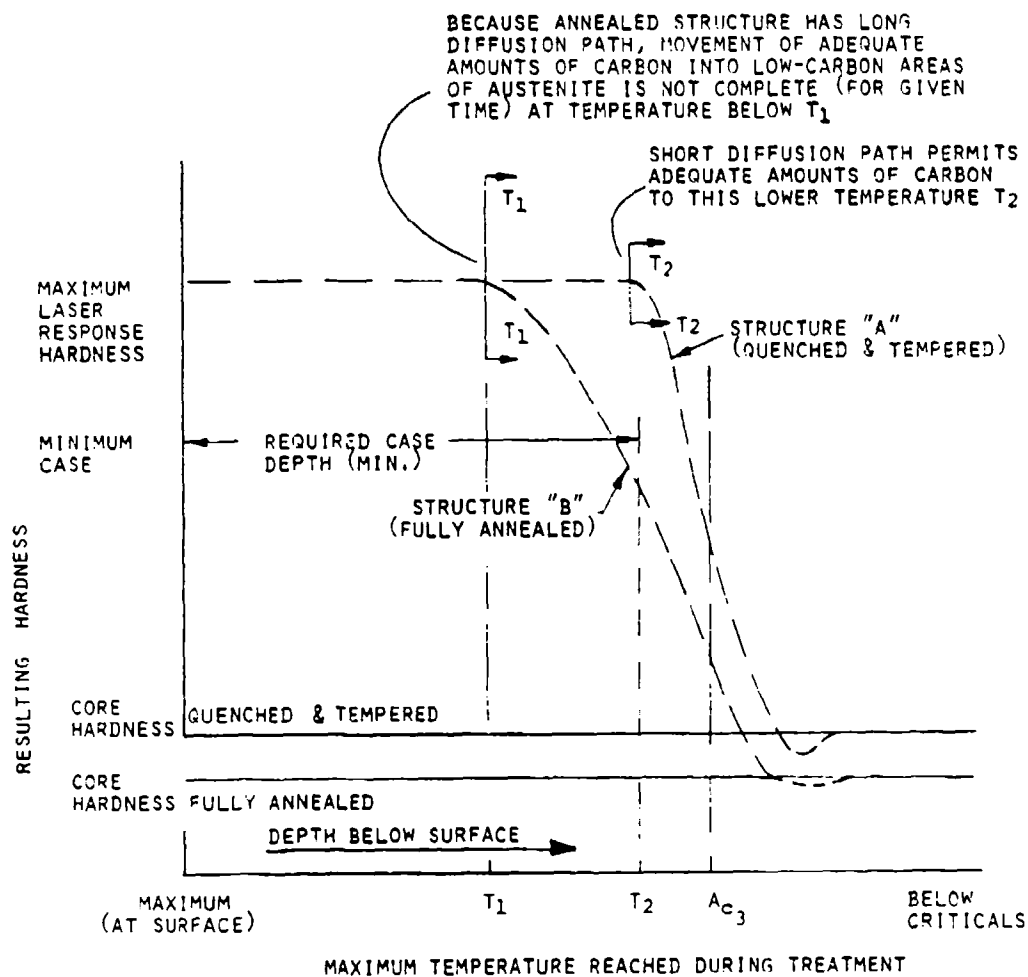


Figure 1. Effects of initial microstructure on laser hardening response.

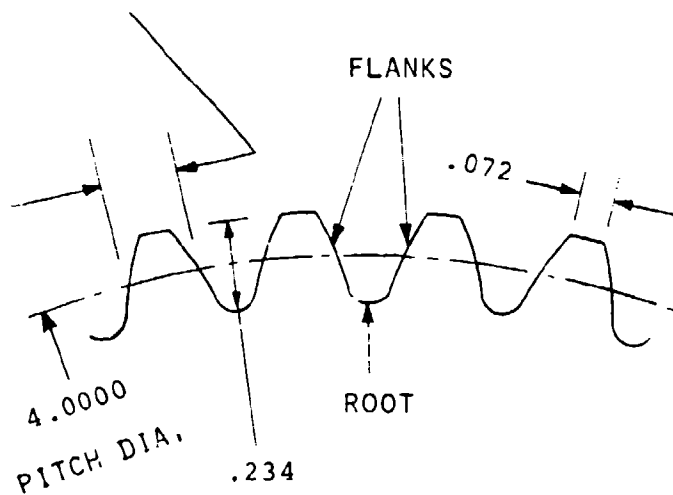
5. SPECIAL REQUIREMENTS IN LASER HARDENING OF SPUR GEARS

In order to meet the case depth and surface hardness requirements around the involute profile of a spur gear and the root, it was apparent that existing laser heat-treating technology would have to be greatly modified during the program. An analysis of the spur gear geometry will explain the reason. Figure 2 shows the spur gear profile, along with nominal dimensions, that was hardened in this program.

A gear profile can be hardened using laser beams in one of two ways:

- Hardening the two flanks of a gear tooth and portions of adjoining roots at one time as shown in Figure 3. This will be referred to as root-flank-flank-root (RFFR) method.
- Hardening the facing flanks of adjacent teeth and the root at one time as shown in Figure 4. This will be referred to as flank-root-flank (FRF) method.

CIRCULAR TOOTH THICKNESS : .1525



(DIMENSIONS ARE IN INCHES)

Figure 2. Details of the as-hobbed spur gear configuration. Dimensions shown are nominal.

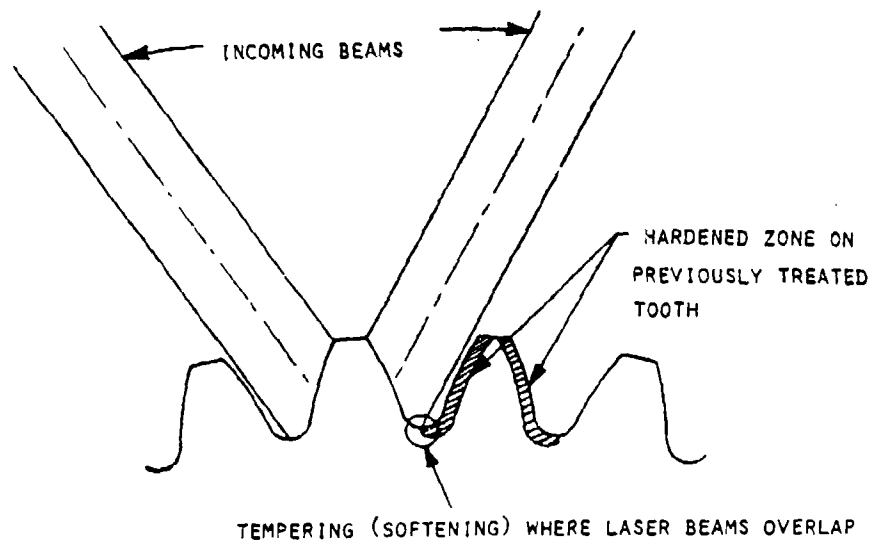


Figure 3. Laser hardening of gear teeth - Root-Flank-Flank-Root (RFFR) technique.

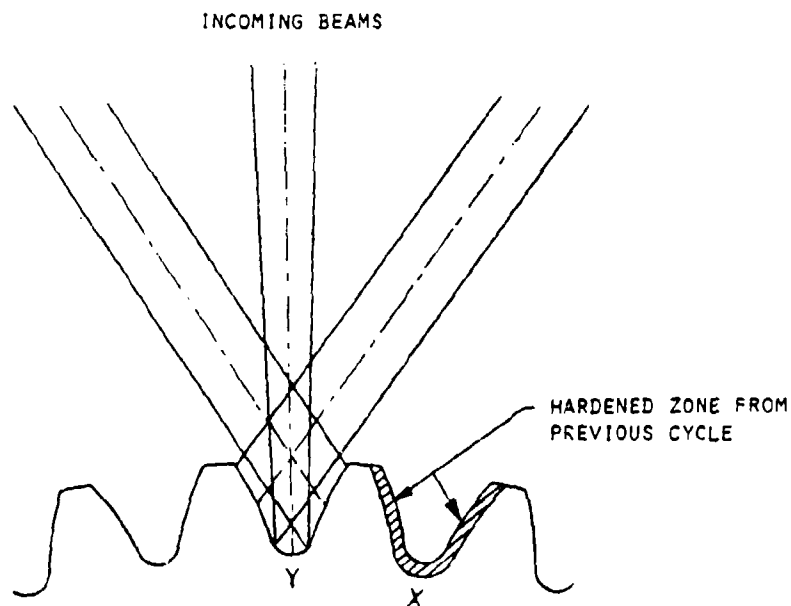


Figure 4. Laser hardening of gear teeth - Flank-Root-Flank (FRF) technique.

The RFFR method has the obvious disadvantage of overlapping laser beams in the root and thereby yielding soft roots due to tempering of previously hardened area. On large gears, e.g., 2 or 3 diametral pitch, this might not present a problem since the root will have enough width to prevent the softening from reaching the root fillet, which is the area of maximum bending stress. For the spur gear configuration used in this program, it was believed that overlapping root beams will certainly soften the root fillet area; therefore, the RFFR technique was not considered from the start.

The FRF method hardens one flank of a tooth at a time. Therefore, when the opposite flank of the same tooth is hardened, there is a possibility of tempering the previously hardened flank. Again, the spur gear configuration used in this program made the task more challenging due to its narrow thickness (nominal circular tooth thickness at the pitch diameter is only .1525 inch). This was perceived to be a problem at the start of the program, but it was felt that it could be overcome by devising appropriate cooling techniques.

The FRF technique of laser hardening gear teeth was the only method used in this program.

5.1 BEAM DIRECTION

To achieve proper placement of hardened zones required a significant refinement of existing laser technology. Notice that Figure 4 assumed the use of three beams. A simpler method would be to use a single beam of sufficient width to hit the exact center of a tooth gap from adjoining tooth tip to tooth tip. From earlier discussion, however, it is noted that this would entail an extremely shallow impingement angle on the flanks of the adjacent teeth. Thus, minimal beam absorption would occur here and reflected energy would bounce into the root area. Further, there are three major geometric constraints that dictate the use of more than one beam to achieve the required heat treat response.

Besides the low impingement angle on the flanks, the other major geometric constraints are:

1. The tip of the tooth is quite thin (Figure 2); thus, rapid heat buildup could occur here.
2. The root area has a large heat sink relative to the available surface area for irradiation.
3. At the base of tooth near the root radius, access of laser radiation may be restricted.

It was IITRI's original contention that these factors necessitated the use of not only multiple beam exposure but also the ability to independently adjust the exposure time and power in each of the beams. The following discussion suggests the reason for this belief.

5.1.1 Tooth Tip Requirements

As seen in Figure 2, the tip of the tooth on the candidate gear is nominally .072-inch thick. Keeping in mind that laser heat treatment relies on a self-quench mechanism, it is seen that the tooth tip would not have sufficient mass below the austenitic zone to provide an adequate conductive quench. In laser and electron beam heat treating technology, a ratio of quench mass depth to case depth of five-to-one (5:1) is suggested as a minimum. This rule allows for thermal diffusivity, specific heat, etc. The required case depth for this application was 0.026 to 0.034 inch. Using the minimum value, it is seen that at the tooth tip, only a .046-inch thickness of cold metal would be available for quenching. The quench/case ratio is 1.8:1 or less depending on case thickness. Thus, an insufficient quench would be expected at the tip. Also, burning of the tip could occur due to extreme overheating. It is not until the pitch diameter is reached that a sufficient quench mass exists. As shown in Figure 2, the pitch diameter tooth width is approximately .1525 inch. The quench/case ratio is close to the 5 to 1 minimum requirement. Techniques had to be devised to obtain auxiliary quench action to compensate for the inadequate ratio at the tip.

The most serious aspect of this thin section is what is known as temper back. As shown in Figure 4, the Y root gap is irradiated after the X root gap. As noted, tip thickness in the direction of heat flow is limited in the test gears. Thus, at the tooth tip, the heat introduced during the Y root gap exposure can flow through the tooth to temper the previously hardened zone on the top of the left flank of tooth gap X. D6AC yields a surface hardness of Rc 62 after laser hardening. During the course of this work, it was found that without some method to cool the X gap during Y gap exposure, the top of the left flank of the X gap could soften to Rc 50 at the tip. Similarly, the tip of the left flank of the Y gap would soften during the subsequent exposure of the next tooth gap. As expected, there was a steep surface hardness gradient down the flank of the test gears heat treated without auxiliary heat dissipation chills. This phenomenon proved to be the most challenging aspect of this effort and is discussed later in this report.

5.1.2 Root Requirements

The concave surface of the root area exhibits the exact opposite behavior of the tooth tip in that it presents an extremely large heat dissipation mass by virtue of its mass/surface ratio. Figure 5 schematically illustrates the effect of a concave surface on heat dissipation. The assumptions here are:

1. The same rectangular beam size ($2R \times t$) is used in both the concave and flat surface.
2. Identical beam power and exposure time are used.
3. Uniform absorption occurs all around the concave profile.

This third assumption is an oversimplification because the impingement angle actually varies around the concave profile. However, to illustrate the heat dissipation phenomenon, this assumption will permit a good qualitative understanding.

As is seen in Figure 5, the exposure of the concave surface and the flat surface at the same parameters results in a 57 percent greater case depth on the flat surface. Thus, a greater heat input is needed in the concave surface to obtain the same case depth as a corresponding flat surface.

We can now identify the need for more laser heat in the root area than is necessary on the flanks to obtain uniform hardening all around. If anything, heat input into the flank had to be minimized in order to avoid heat buildup and temper back.

5.2. DUPLEX HEATING

Maintaining extra heat input into the base of the tooth flank near the beginning of the root area while minimizing heat to the teeth meant that a duplex power delivery system would be needed. There are two reasons for this. First, the "profile" of the tooth near the pitch diameter would stop much of the radiation from striking the base of the flank if a single laser beam directed along the tooth gap centerline were used. Second, the shallow impingement angle here would decrease absorptivity. IITRI's multiple beam system (see Section 7) provided duplexing in terms of angle and power.

A summary of this geometric analysis of the spur gear suggests that realization of the desired project objectives requires that the laser optical system have the following features:

1. Multiple beams are needed to cover the tooth gap profile at effective impingement angles.

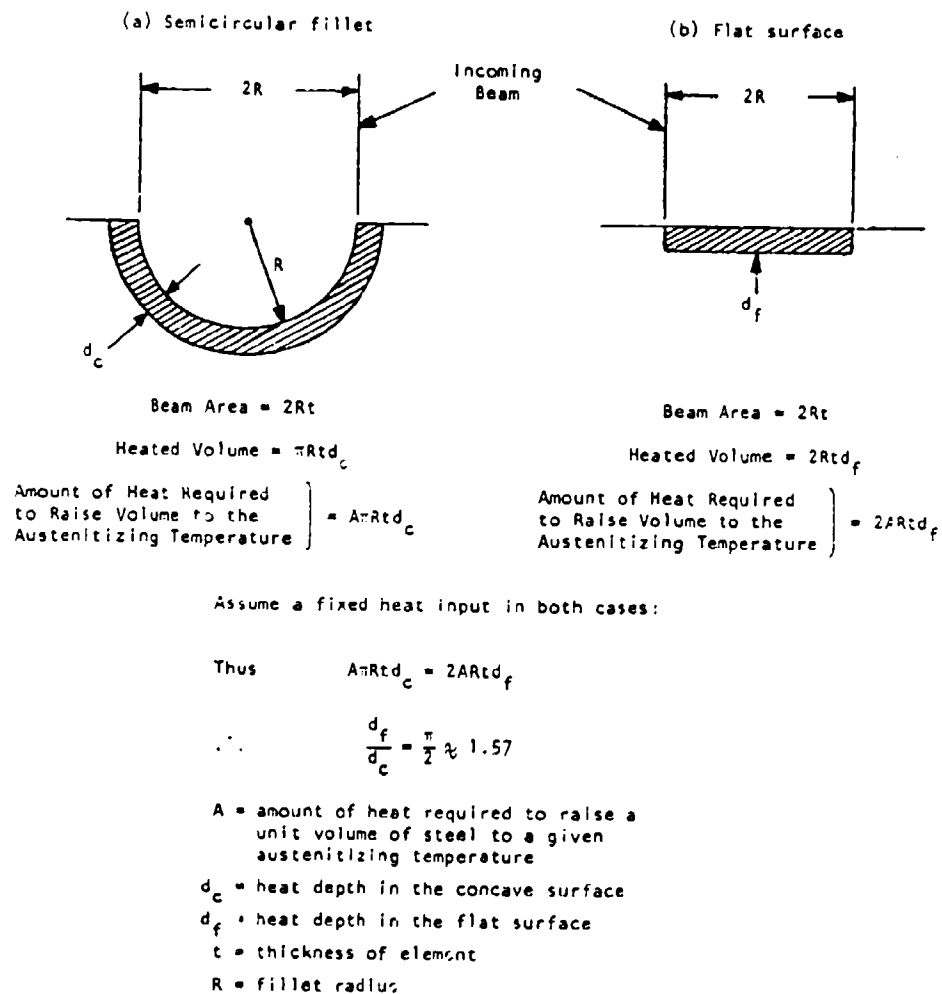


Figure 5. Geometric heat dissipation consideration during laser heat treatment.

2. The root area needs more heat as a result of its heat dissipation characteristics.
3. Overheating of the tooth tips must be avoided. External cooling is undoubtedly necessary.
4. The above factors necessitate an ability to independently control both the power and exposure time in each of the multiple beams to deal with the different thermal requirements of the gear geometry.

Initially, static exposure was selected over a scanning motion of the part in order to simplify part tooling. This decision assumed full coverage of the tooth surface from end face to end face of the gear through matching of the beam spot size with the gear width. There was concern that use of an over-size spot would melt gear edges, particularly near the tip.

Section 7 describes in detail the optical and equipment requirements.

6. SELECTION OF GEAR STEEL

6.1 300M VS D6AC

Two low alloy steels were considered for use in this program. Preliminary work was conducted on AMS 6419 steel, commonly known as 300M. 300M is a modification of AISI 4340 with higher carbon, molybdenum and silicon. (The chemical composition of 300M material used in this program is shown in Table 2). 300M per AMS 6419 is a premium quality consumable electrode vacuum melted steel suitable for aircraft accessory gearing. BHT uses this steel in a through-hardened condition in some accessory gears on the AH-1T helicopter.

Figure 6 shows the hardness profile of a 300M specimen laser hardened and tempered at 300°F. This temperature is the lowest tempering temperature that is used in aircraft gearing application. As seen from Figure 6, 300M does not retain Rc 60 hardness after a 300°F temper. Since Rc 60 was the minimum surface hardness desired on laser hardened gears, 300M was not given any further consideration in this program.

The second material selected for this program was D6AC per AMS 6431. D6AC, in accordance with AMS 6431, is a low alloy steel of premium quality produced by consumable electrode vacuum melting. It is an alloy used commonly in the aircraft industry. D6AC has higher carbon and molybdenum than 300M and therefore was expected to yield Rc 60 minimum hardness after 300°F temper. A small quantity of D6AC material was obtained to perform preliminary temper resistance tests. The chemical analysis of this batch of D6AC is given in Table 3. The hardness profile of the laser hardened case of D6AC before and after 300°F temper is shown in Figure 7 and demonstrates that the material meets the minimum hardness requirement of Rc 60 after tempering.

TABLE 2. CHEMICAL ANALYSIS OF 300M PER AMS 6419
(4.5-inch-diameter bar)

	C	Mn	Si	Cr	Ni	Mo	V	Cu	P	S
Actual:	.41	.71	1.60	.83	1.78	.42	.07	.10	.004	.003
Requirement:	.40/.45	.60/.90	1.45/1.80	.70/.95	1.65/2.00	.30/.50	.05/.10	.35 max	.010 max	.010 max

TABLE 3. CHEMICAL ANALYSIS OF D6AC PER AMS 6431
(Material procured for preliminary temper resistance study)

	C	Mn	Si	Cr	Ni	Mo	V	P	S
Actual:	.49	.85	.22	1.06	.56	1.00	.11	.010	.004
Requirement:	.45/.50	.60/.90	.15/.30	.90/1.20	.40/.70	.90/1.10	.08/.15	.015 max	.015 max

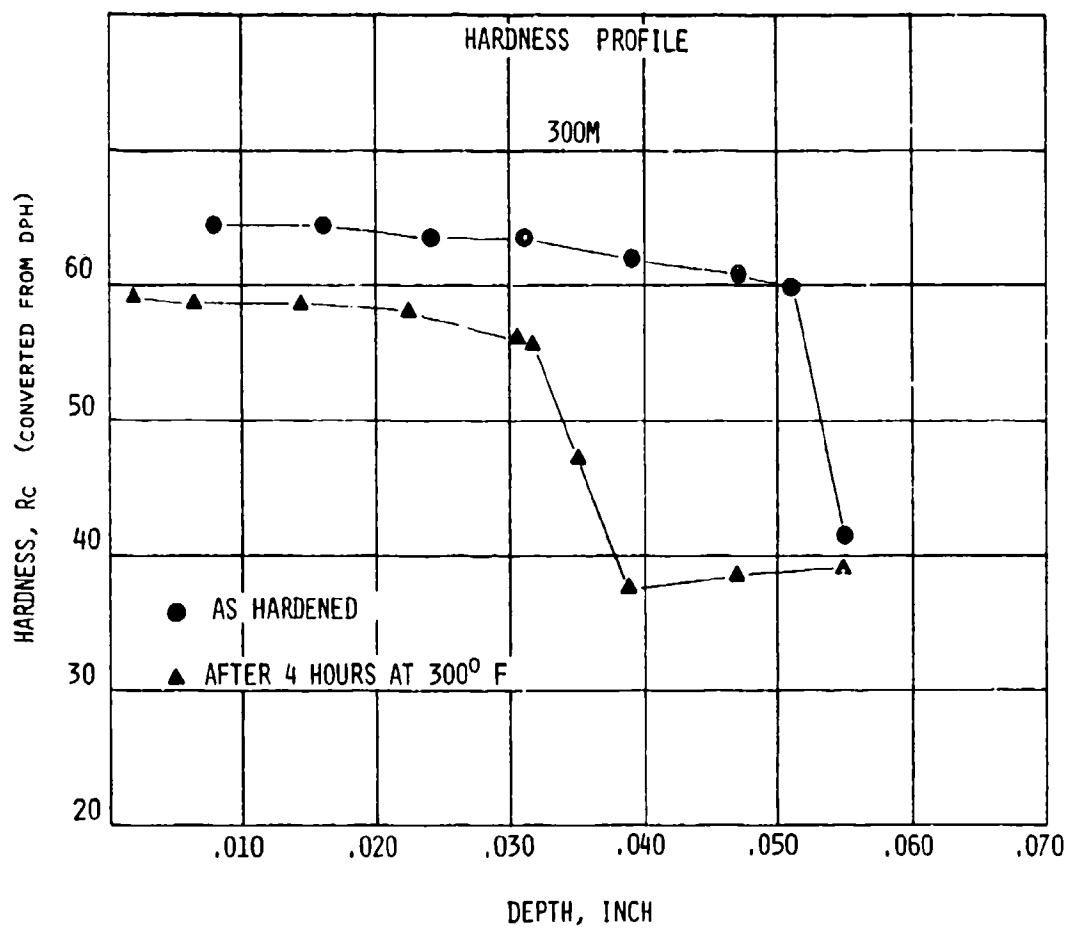


Figure 6. Laser hardened case profile for 300M before and after temper.

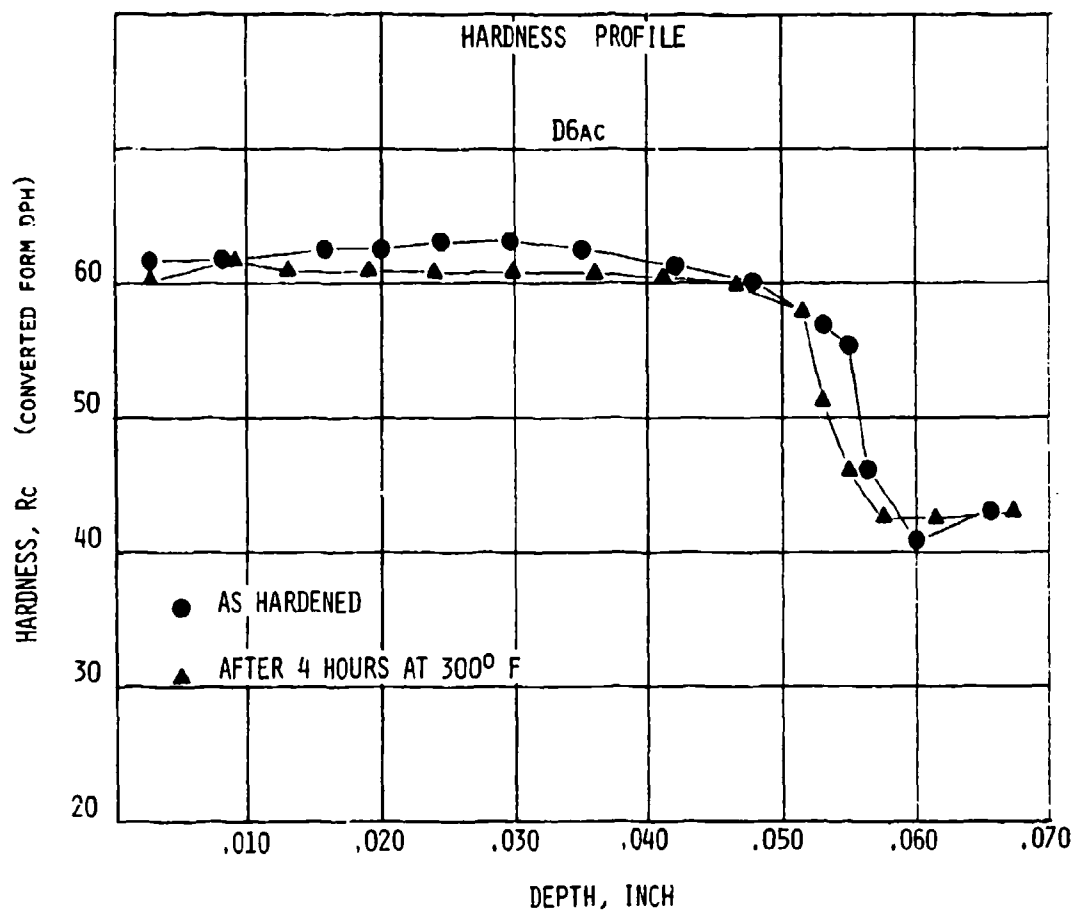
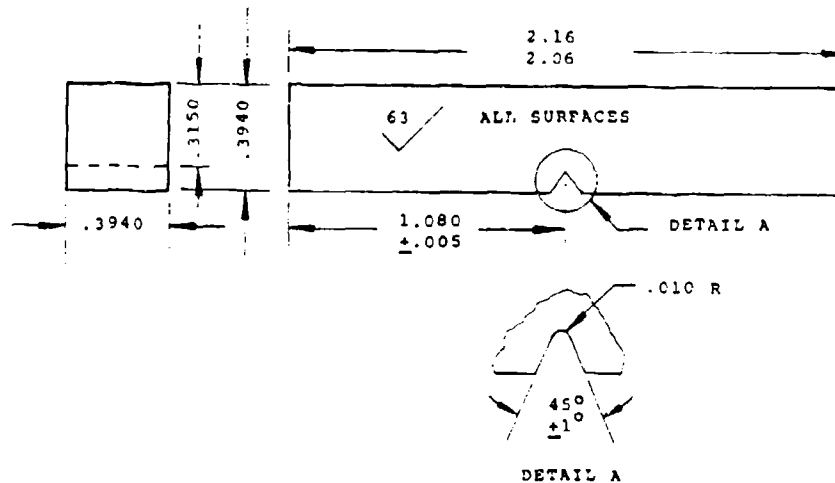


Figure 7. Laser hardened case profile for D6AC before and after temper.

6.2 METALLURGICAL PROPERTIES OF D6AC

After selecting D6AC as the primary material for this program, two heats of the material were obtained. Raw material evaluation tests were conducted on samples from both heats and results met the requirements of AMS 6431. Results of raw material evaluation tests are presented in Appendix B.

The toughness of D6AC was evaluated by conducting Charpy V-notch impact tests and fracture toughness tests. Specimen configuration used in the impact testing is shown in Figure 8. The results of impact tests are shown in Table 4 and Figure 9. (The difference in impact strength between the two bar sizes is primarily due to the difference in mechanical working and is not uncommon in alloy steels.) Fracture toughness tests were performed in accordance with ASTM-E399 using 1/4T compact tension specimens described in Figure 10. The specimens were laser hardened on both sides near the crack tip as shown in Figure 11. The results of fracture toughness tests are shown in Table 5. Figure 12 compares the fracture toughness of D6AC with that of carburized AMS 6265. The AMS 6265 specimens were also 1/4T compact tension specimens and were carburized after final machining to the case depths shown in Figure 12.



TOLERANCE: ±.001 UNLESS SPECIFIED OTHERWISE

ALL DIMENSIONS IN INCHES.

Figure 8. Charpy V-notch impact test specimen configuration.

TABLE 4. LONGITUDINAL CHARPY V-NOTCH IMPACT STRENGTH
OF D6AC AT TWO DIFFERENT HARDNESS LEVELS FROM
TWO DIFFERENT HEATS AND BAR SIZES

Specimen No.	Bar Diameter (inch)	Core Hardness (Rc)	Impact Strength (Ft-lb)
5H-1	5.25	36.0	57.5
5H-2	"	"	60.0
5H-3	"	"	57.0
5H-4	"	"	57.0
5H-5	"	"	59.0
5H-6	"	"	59.0
5H-7	"	"	57.0
5H-8	5.25	36.0	57.0
			Average = 57.9
5L-1	5.25	41.0	35.5
5L-2	"	"	34.0
5L-3	"	"	40.0
5L-4	"	"	37.0
5L-5	"	"	38.0
5L-6	"	"	38.0
5L-7	"	"	38.5
5L-8	5.25	41.0	35.5
			Average = 37.1
8H-1	7.0	36.0	38.0
8H-2	"	"	36.5
8H-3	"	"	36.0
8H-4	"	"	40.0
8H-5	"	"	34.0
8H-6	"	"	37.0
8H-7	"	"	37.0
8H-8	7.0	36.0	36.0
			Average = 36.8
8L-1	7.0	41.0	28.0
8L-2	"	"	19.5
8L-3	"	"	21.5
8L-4	"	"	21.0
8L-5	"	"	20.8
8L-6	"	"	21.0
8L-7	"	"	22.0
8L-8	7.0	41.0	21.5
			Average = 21.9

Note: Above values may be compared with the average longitudinal impact strength of VAR 9310 after postcarburize heat treat - 4.0-inch bar: 62.1 ft-lbs; 8.0-inch bar: 56.4 ft-lbs.

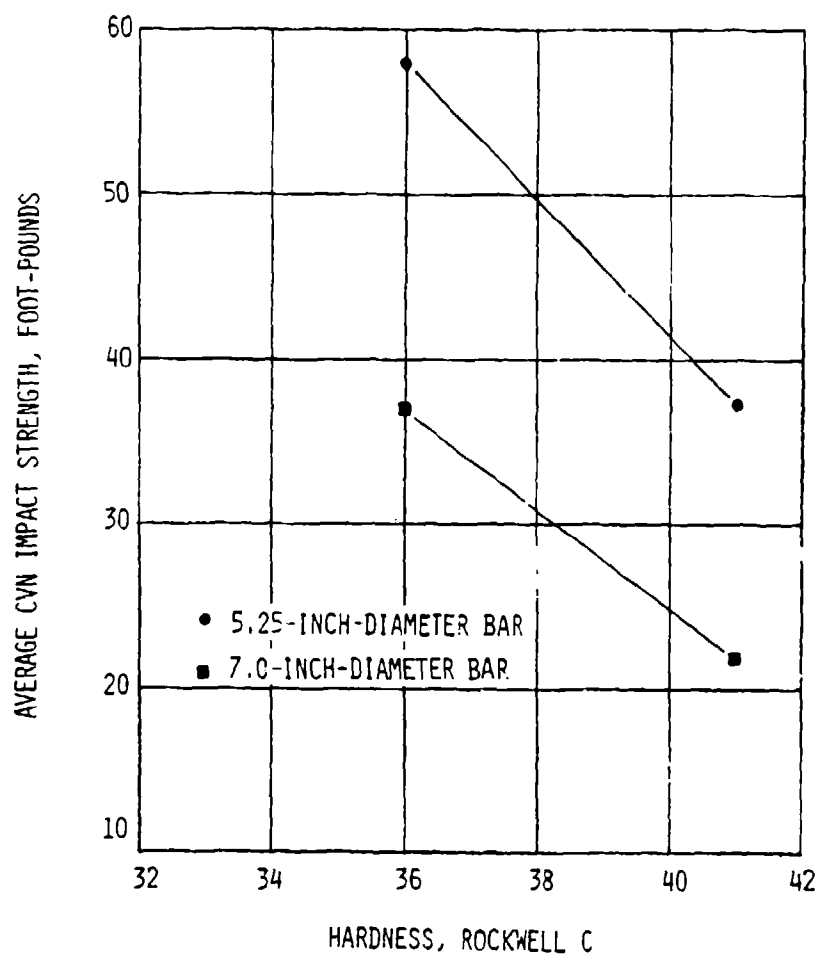


Figure 9. Charpy V-notch impact strength of D6AC at two core hardness levels.

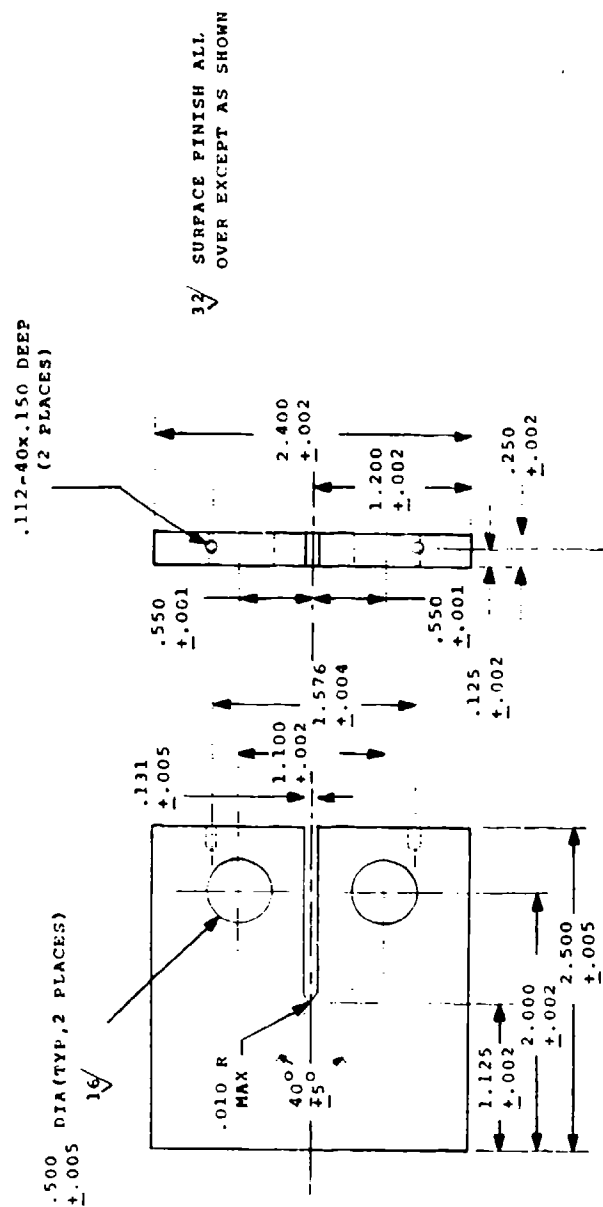


Figure 10. Compact tension fracture toughness test specimen configuration.

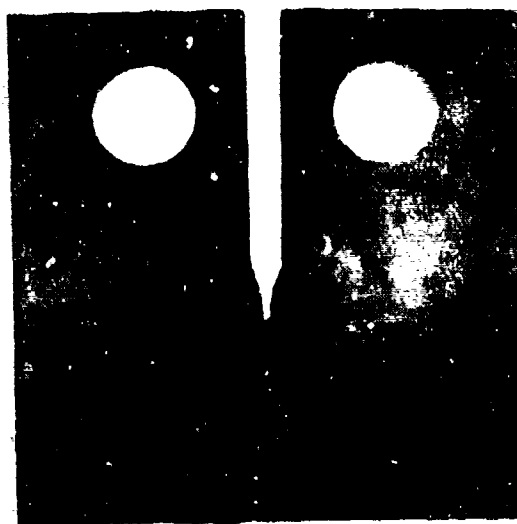


Figure 11. Failed D6AC fracture toughness (compact tension) specimen. The specimens were laser hardened at the crack tip on both sides.

TABLE 5. K_q FRACTURE TOUGHNESS OF D6AC AFTER LASER
HARDENING AT THE CRACK TIP (1), (2)

Crucible Heat No.	Bar Diameter (in.)	Core Hardness	K _q Fracture Toughness (KSI $\sqrt{\text{in.}}$)
7153726	5.25	Rc 41	95.1
7147356	7.0	Rc 41	94.1
7153726	5.25	Rc 36	(3)
7147356	7.0	Rc 36	108.23

- Notes: 1) Laser hardened case depth measured approximately 0.25 inch on all specimens.
- 2) All specimens tempered 300°F for 4 hours prior to testing.
- 3) Invalid test due to excessive fatigue crack length.

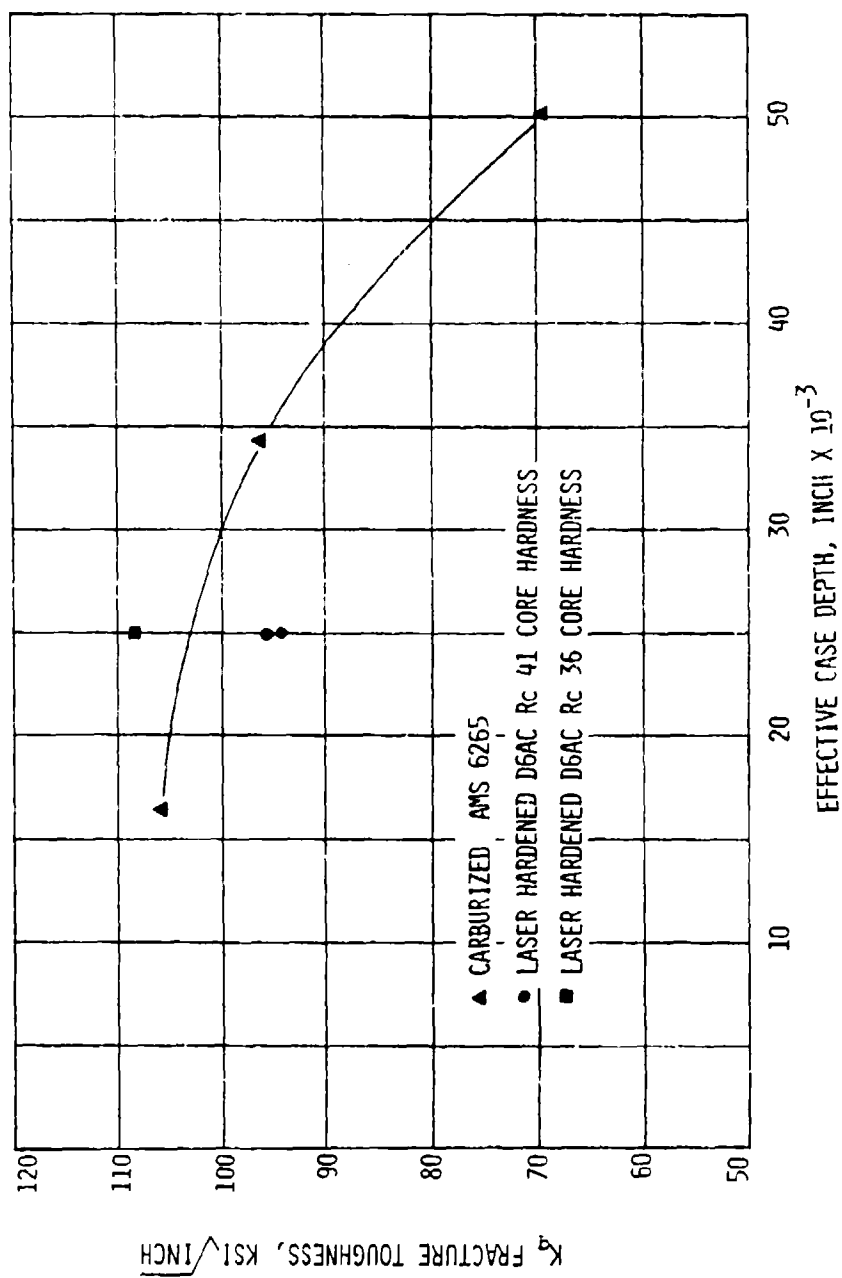


Figure 12. Kq fracture toughness of laser hardened D6AC compared against that of carburized AMS 6265.

6.3 PRE-LASER HARDENING HEAT TREATMENT

The heat treat condition of steel prior to laser hardening has a significant effect on the case properties. For this reason, all 300M and D6AC specimens were normalized, hardened, and tempered before laser hardening. The specific heat treat cycles are shown in Table 6.

TABLE 6. PRE-LASER HARDENING HEAT TREAT CYCLES
USED FOR 300M AND D6AC

	300M	D6AC
Normalize, 1 hour at	1675°F	1650°F
Harden, 1 hour at	1575°F	1550°F
Quench	Oil (130-170°F)	Oil (130-170°F)
Temper, 4 hours at	1100-1150°F	1100-1150°F

Note: Typical section thickness of specimens at the time of heat treatment was 5/8 inch.

7. SYSTEMS ENGINEERING AND OPERATION

This portion of the program was actively directed toward making available a system that could demonstrate laser treatment on complex shapes such as gears. The effort had to be confined to existing equipment and facilities. This constraint led to certain problems that revealed broader facets of the system. For example, the need to deal with an unusually long beam transmission led to a number of observations regarding suitable types of mirrors and management of beam path atmosphere, among others. The following section deals with the specific task of adapting the IITRI Laser Center to the gear treatment requirements of the contract. However, general observations regarding the design aspects of an industrial system dedicated to gear hardening specifically have also been included.

Figure 13 is a layout of the IITRI laser facility. IITRI employs an Avco-Everett 15 kW, continuous wave CO₂ transverse flow type laser (shown in Figure 13). The characteristics of this device are given in Appendix C. As shown in Figure 13, IITRI has a multiple work station capability for laser welding, cutting, heat treatment, surface alloying/cladding and laser-assisted machining. The performance of this work necessitated the installation of a totally new hardening work station (Station 2A) by IITRI. This station is shown at the far left of the figure.

It should first be noted that a collimated laser beam is delivered to all nine of the work stations. To transfer the beam from the laser and from station to station, movable flat mirrors are employed to steer the collimated beam. The approximate location of these transfer mirrors is shown in Figure 13. An additional beam transfer mirror was installed for this work. From this transfer mirror, the beam is directed through a long vented duct extending the length of the facility to the gear work station. The high available power in the IITRI facility (15 kW) dictates the exclusive use of front surface metal mirrors (water cooled and mass cooled). Transmission optics are not employed, although they would be acceptable at power levels below about 5 kW.

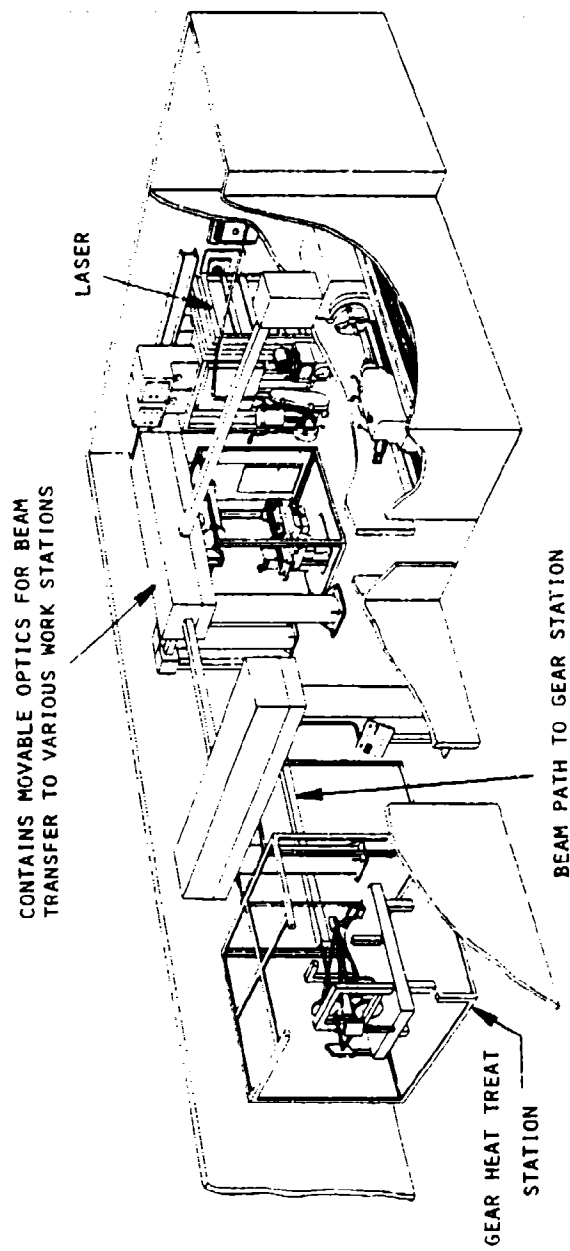


Figure 13. Layout of the IITRI laser facility.

Figure 14 is a photograph of the gear heat treatment tooling package. At the right the gear positioner is shown. The cylindrical objects are microprocessor-controlled stepping motors for tooth indexing and workpiece oscillation. To the left of the work positioner is the first optical frame. Next in line is the frame supporting the calorimetric beam shutters. To the left of this is the second optical frame.

7.1 BEAM TRANSMISSION

Certain precautions are necessary for the transfer of an infrared laser beam through air. The chemical bonds of certain molecules can resonate at a frequency corresponding to the CO_2 laser's $10.6 \mu\text{m}$ output wavelength. As a result, they act as energy absorbers. These include such common compounds as H_2O , CO_2 , and various hydrocarbons. Absorption of the laser light by these compounds causes heating of the air in the beam path. Since hot air and ambient air are of different densities, refractive effects alter the spatial power distribution within the beam. Atmospheric absorption also implies a lowering of beam transmission efficiency.

The profile of the beam employed in this work represents a ring-like energy distribution. In other words, a transverse profile of the beam energy is annular. This shape is derived

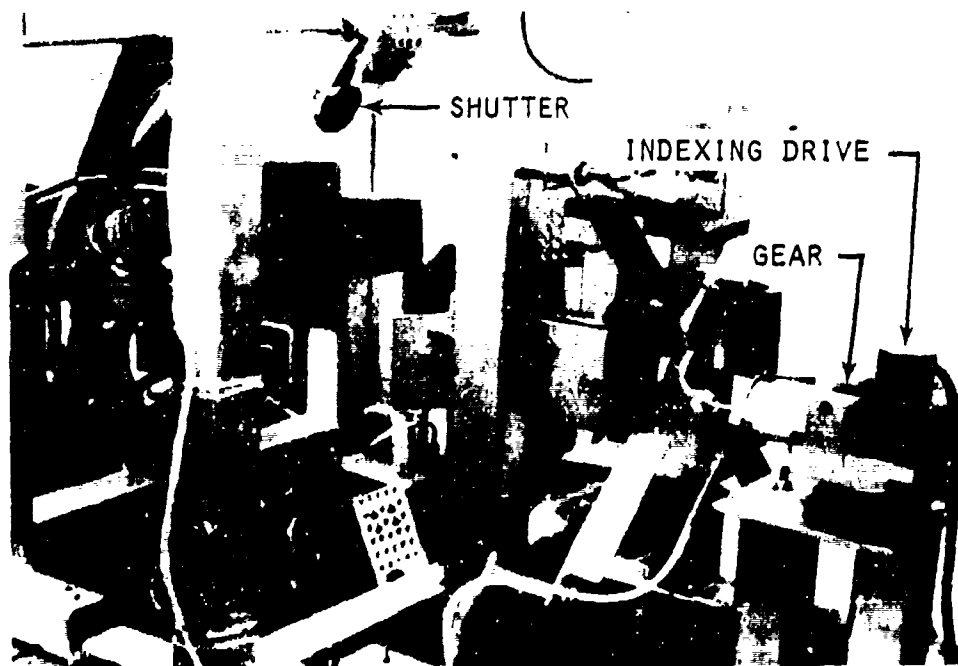


Figure 14. Overview of gear heat treatment tooling.

from the annular shape of the laser chamber output mirror. This annular mirror directs the energy out of the laser as an $f/25$ diverging beam, which is then collimated with a concave front surface copper mirror to produce the aforementioned ring shape. The beam OD is nominally 2.5 inches while the ID is about 2 inches. These dimensions are observed only very close to the collimating optics (i.e., near the laser output) and are averages because the energy pattern is not uniform around the circumference of the concentric beam. Additionally, during this program the distribution of power within this concentric beam appeared to be nonuniform and subject to change from time to time. The source of spatial variation, however, does not appear to be the laser. This was demonstrated by producing beam prints using fixtured acrylic plates that had been carefully machined to bring their edges to the same reference line as each print was made. These beam prints, shown in Figure 15, were made using:

The laser beam in a crescent mode directly from the laser (for the laser hardening of gears a full annular beam was used and the prints shown in Figure 15 do not show quartered annular beam produced by the optics shown in Figure 17), and

Five water-cooled mirrors (in this program only mass-cooled mirrors were employed).

A shutter was used to control the exposure time. The principle feature of the beam prints is the outside of the half-moon configuration and the contour (representing power), which lies just inside of it (and is not shown in the sketches). Figure 15 shows that the location of the beam, with reference to the upper right-hand corner of each plate, was essentially unchanged throughout the 900 seconds of continuous exposure. These tests were conducted by IITRI in support of a proposal to abandon the beam path used in the program in favor of the above-described beam path using water-cooled optics. The program was terminated before the proposal could be acted on, but these tests show that laser beam is inherently stable and remains that way if the mirrors in the path are water cooled. Since instability was observed at the work station, the conclusion can be drawn that the mass-cooled mirrors between the laser and work were the cause.

In any event, the refractive effects served to magnify the irregularity of the output power profile. The two common refractive effects encountered with infrared beam transmission are known as "blooming" and "steering." Blooming involves the circumferential expansion of the beam. Steering involves the movement of the rays in the beam off of their previous centerline. The combined effect of these phenomena was seen to cause the 2-inch beam to spread out as much as 1.5 inches as it traversed the beam path between the laser and the work station about 90 feet away.

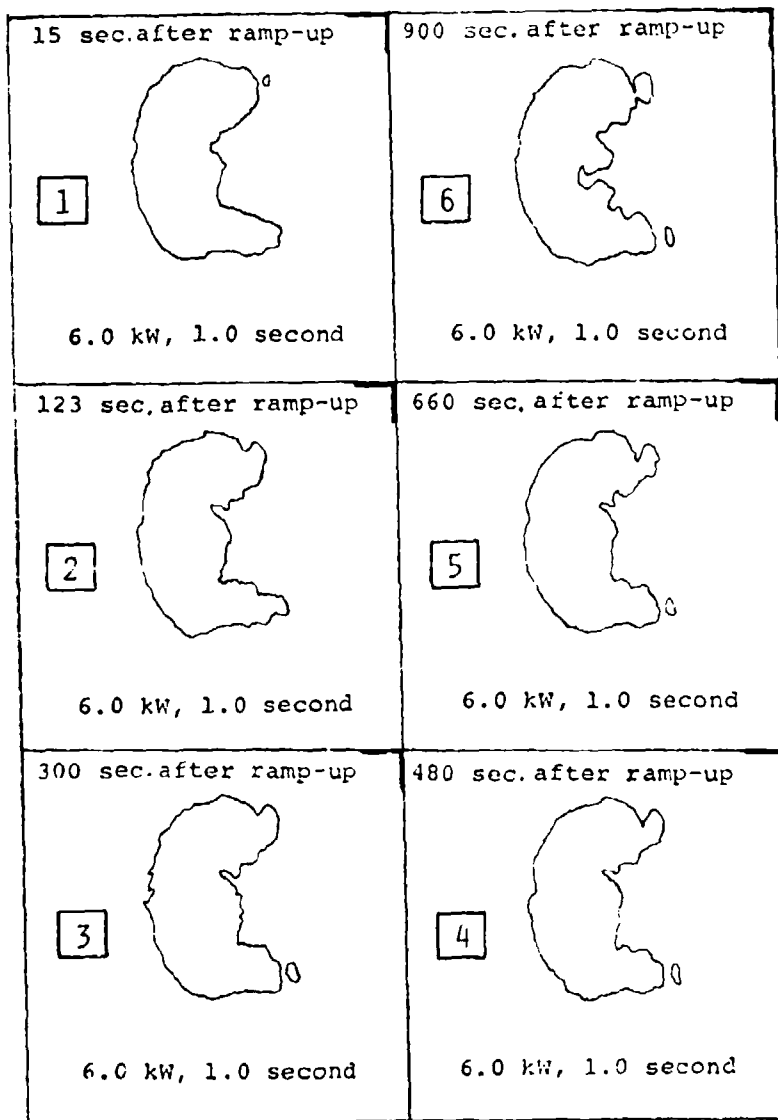


Figure 15. Laser beam (crescent mode) profiles obtained with acrylic plates showing stability of the beam with respect to time. (The upper right corner of each plate represents a reference point which was at the same location as each exposure was made.)

During the program, several precautions were considered to minimize these effects. The first is to minimize the distance between the work station and the laser. The IITRI room layout did not permit this option. The total beam path, from laser to workpiece, was approximately 90 feet and observations suggested that considerable effort should be made in a manufacturing situation to place the laser head as close to the workpiece as possible.

The second beam transfer precaution was to prevent the formation of heated air pockets in the beam path. For this project, cross-vented ducts were employed to keep fresh air blowing through the beam path. A small fan was placed every 6 inches along 40 feet of the beam path. As was seen in Figure 14, the optical package used for gear heat treatment restricted the use of vented ducts in the actual work station. However, fresh air was kept circulating through the station by using floor fans. The fans definitely reduced blooming over stagnant air.

Another precaution was to assure, as much as the schedule permitted, that clean dry air circulated through the beam path. It was noted during this work that blooming and steering were noticeably more pronounced if tests had to be run during very humid weather. In a manufacturing setting, a totally enclosed beam duct employing an axial flow of clean air would be recommended.

The final precaution to ensure optimum beam quality is not related to any atmospheric beam interaction. Instead, it is related to the surface condition of the transfer optics. Since the reflective optics employed in this effort were of oxygen-free high conductivity (OFHC) copper, this discussion centers around copper mirrors. Copper was used in the system that was designed for this program because it permits a lower-cost optic to be built. Copper can be fabricated into mass-cooled mirrors for a few hundred dollars each. Simple low-cost mirrors permitted maximum experimental flexibility as the process evolved, but thermal instability and environmental sensitivity to scratches, tarnish, etc., were observed. Once a fully approved process was available, an investment in water-cooled, molybdenum mirrors would appear to be justified for long-term production stability. Although it is less reflective to 10.6 μm radiation than copper, its higher thermal diffusivity, lower thermal expansion, high thermal damage threshold, higher scratch resistance, and better resistance to atmospheric attack make molybdenum a more logical production optic material.

Observations made in this program with respect to beam transmission in an industrial environment suggest other sources of beam degradation. Portions of a collimated beam striking a

flat copper mirror surface can be scattered in the following ways:

1. Roughness from diamond tip machining or polishing of the optic
2. Scratches or gouges caused by careless handling
3. Shrink porosity or other internal defects in the copper that are exposed at the mirror surface*
4. Dust collection on the mirror surface
5. Thermal distortion of the optic. Even the amount of heat absorbed by a highly reflective metal such as copper can be significant over long exposure times. The high expansion coefficient of copper, coupled with improper optic mounting techniques, can result in appreciable beam distortion. For this reason, water cooling of all optics is recommended. Warm water is preferred to minimize condensation on the mirror surface.

The greater the number of optics employed, the more the scatter in the beam. Additionally, a long beam path magnifies the optic scattering effect. It is important to note that the laser heat treatment process such as employed in this program is not as affected by beam scattering as is laser welding, where a very coherent beam is necessary to assure a sharply focused beam.

7.2 WORK STATION ENCLOSURE

Figure 13 shows the gear heat treatment optics and tooling mounted inside an enclosure. The work station enclosure is 10 x 10 x 8 feet high. The frame of the station is made from 4- x 4-inch steel channel. The walls and sliding doorway are comprised of transparent acrylic plastic (1/4-inch thick).

Acrylic affords two advantages:

- Transparent station walls allow the operator to watch the heat treatment process.
- While transparent to visible light, it is quite opaque to 10.6 μ m infrared light. Thus, it acts as a shield to protect the operator from stray radiation.

*A soap solution is used to clean the copper mirrors, which are highly susceptible to atmospheric "tarnishing." This could etch out the grain boundaries and provide another source of beam scatter.

Figure 14 shows a large 6- x 6-foot steel base on which the optical frames rest. It stands 1-1/2 feet off the floor.

7.3 OPTICAL DESIGN

7.3.1 Beam Shaping Methodology

In earlier discussions of laser heat treatment, the effect of spatial power variations within the beam on hardening response was not mentioned. It was assumed that a uniform (flat) power profile was employed. This would result in a hardened zone of uniform thickness. It was observed in this program that a transverse flow laser does not necessarily provide such a power profile and, as such, certain methods to "shape" the beam to obtain a flat profile had to be developed and employed.

The common shaping methods are illustrated in Figure 16. This program was based on the concept of beam integration which had been used by IITRI in previous programs. Low-cost integration techniques were introduced, consistent with the economic emphasis of the program.

7.3.1.1 Beam Integration

Beam integration starts with the division of a nonuniform incoming beam into many parts. If each of these parts is then directed to the same area on the work surface, a uniform, "integrated" beam power profile is obtained. "The power density on the work is independent of the laser beam profile and depends only on the total power in the beam."⁵

Before the initiation of this effort, beam integration at IITRI was commonly implemented via a concave beam integrator produced by Spawr Optical, Inc. This optic consisted of a series of half-inch square polished flat facets that are hand-mounted together on a 50-inch radius-of-curvature concave backing. In this way, the incoming collimated beam is broken up into a converging stream of square beams, each of a size relating to that of the flat facets. The reimage distance, or the point where each of the square divided beams is piled on top of another, is 25 inches away. At this point, a nominally "flat" power profile is obtained.

Consider how such a device works in order to understand its importance. If a circular laser beam with a 2-inch diameter were directed at the 36 facets of the above integrator, it would illuminate almost the full area of 12 facets and portions of 4 or more. The work would see a single facet image which is a compilation of the above 16 full or partial images. The

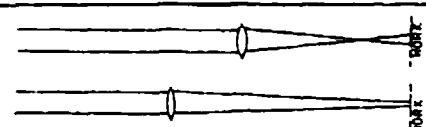
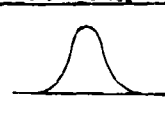
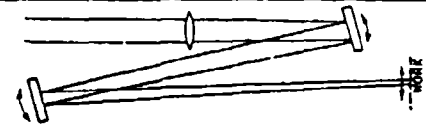
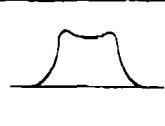

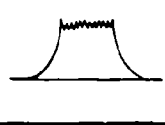
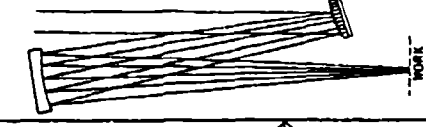
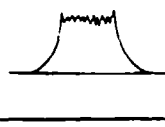
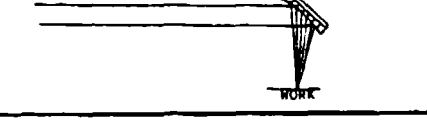
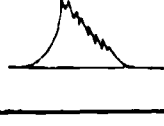
	SHAPING OPTICS SCHEMATICS	ENERGY PROFILE	DESCRIPTION
(a)			OUT OF FOCUS OR LONG FOCUS OF INCOMING BEAM BEAM PROFILE IS THAT OF LASER OUTPUT POWER
(b)			LONG FOCUSED BEAM, SCANNED OR OSCILLATED IN ORTHOGONAL DIRECTIONS
(c)			CONCAVE BEAM INTEGRATOR
(d)			CONVEX BEAM INTEGRATOR AND SPHERICAL REIMAGING MIRROR.
(e)			REPLICATED DOWNHAND PARABOLIC CONCAVE BEAM INTEGRATOR WITH POWER PROFILING

Figure 16. Beam integration schemes: (a) simple focusing lens; (b) two oscillating mirrors; (c) concave surface with several molybdenum facets; (d) convex beam integrator (CBI) made from single copper block; and (e) parabolic integrator.⁵

power on the work would be the reflected power of the 2-inch beam. If the beam bloomed to 3 inches without changing power, 24 facets and portions of 4 more would be involved, but the single-facet image on the work would not have changed. The beam could shift across the face of the integrator and the single-facet image on the work would not change (unless some of the beam spilled off the integrator and was lost).

There are, however, certain unattractive characteristics of integrated power profiles. As shown in Figure 16c, geometric patterns of variable power exist within the beam. This is due to the reinforcement/cancellation and refractive phenomena.⁵ "The large peaks at the edges result from the sides of the

⁵S. L. Ream, "A Convex Beam Integrator," Laser Focus, November 1979.

facet from which the portion of the beam has been directed, and the finer peaks and valleys result from interference among the beams from the different facets."⁵ These peaks represent areas within the gross power profile that are of locally higher power density than the average. Thus, surface melting during heat treatment is usually more prevalent with integrated optics than with the other common shaping method that is shown in Figure 16b. Part oscillation was employed to minimize the effects of these irregularities.

However, beam integrators are easy to use and are preferred for applications where complex optical systems are not feasible; for example, where multiple beam paths are required. This program required multiple beams and also beam sizes that were not available in commercial integrators.

7.3.1.2 Convex Beam Integrator

Accordingly, a convex beam integrator (CBI) was manufactured by IITRI for this program. The CBI is a series of rectangular facets described on a convex spherical surface. The resulting negative focal plane is then reimaged with an additional concave spherical mirror.⁵ This concept is illustrated in Figure 16d. Since this optic is produced from a solid copper block by diamond tip flycutting employing N-C control, it was feasible to tailor mirrors to the specific test gear requirements for this program. Such low-cost mirrors would also serve as low-cost quick-change "tools" in a commercial operation. Another advantage of CBI's is that custom power distributions, similar to Figure 16e, are possible. This sort of power profile has been shown to provide numerous advantages when heat treating a moving part.⁵

The facet sizes on the CBI's fabricated for this effort were nominally 0.300 x 0.200 inch to accommodate the spur gear geometry (refer to Figure 2). The actual beam size "seen" by the work, however, was different (approx. 3/8 x 1/4 inch) due to diffraction. Optic errors introduced during the diamond tip machining of the CBI produced a power profile wherein the characteristic peaks of energy were grouped in the center of the beam spot. Normally, as optic manufacturing techniques are refined, these reinforcement peaks can be spread out over the area. However, when they are grouped they tend to concentrate too much of the energy in the center of the area so that the power profile begins to look like that of a very large diameter focused beam with a pronounced center concentration of energy. Such a profile overtreats the center of the spot causing an increased depth and a strong potential for melting at this area. This can be corrected by more refined optics or by moving the parts through the power profile, a technique under discussion when the program was terminated.

7.3.1.3 Beam Splitting and Subsequent Management

Energy duplexing by means of multiple beams was deemed the only way to approach the achievement of a uniform hardened zone around the tooth gap. In a system designed specifically for multibeam gear hardening, these beams might be most effectively produced by four small lasers. This would provide good beam positioning, improved flexibility in system layout, and possibly a lower capital investment (depending on the relative power involved). To simulate such a production system, IITRI had to devise a method for splitting the collimated concentric beam from its single large laser into four segments. Each of these beam segments is then sent through its own integrator/optical train. As shown in Figure 17, a copper pyramid comprised of four copper wedges butted together performed the splitting operation. Figure 17 then shows the details of what happens to one of these segments (or "legs"). It must be kept in mind that each of the other segments has its own optical train identical to that shown in Figure 17. Thus, the final IITRI gear heat treatment optical package consisted of four CBI's, four spherical reimaging mirrors, four flat mirrors as shown in Figure 17, four targeting mirrors, and one pyramidal beam divider.

Figure 18 is a sketch of the final placement of the four integrated beams on the spur gear tooth gap. Also shown is a review of the geometric factors affecting the heat treatment. To overcome the severe heat sink at the root, two beams were placed on top of each other here. (Only one is shown in Figure 18 for illustration purposes.) To cover the whole flank area, each flank of tooth gap was struck by a separate beam at a nominal impingement angle of 52° . Notice that the root and flank beams overlap at the base of the tooth. Optimization of the sequencing of exposure and methods to achieve the relative power balance in each of the beams is discussed later.

7.3.2 Optical Fabrication and Specifications

In pursuing lower cost beam transfer optics as an element in production gear treatment tooling, IITRI investigated the diamond machining process for producing flat copper mirrors.

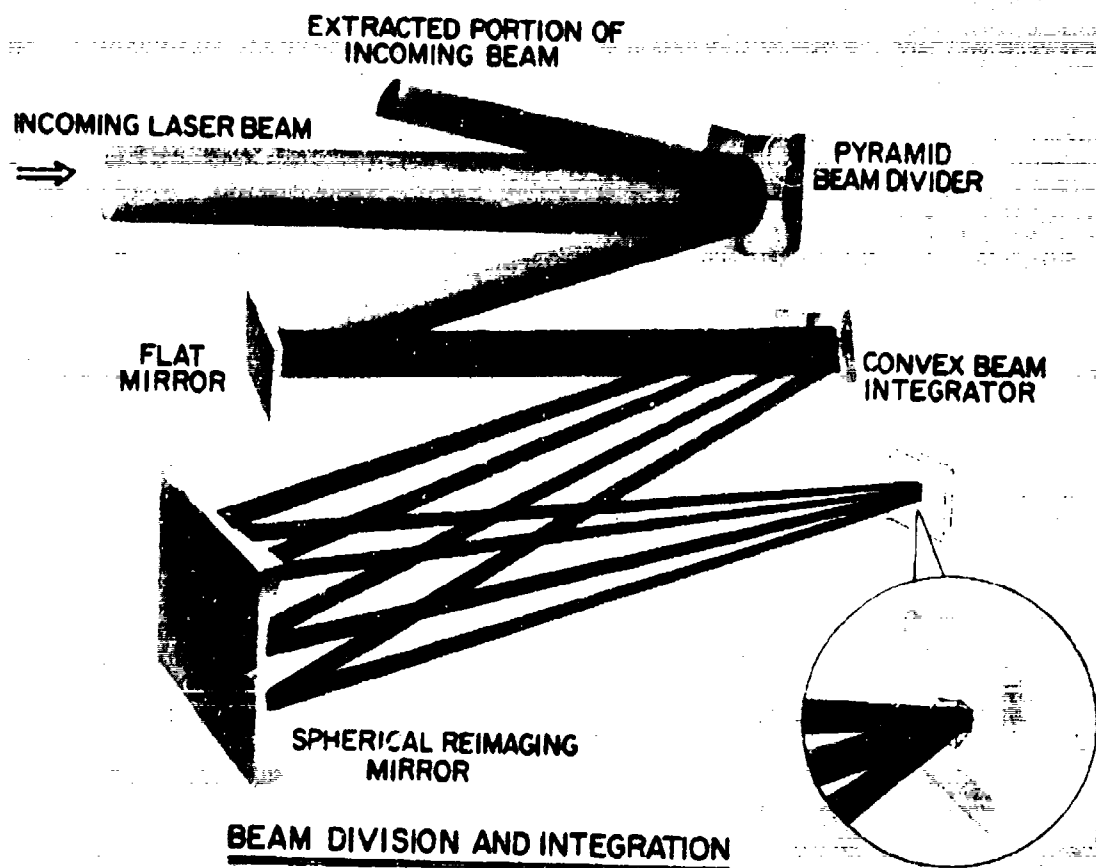
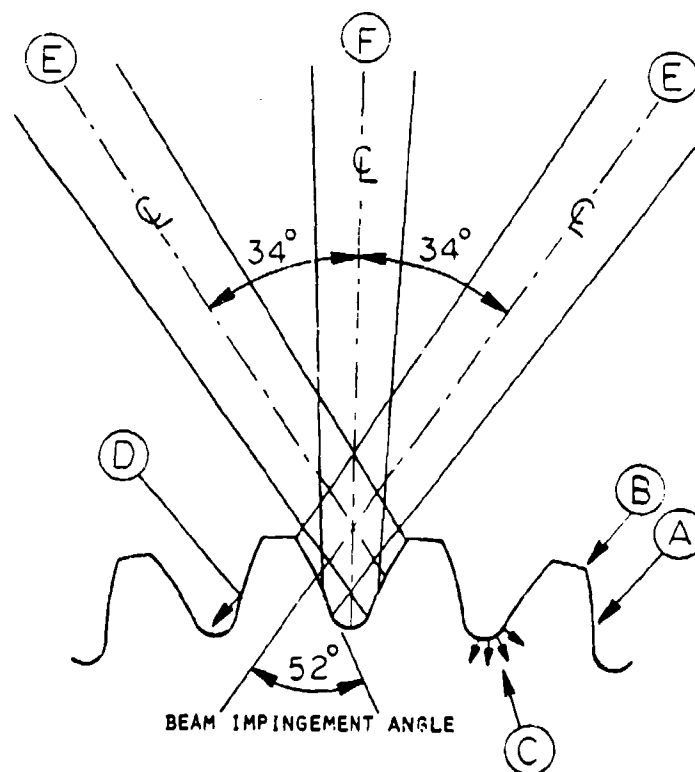


Figure 17. Beam division and integration scheme used in this program.



- A - BEAM IMPINGEMENT ANGLE AFFECTS ABSORPTION
- B - TOOTH TIP IS SENSITIVE TO MELTING
- C - ROOT HAS LARGE HEAT SINK RELATIVE TO SURFACE AREA
- D - REFLECTION FROM FLANKS MAY ADD HEAT TO ROOT
- E - FACE OR FLANK HEATING BEAMS
- F - ROOT HEATING BEAMS (ONE SHOWN)

Figure 18. Laser heating of a tooth gap using the FRF technique employed in this program.

Most of this work was performed by the Micro-Surface Generating Laboratory of Pneumo Precision, Inc., using their MSG-500 flycutter, which routinely produces surface finishes better than 1.0 μ in.(AA) with overall flatness of about 5 μ in. over a 6-inch-long cut. The performance of the flats produced on this equipment proved equal to that of ground and polished flat mirrors. Our success in producing beam transfer flats using diamond machining led to consideration of the possibility of producing a beam integrator mirror by the same method.

Because diamond machining cannot produce the concave faceted surface of such an integrator, a CBI used in combination with a concave spherical reimaging mirror was considered as a cost-effective alternative. With a convex facet pattern, all other facets remain below the plane of the cutter while an individual facet is being machined.

The problem of manipulating the copper blank into the exact positions necessary for machining each facet proved to be a difficult task, requiring that special tooling be designed and fabricated. The resulting hardware resembled a compound sine plate and consisted of a 10- x 10-inch steel plate, supported by three ball screw assemblies located on three corners of a 27-inch square (Figure 19). Elevating and lowering the ball screws gave two-axis tilting of the top plate over a range of

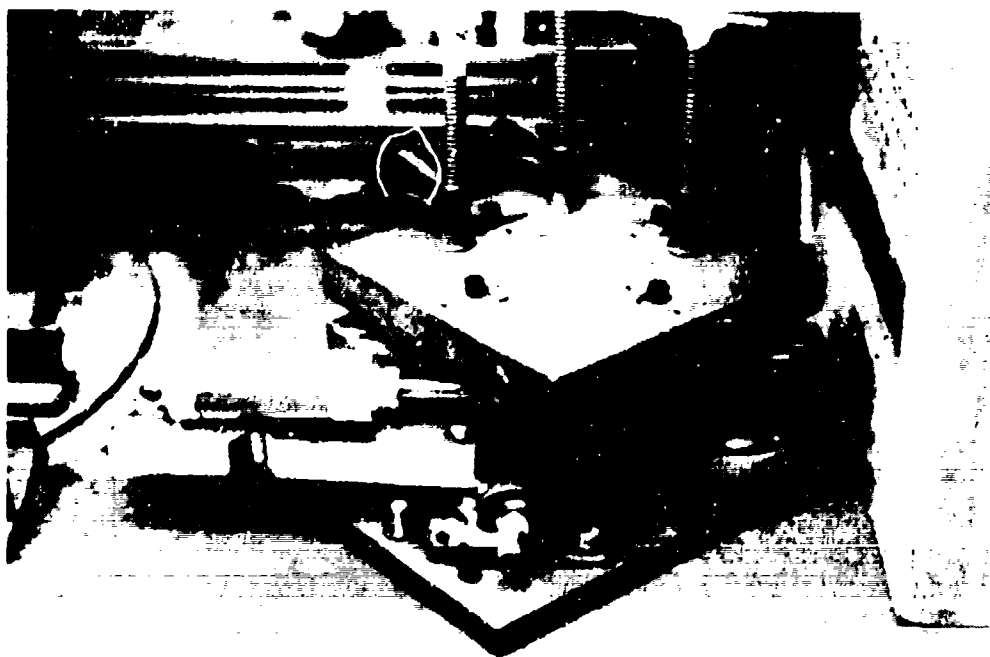


Figure 19. Tooling for locating mirror facets for the convex beam integrator (CBI).

about $\pm 5^\circ$ from horizontal. Fabricating a CBI that would give the desired beam shape required a 0.2- x 0.3-inch rectangular facet size. Since the CBI was to have a 40-inch radius of curvature, this amount of tilting would allow more than 200 individual facets to be machined within the range of the tooling fixture.

In order to prove the feasibility of the CBI concept, a test piece having about 90 facets was initially machined using manual positioning of the ball screws on the tooling fixture. This task required that hundreds of indexing moves be correctly "dialed-in" on the ball screws, and required an even larger number of machining cuts on the diamond flycutter with the depth of cut being carefully monitored and adjusted. After three days of painstaking effort, a 3-inch-diameter CBI was produced that, in conjunction with a 6-inch-diameter reimaging mirror, produced an integrated beam having a rectangular shape slightly larger than 0.2 x 0.3 inch.

Based on successful tests with this first CBI, plans were made to produce four larger CBI's to be incorporated into the gear heat treating work station. An ICON UMC three-axis numerical controller with stepper motors and driver circuitry was purchased and interfaced with the ball screws of the tooling fixture. The combination of 1/8-inch lead ball screws with the 400 steps per revolution of the ICON stepper motors, along with a 14- to 16-gear reduction, resulted in a mechanical resolution of 7.292×10^5 inches of linear displacement per stepper motor pulse, allowing manipulation of the workpiece to within 2 arc seconds of accuracy. The manipulator tooling positions were calculated and programmed into the ICON controller to facilitate more rapid and reliable indexing during fabrication of the larger CBI's.

In machining the first 4-inch-diameter CBI with the upgraded tooling fixture, it became apparent that although the calculations for tilt positions were quite accurate, the calculations for setting the cutter depth were unreliable.

It should be pointed out that the geometry of these mirrors is such that the plane of each facet lies only 0.0002 inch down from the sphere tangent to its corners, and a cut only 0.0003 inch too deep effectively doubles the size of the resulting facet. Consequently, producing an entire CBI with uniform facets required that 164 successive cuts be made, each to an accuracy of ± 0.0001 inch.

Despite the problem with programming the depth of cut on the UMC, it was still possible to complete one 164-facet CBI in less than 8 hours. However, since the depth of cut was determined on a trial-and-error basis, the resulting CBI's all have a few oversize facets scattered about their surfaces, and the

pattern is not always a perfect checkerboard. By analyzing the depth-of-cut data recorded during fabrication of the first few CBI's it became apparent that the deviations from the calculated depths of cut were the result of surface irregularities on the fixture components linking the ball screws with the top plate. By compensating for these irregularities, successive CBI's were machined with greater consistency in their facet patterns. However, this stepwise refinement process consumed several hours of extra machining time, and future CBI fabrication will require remachining the critical components of the tooling fixture.

In order to utilize the beam shaping and integrating capabilities of the CBI's produced by this process, four concave spherical reimaging mirrors with the same 40-inch radius of curvature also had to be fabricated. The constraints of the gear heat treating work station dictated that these reimaging mirrors have a minimum diameter of about 10 inches. Since a 12-inch diameter mirror was about the largest size that could be machined and polished on in-house equipment, this diameter was used for the four reimaging mirrors. They were machined from 1-inch thick, half-hard OFHC copper plate using a 24-inch-diameter flycutter on a vertical milling machine. By mounting the copper blank on a motor-driven rotary table with its axis tilted 16.7° from vertical, and positioning the table so that the arc of the cutter intersected its center of rotation, a concave surface was machined on the blank by slowly rotating the blank through 180 degrees. After repeating this procedure until the concave surface was machined out to the full 12-inch diameter, the blanks were then abrasively polished using conventional optical polishing techniques.

7.4 OPTICAL PACKAGE FOR GEAR HEAT TREATMENT

Previous discussions described how the primary laser beam was split into quadrants, and how each quadrant was then integrated in its own optical array and subsequently positioned on the spur gear tooth gap. Methods for manufacturing the mirrors that constitute the optical tools of the system are also described. This subsection discusses how each of the four optical trains were consolidated into a demonstration gear heat treatment package.

Figure 14 showed the heat treatment optics and tooling. Figure 20 is a schematic of the optics looking down from the top of the work station. A side view of the optical package would be identical. Only two of the four legs are shown. Note that only the incoming beam centerline is shown and that the actual incoming beam diameter was between 3 and 3.5 inches (depending on the atmospheric quality within the beam path).

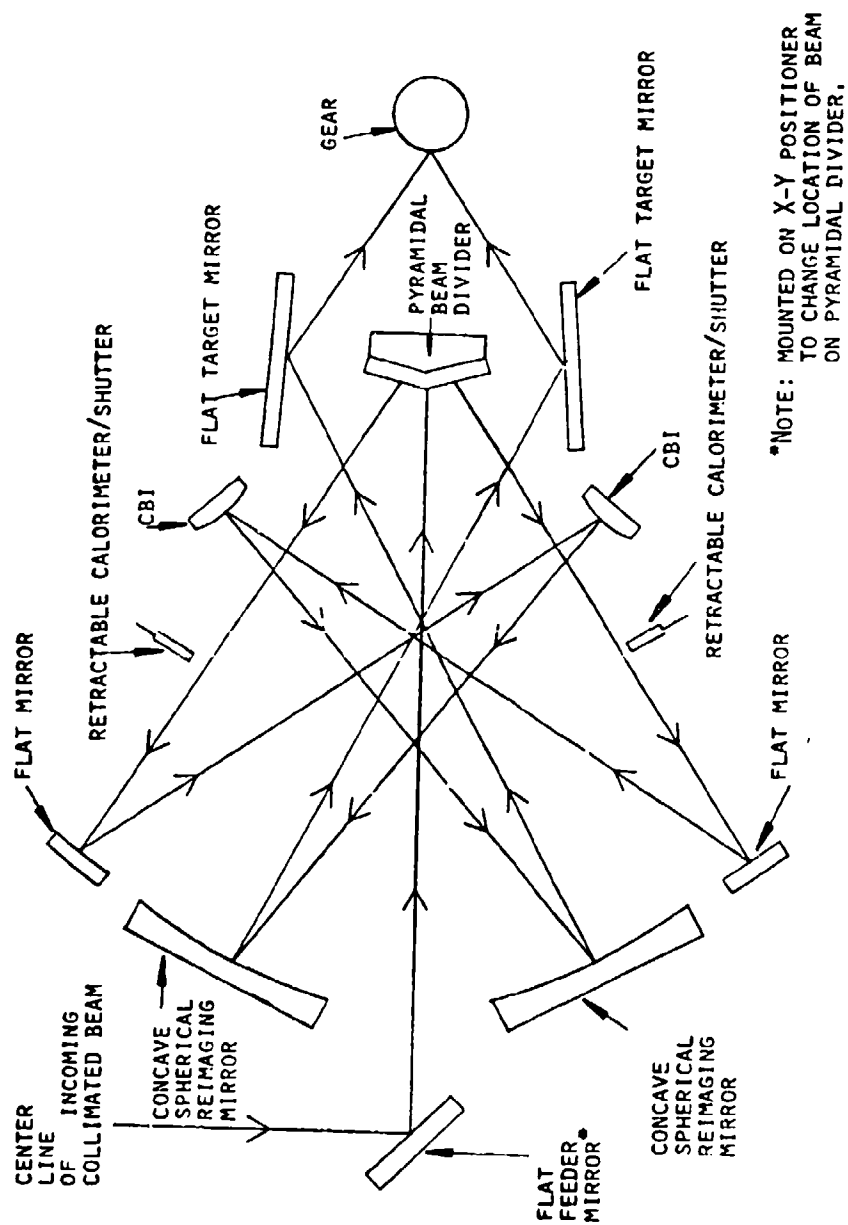


Figure 20. Optics arrangement used in the program. (For clarity only two of the four beams are shown.)

Some of the distances between the optical elements shown in Figure 20 are:

- a) From beam divider to flat mirror: 44 inches
- b) From flat mirror to CBI: 40 inches
- c) From CBI to spherical reimaging mirror: 40 inches
- d) From spherical reimaging mirror to target mirror: 46 inches
- e) From target mirror to work: approximately 13 inches

The folding angle (i.e., the angle between the incident and reflected beam) on the CBI was nominally 12° . It is important to minimize the folding angle on integrators in order to avoid astigmatic distortion of the reimaged spot. Folding angles less than 10° are ideal, while under 15° is considered the upper limit if the image of the facet is to be returned.

The optical frames shown in Figure 15 were constructed from 4-x 4-inch steel channel. The mirror holders were welded to these frames. In order to allow independent alignments between each optical element in the system, a triangular array of holes was drilled and tapped into the backs of each mirror. A mating hole pattern was then built into each mirror holder, and a threaded rod was placed through the holes in the mirror holder into the back of each mirror. Rotation of these threaded rods provided adjustment of the angular position of each optical element. This was necessary not only to obtain initial alignment but also to adjust the target mirror angles to position the integrated beams at different points on the tooth gap. The aforementioned errors in the CBI fabrication left "bad" spots on their surfaces. The collimated beam quadrants had to be positioned on the CBI's by adjusting the flat mirrors (Figure 20) to avoid these areas.

Figure 20 illustrates how the single beam from the laser was directed into the demonstration gear treatment package and how adjustment of the power levels in each of the four split quadrants was obtained. The pyramidal divider is fed from a flat feeder mirror mounted on an X-Y positioner. Thus, any change in attitude of this feeder mirror corresponds to a change in position of the incoming concentric beam on the pyramidal divider. Also shown are the two legs of the system corresponding to the beams striking the flanks of the tooth gap. The other two optical trains would lie above and below the plane of the page in Figure 20. These legs would correspond to the beams striking the root area of the tooth gap. Thus, the feeder mirror was built to permit changes in beam position on the divider in both the plane of the page and perpendicular to the plane of the page in Figure 20. Changing the position of the beam on the pyramidal divider implies changing the relative power balance in each of the beams split off from the divider. This is easier to visualize by studying

Figure 17. Consider the case where the incoming beam moves up toward the upper left corner of the divider. This would mean that less light would go through the depicted optical train, while more light would be available in the adjacent quadrant. This latter point is critical in that it is not possible with this system to independently adjust the power in each of the split beams. A change in position of the incoming beam on the pyramidal divider affects the power level in all the legs by virtue of this beam-splitting method. This constraint imposed certain problems in the maintenance of power balance in each leg during actual gear heat treatment trials. The variable nature of the power distribution in the laser beam plus beam blooming and steering further aggravated this situation.

The need to control beam direction before and during runs could be eliminated in a custom-designed heat treater by using multiple lasers that avoid the detrimentally enhanced power/direction variation caused by a beam splitter. Under such circumstances a dedicated production system could also simplify much of the calorimetry/shutter complexity (described next) because the laser controls could be used.

7.5 CALORIMETER/SHUTTER DETAILS

It became obvious in the program that the beam splitting method used in the demonstration package mandates some method of monitoring the power balance in each of the split beams. In response to this, calorimetric hardware was devised.

Shown in Figure 20 are the locations of the retractable calorimeter/beam shutters used to measure beam power and control exposure time in each of the four beams. Such a shutter was provided for each of the four split-off beams. The rationale for placing these shutters between the divider and the mirrors was that, at this point, the beam is still fairly spread out. Thus, a lower power density strikes the shutter, minimizing ablation and damage of the absorptive coating. In Figure 15 it can be seen that the shutters are held in place on their own frame. This frame lies between the two major optical frames and was also fabricated from the same 4- x 4-inch steel channel.

7.5.1 Calorimetric Aspects

In their fully extended position (closed), these four shutters block off all the radiation reflecting off of the pyramidal divider. In this position, measurement of beam power in each of the four legs is possible. The calorimeter/shutter consisted of a 1-inch-thick block of aluminum drilled out for adequate circulation of cooling water. Each shutter was identically drilled so that the water cooling action would be the same in each one. A flat black Krylor spray paint was

applied to the exposure side of the shutters to act as an absorptive coating. Pressure-regulated Dwyer flowmeters were placed on the input water lines to each shutter. These meters provided uniform controllable flow from 0.1 to 1.0 gpm. A bucking thermistor circuit was placed across the input and output water lines from each shutter. To avoid calcination of the thermistors, they were not placed directly in the water stream. Instead, a short length of .25-inch-diameter copper tube was spliced into the lines. The thermistors were then potted onto these copper tubes with epoxy. A bucking thermistor circuit can provide a direct correlation between the microamperage of the circuit and the change in temperature between the input and output water from the shutters. To do this, a reference voltage of 0.5 was placed across the circuit. Figure 21 shows the four microammeters and reference voltage

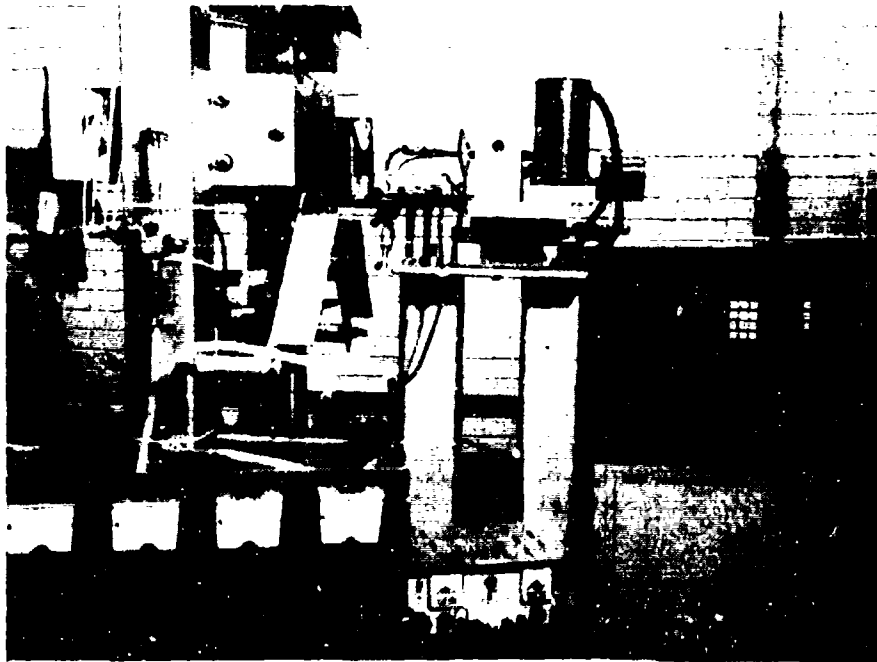


Figure 21. Location of calorimeter meters (left foreground), work positioner (center) and microprocessor (right).

power supply. The ICON microprocessor shown was used for the optics fabrication, exposure time control, and workpiece positioning. The workpiece positioning assembly is also shown.

In order to obtain a correlation between the bucking thermistor output amperage and the beam power striking the surface of the shutters, a calibrated cone power calorimeter had to be used. This calorimeter is provided as part of the AVCO laser and is the only way to measure total beam power at these high power levels. The objective of the calorimetry was to obtain a circuit gain factor relating microamperage to beam power, i.e., watts/microamp.

First, the total beam power reaching the gear work station had to be measured. Atmospheric effects and optical imperfections can cause beam attenuation and absorption. Thus, the power setting on the laser controls did not always relate to the actual beam power 90 feet away from the laser in this test facility. In addition, this power loss was not necessarily consistent from day to day because of open beam paths. The output power of the laser was measured near the output window and was found to be consistent. The problem is that atmospheric changes from day to day occur in the experimental facility, so that far-field effects are variable.

In response to this, the following calibration procedure was used in order to obtain a reliable system gain factor

1. The cone power meter was placed directly in front of the pyramidal beam divider. This position allowed the closest possible estimate of power at the beam divider. The relationship between beam power in front of the divider to the power set on the laser control was obtained. Losses from the mirrors remaining in the beam path between the position of the calorimeters and the work surface were neglected in reporting the treating power at the workpiece. (These losses can be estimated to be about 1 percent per mirror, or less than 60 watts in 1000. They approximate the manufacturer's specified tolerance for this laser.)
2. As quickly as possible, the cone power meter was removed from the work station. Simultaneously, the water flow was started through the calorimeter/shutters. As all four shutters were fed from the same main line, a maximum of 0.7 gpm would be obtained in each of the shutters simultaneously. (Some drift in the flow rates was noticed but is accounted for later.)

3. With all of the shutters in the fully extended position (closed), the laser was again turned on and all four beams from the pyramidal divider were collected on their respective calorimeters/shutters.
4. At each power setting, the microamperages from each of the shutters were recorded along with their respective flow rates. Three minutes of continuous exposure were allowed on the shutters before the readings were taken. (This 3-minute stabilization period was used only during these calibration procedures. A one-minute stabilization time was employed for subsequent experiments and was found to be sufficient.)
5. The microamperage from each calorimeter was multiplied by its respective water flow rate to obtain a flow-normalized microamperage value (to compensate for flow rate drift). All of the flow-normalized microamperages were then added at a given power setting.
6. These totals were then divided to obtain the beam power as measured by the cone power meter. Thus, at each power setting a system gain factor was obtained.

The above procedure was repeated ten times. A consistent gain factor was obtained, but the gain factor decreased as the beam power increased. For example, at a power setting of 10.0 kW, 8.3 kW reached the cone power meter in the work station. At this power the total of the flow normalized microamperages was found to be 112. Thus, 8300 W divided by 112 resulted in a system gain factor of 74.2 W/microamp*. A similar observation of 5.0 kW set power (4.5 kW actual power) indicated a circuit gain factor of 82.8 W/microamp. Fortunately, subsequent optimization studies revealed that the majority of the gear hardening work required between 7.5 and 9.0 kW actual total beam power. Within this range, the circuit gain factor varied only slightly (76 to 74.7). Thus, an average of the system gain factor at these two beam powers was found to be about 75.4 W/microamp. This value was used for the remainder of the work. To obtain the actual power in each of the split beams, the flow normalized microamperage in each calorimeter was multiplied by the system gain factor given above.

7.5.2 Exposure Time Control

The advantage of this calorimeter system is that these devices could also serve to independently control exposure time. Each

*The microamp used in system gain factor is a flow normalized microamperage.

of the calorimeter/shutters was mounted on pneumatically actuated Bimba air cylinders. Care was taken to ensure consistent air pressure in each of the cylinders. A solenoid valve was used to actuate the cylinder. The solenoid was controlled and triggered by the UMC/N-C microprocessor using an external function command.

Exposure time as a function of the microprocessor settings was obtained using a photodiode connected to an oscilloscope. A collimated visible light source was masked down and aimed at the beam splitter. The photodiode was then placed at the work position. The shutters were cycled at various microprocessor settings. The resulting oscilloscope traces were photographed and measured. With the existing system, the shortest exposure time possible was 0.175 second. The exposure times were found to be repeatable to within 3 percent.

7.6 WORKPIECE POSITIONING

Figure 22 is a photograph of a test gear on the workpiece positioner. A time exposure photographic technique using the He-Ne alignment laser allowed the paths of the invisible CO₂ beam to be shown. Two N-C controlled stepping motors were fitted to this fixture to control gear oscillation during laser treatment, indexing of the tooth gaps between treatments, and synchronization of the gear motion with the beam shutters. The stepping motor at the far right in Figure 22 controlled the gear rotational motion via a timing belt and pulley. The stepping motor to the left of this control oscillated the gear in the up and down direction using a cam follower, not visible in Figure 22.

The gear was oscillated in both the rotational and up and down directions. The oscillation amplitude up and down was approximately 0.1 inch. The rotational oscillation was about 5 degrees. Since the gear motion was synchronized with beam shutters, frequency of oscillation was a function of exposure time. The shorter the exposure time, the faster the oscillation. One Hz was a typical value.

Another characteristic of the CBI power profile was nonuniformity. The profile was hyperbolic wherein the center of the beam was hotter than the edges. This, of course, resulted in a hardened zone of nonuniform thickness, where the center of the case was deeper than the edges. Oscillation of the gear would tend to move the hot center portion over more of the surface to promote more hardened zone uniformity. Also, heat buildup at the edge corners of the teeth was anticipated. As will be seen in the next section, perfect uniformity was not obtained across the thickness direction of the tooth gap using the "shot" or timed exposure technique.

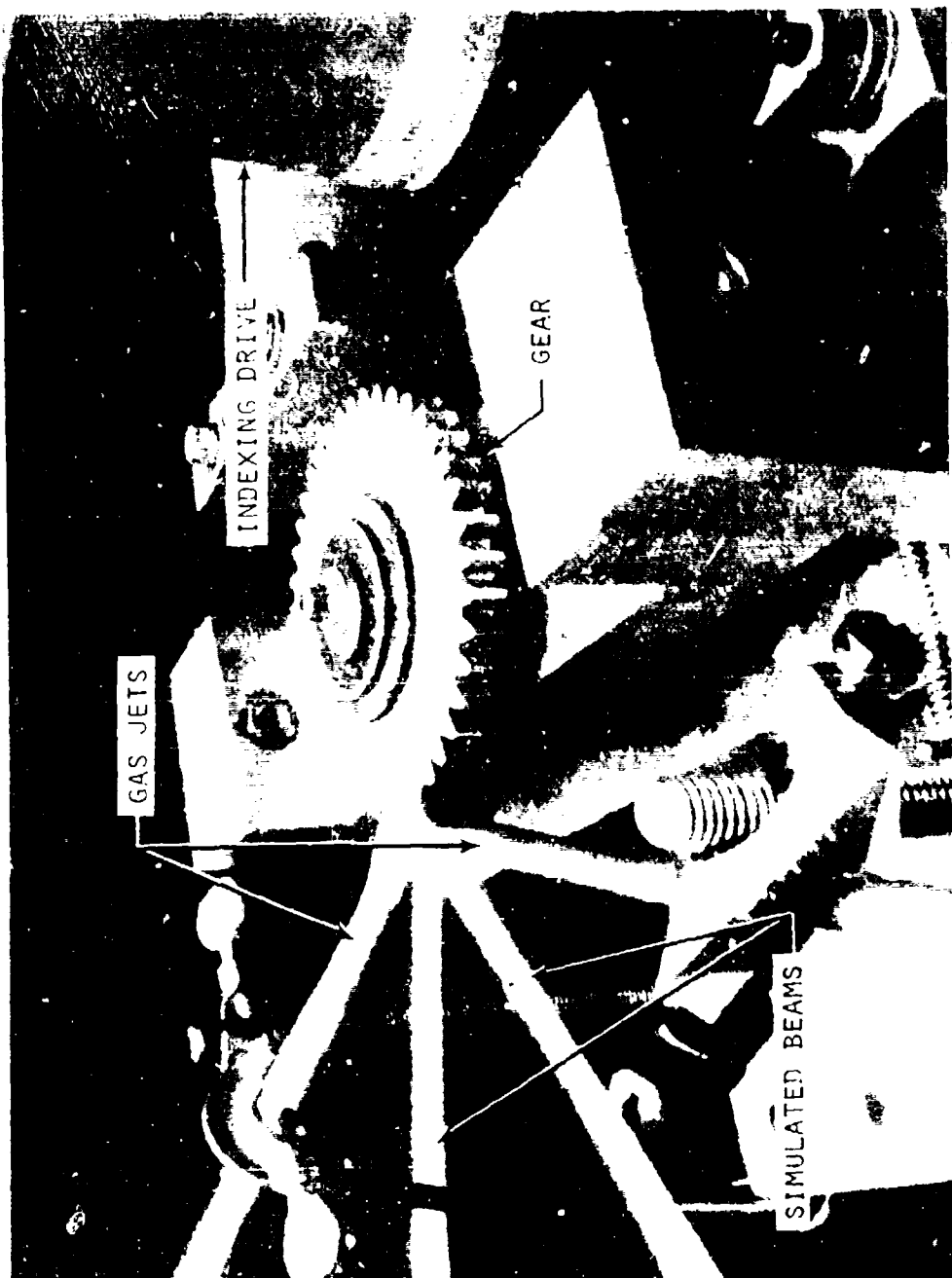


Figure 22. Close-up of gear on the workpiece positioner and simulated beams.

7.7 TREATING SEQUENCE

Before the data are presented, it should first be noted that after the installation of all of the equipment, the system could be operated on a totally automatic basis (after initial manual alignment of the gear). A remote switch to the micro-processor allowed the operator to stand outside of the work station while initiating the heat treat sequence. Typically, a sequence of events to harden a gear was as follows:

1. The gear was painted with flat black Krylon spray paint.
2. The gear was positioned and aligned using a reference He-Ne laser beam. This beam was coaxially aligned with the power beam, and permitted alignment (remember, the CO₂ beam is invisible).
3. With the shutters in the closed position, the water flow rate through each was set as closely as possible to 0.7 gpm.
4. The safety interlock on the work station was engaged, and the laser was turned on.
5. With the split beams striking the calorimeter/shutters, 1 minute was allowed for the calorimeters to reach a dynamic thermal equilibrium.
6. Each microamperage and flow rate was then noted.
7. If the calorimeters indicated a power imbalance, the feeder mirror to the beam divider was then re-positioned from an external control to change the power balance in the beams to the desired settings. This would typically take 2 minutes.
8. After the appropriate power balance was obtained, the N-C program sequence was initiated (note that the desired parameters were preprogrammed into the controller).
9. The program sequence was as follows:
 - a. Gear indexed to next tooth gap. Preset helium gas flow directed into tooth gap.
 - b. Gear oscillation commenced simultaneously with the opening of the two root beam shutters.
 - c. One of the root beams shut off after the programmed time.

- d. With the other root beam still on, the two flank beam shutters opened.
- e. These stayed on for the programmed time.
- f. All shutters closed, and gear oscillation ceased. Simultaneously, a quenching "blast" of helium struck gear.
- g. The program was then ready for another sequence.

7.8 BEAM POWER CONTROL DURING RUNS

Maintaining a stable beam position and power distribution in the beam proved to be very difficult. Several variances tended to occur once the laser was started. IITRI was able to take corrective measures against some variances but not others. Fortunately, the latter uncorrectable shifts (in the power through each leg) did not occur during the test runs. They did cause difficulty in process development.

7.8.1 Spatial Drift Correction

Systematic calorimetric measurement of each of the four quadrants into which the primary beam was split permitted the documentation and correction of a spatial drift with respect to the area of impact on the pyramidal beam splitter. IITRI was able to correct for this displacement by moving the mirror that fed the pyramidal divider while monitoring the calorimeter. Beam displacement was not exactly parallel to the movement of the feeder mirror. The displacement was diagonal down the front of the divider so that only a partial correction could be made.

7.8.2 Correction for Total Power Variation

The calorimeter diagnostics indicated that the total beam power tended to decrease during a run of 5 or 10 minutes. Occasionally, total energy was found to increase slightly after the initiation of a run. When the cone power meter was mounted at the pyramidal divider, it also showed a similar tendency. It should be noted that the laser is equipped with a real-time monitor that corrects the laser power should it drift. However, this is only effective just outside of the output window.

It may be that a certain amount of power drift was unavoidable because of the long, complex, optical path between the laser and the work (90 feet). Mirrors in this path absorb small amounts of beam energy (2-5 percent) and thus heat up. Additionally, absorption increases with this increased heating. Although the beam path was cross-vented every few inches,

pockets of stagnant air could have still existed. Suspected pockets were provided extra ventilation using floor fans. Mirror heating, which undoubtedly caused the previously described beam displacement, could have caused some spillover (and loss) of the beam from the mirrors under certain circumstances, such as stagnant air beam bloom. Mirrors that allowed access of a cooling fan were cooled in this way.

Another problem aggravated the situation of total power drift. If a general decrease in total incoming beam power was detected, a logical solution was to increase the laser power setting. However, the amount of corresponding increase in each of the split beams was not necessarily uniform. This appeared to be caused by the nonuniformity of the spatial power distribution within the incoming concentric beam. The long beam path may have further promoted nonuniformity.

In any event, these total power drift characteristics, like the beam displacement, could be partially controlled by repositioning the feeder mirror using the calorimeters as guides.

7.8.3 Independent Power Drift in Individual Legs

A final condition of imbalance between the power in the four beams proved to be more difficult to correct. Once properly balanced, it appeared possible for two of the beams (assigned to the root) to calorimetrically indicate an independent drift with respect to the remaining beams (the flank beams). No fixed pattern was observed. One root beam increased, while the other decreased for a net change of zero on the root; or both increased (or decreased). In such circumstances a general power correction was not deemed appropriate. Repositioning the feeder mirror would correct the root beams, but would then unbalance the flank beams. These observations suggested a rotation of the power distribution within the perimeter of the annular beam from the laser.

The power distribution is a function of gas and discharge dynamics within the cavity of the laser and is not subject to any control available to the operator. New laser cavity optics were purchased and installed and the anode/cathode assemblies cleaned and replaced in an attempt to correct the condition of root beam independent drift. However, this was found to have little effect on the drift phenomenon.

Root beam independent drift often caused a drop of up to 20 percent in the power going into the root, provided the power and balance of the two face beams was undisturbed.

7.8.4 Summary of Corrective Action and Impact

As a summary of this systematic attempt to characterize the beam energy distribution using the calorimetric hardware, it appeared that the system could be corrected by the operator on a tooth-by-tooth basis for conditions of beam displacement and total power drift.

Independent drift of the individual beams was beyond the operator's control. However, while independent beam drift hindered systematic studies to optimize the process, the prototype production trials were relatively free of independent power drift in individual legs and root uniformity was good. This indicates that the calorimeter sensitivity was sufficient to allow beam power correction to within the required tolerance. To further minimize the complexities of simultaneously correcting for these several conditions, studies were made with only one root beam.

However, one root beam could not supply sufficient hardened depth. First, the beam-splitting technique allowed for only limited power differences between the root beam and the flank beams. To compensate, an extra long initial root beam cycle was attempted. This, however, extensively preheated the flanks prior to their exposure cycle; thus, melting on the flanks was hard to control. This root cycle/face cycle interaction was further studied and is discussed later in this report.

The problems associated with beam power control during the operation of the laser appear to be specific to the concept of splitting the beam of a large single laser. In designing a system specifically for multibeam operation, two solutions were suggested during the effort to control the demonstration system:

1. Employ individual lasers to provide each leg of the system.
2. Integrate (and magnify) the beam ahead of the splitter so that power shifts are evened out if not entirely eliminated.

8. RESULTS AND DISCUSSION

8.1 LASER-GEAR STEEL INTERACTION

At the start of this program, basic laser exposure curves for both 300M and D6AC were established using 1/2-inch-thick flat specimens. The specimens were prepared by cutting transverse slices from the starting bar stock, heat treating as described in Section 6, and grinding to produce parallel surfaces. Each slice was spot hardened at several places using different laser hardening parameters. 300M specimens were hardened using the laser beam in a concentric mode while D6AC specimens were hardened using the beam in a crescent mode. Figure 23 shows the visual case depth of 300M as a function of laser exposure for two power levels. Figure 24 shows the visual case depth of D6AC as a function of laser exposure for two core hardness levels. It is apparent from comparison of these two figures that D6AC develops a deeper case than 300M at a given laser exposure. This is primarily due to higher carbon content of D6AC. During this phase of the program, certain specimens were double-exposed to the laser beam. Double exposure appeared to have no noticeable effect on the surface hardness and case depth.

Residual stress analysis of a laser hardened spot was performed using the two-exposure X-ray diffraction technique. The results of this analysis are presented in Table 7. The presence of tensile residual stresses on the laser hardened surface was contrary to general expectations and may be due to the fact that only a small spot, approximately 1/2 x 1/2 inch, was laser hardened.

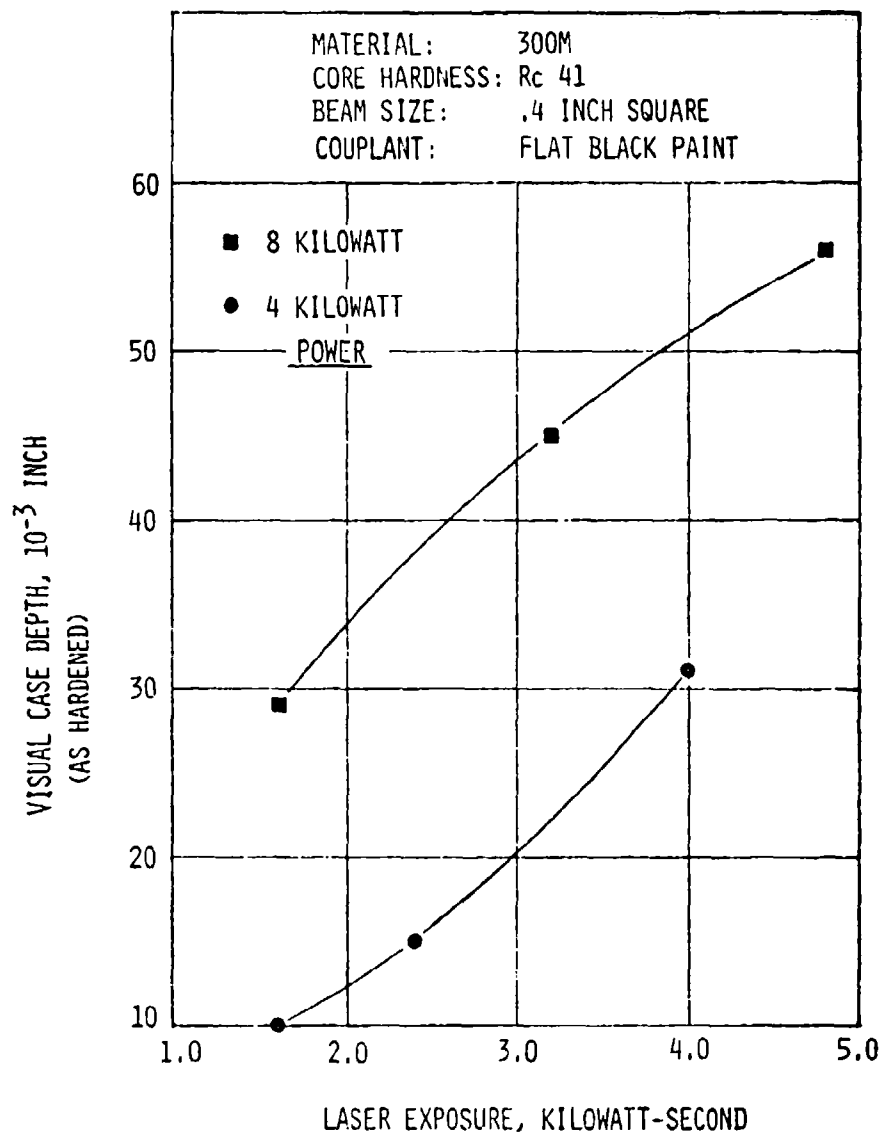


Figure 23. Lazer exposure vs visual case depth for 300M at two different power levels using flat disc specimens.

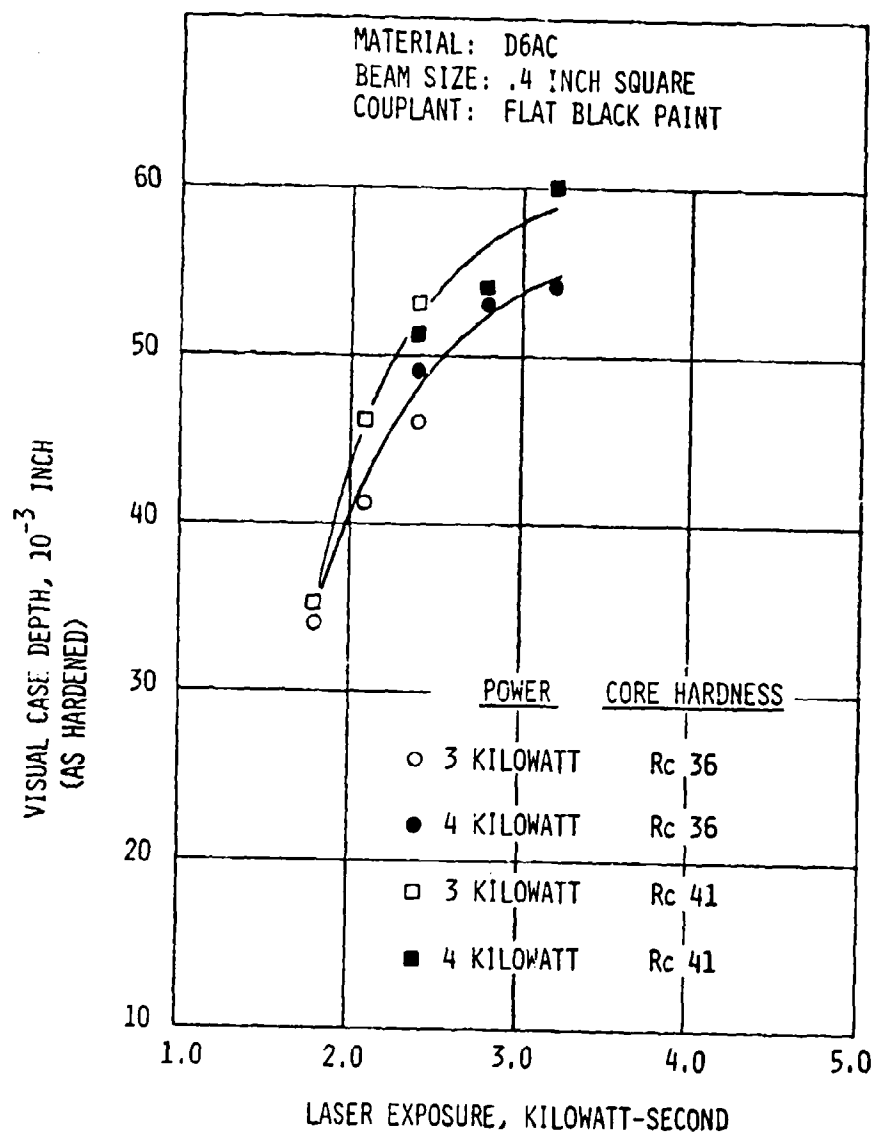


Figure 24. Laser exposure vs visual case depth for D6AC at two different core hardness levels using flat disc specimens.

The presence of a hard spot such as this in a relatively "soft" matrix could create unpredictable residual stress distribution. Later on in the project, a more rigorous residual stress analysis of laser hardened gear teeth was planned but not carried out due to termination of the program.

The laser-gear steel interaction tests also established the laser exposures at which surface melting first occurs. As expected, the point at which melting occurred was a function of both the power setting and laser exposure time, and is described in Table 8.

TABLE 7. RESIDUAL STRESS ANALYSIS OF LASER HARDENED D6AC SPECIMEN (.032-INCH CASE DEPTH)

Depth Below Surface (inch)	Residual Stress (KSI)
Surface	+20.2
.001	+24.7
.005	+19.9
.010	+32.5

TABLE 8. LASER EXPOSURE AT WHICH SURFACE MELTING WAS FIRST OBSERVED IN 300M SPECIMENS

Power Setting (Kilowatt)	Laser Exposure at which Melting Occurred (Kilowatt - Second)
4.0	4.0
6.0	4.8
8.0	3.2
10.0	2.0

One set of experiments was conducted to compare the laser hardened case hardness with that obtained by conventional hardening followed by oil and water quench. The results are shown in Figure 25 and they demonstrate clearly, that the laser hardened case is harder than that obtained by conventional heat treatment.

Figure 26 is a photomicrograph showing a typical laser hardened case in D6AC.

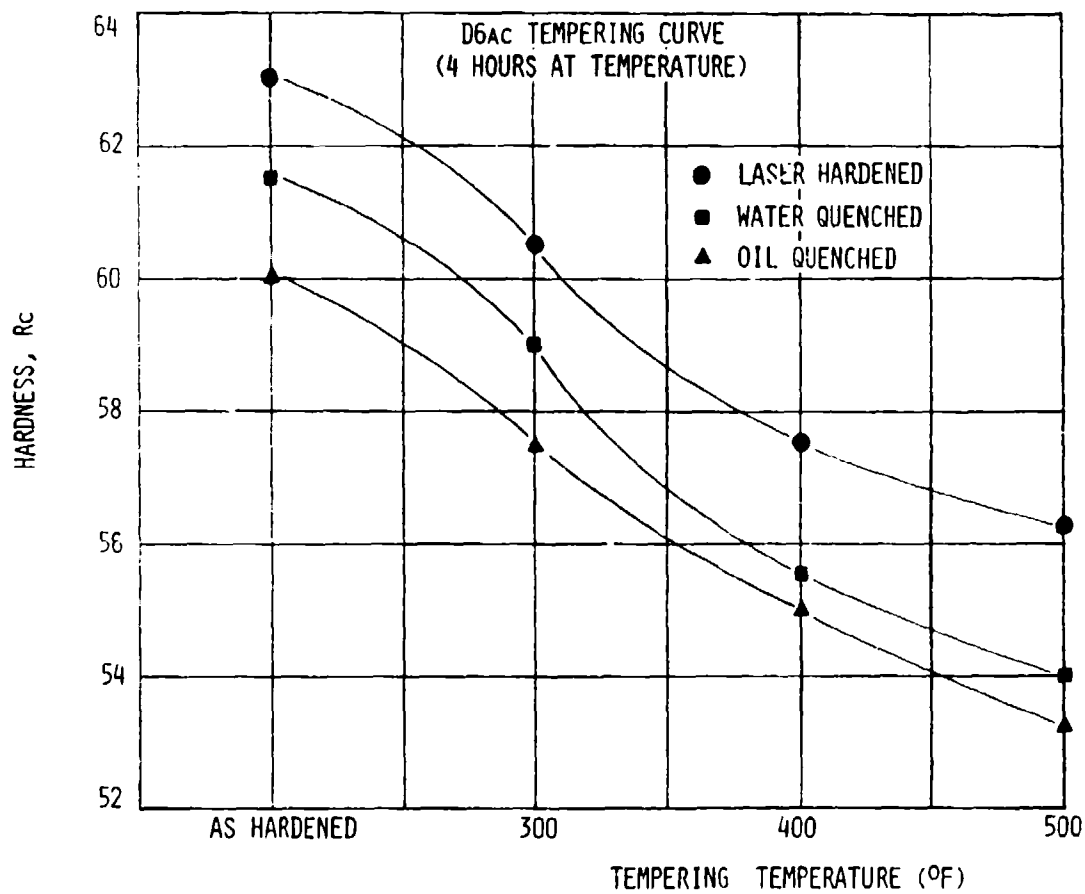


Figure 25. Surface hardness of D6AC - comparison of laser hardening, water quench and oil quench.

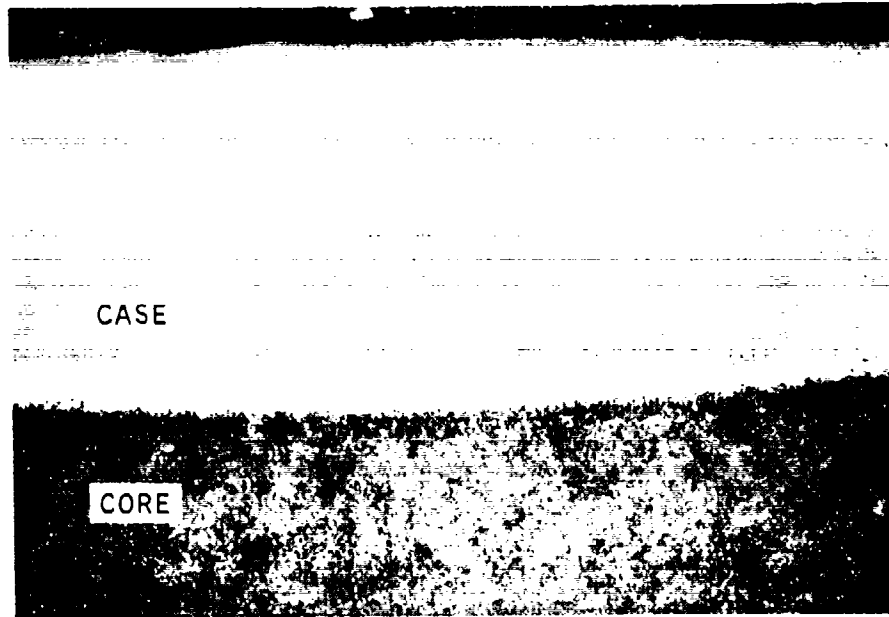


Figure 26. Photomicrograph showing laser hardened case in D6AC and the case/core transition (2% nital, 66X).

8.2 EFFECTS OF ABSORPTIVE COATINGS

The effect of absorptive coating was evaluated early in the program by using graphite and flat black Krylon paint during the laser-gear steel interaction study. In general, Krylon was found to be a better absorber. It is felt that the silicate binders are primarily responsible for this behavior. This fact in conjunction with the ease of applying the spray paint, defined the spray paint as the logical absorptive coating choice for subsequent work.

The flat black paint used was the Krylon brand which is readily available in spray cans for ease of application. A more detailed evaluation of absorptive coatings was conducted a little later in the program using D6AC gear steel. The following four couplant conditions were evaluated:

1. Specimens coated using a new spray can of Krylon.
2. Specimens coated using a half-full spray can of Krylon.
3. Specimens coated by dipping into a Krylon/propanol mixture.

4. Specimens coated by dipping in a colloidal graphite/propanol mixture.

The coating thicknesses on all specimens were measured using a precision dial micrometer. The purpose for using a half-full can of Krylon was to evaluate the effect of possible paint composition variation. Coated samples were then exposed to a single integrated beam, approximately 3/8 inch x 1/4 inch, at about 2.2 kilowatt for 0.2 second. The results are summarized in Table 9 and shown graphically in Figure 27.

From these results it was concluded that within the coating thickness and composition range studies, variations as high as 25:1 in coating thickness have no effect on the hardened zone profile. It was noted, however, that the tendency toward surface fusions was increased with the heavier paint coats. Based on these findings, all subsequent work incorporated a three-coat paint thickness in the range of .001 to .002 inch. Gear specimens were coated by spinning the gear on an electric drill through the fixed paint spray.

TABLE 9. RESULTS OF ABSORPTIVE COATING ASSESSMENT

1. Fresh spray can samples (3 samples)--

Coating thickness range: .0006-.0039 inch
Visual case depth range: .030-.031 inch
Visual case width range: .185-.189 inch

2. Half-full spray can samples (5 samples)--

Coating thickness range: .00015-.0024 inch
Visual case depth range: .030-.031 inch
Visual case width range: .173-.189 inch

3. Paint dip samples (4 samples)--

Coating thickness range: .0003-.0070 inch
Visual case depth range: .030-.031 inch
Visual case width range: .181-.189 inch

4. Graphite dip samples (4 samples)--

Coating thickness range:* .0003-.0045 inch
Visual case depth range: .022-.024 inch
Visual case width range: .138-.150 inch

*Gravity segregation caused widely varying thickness.

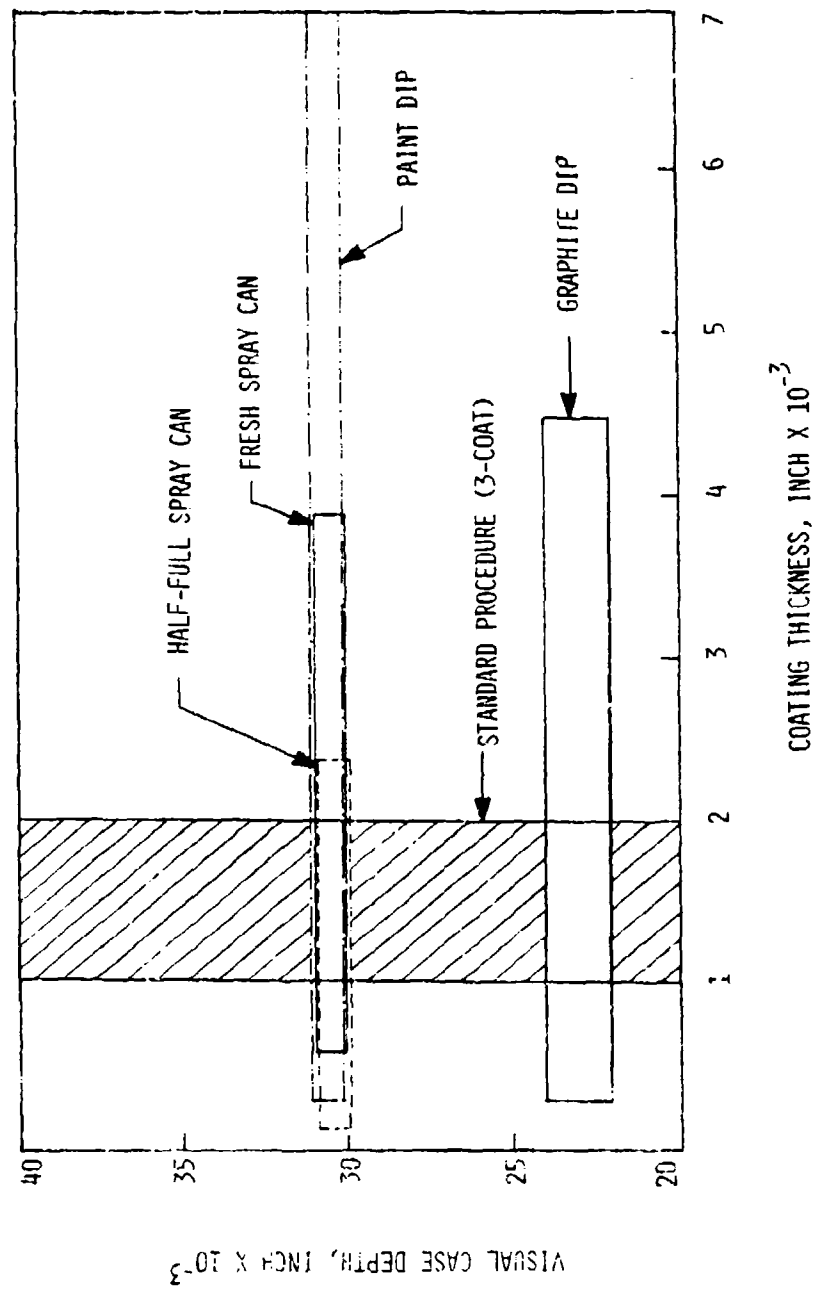


Figure 27. Effect of coating type and thickness on laser hardened case depth of D6AC.

The results in Figure 27 show excellent uniformity of depth and were reproducible enough to permit differentiation between paint and graphite. These tests were run on the station in the same manner as gears that show much less uniformity. This suggested the role of geometry rather than total power as a major factor in uniformity.

8.3 EVALUATION OF QUENCHING MODES

Earlier in this report, the problem of heat flow through a gear tooth to temper back the hardened zone on its opposite side was discussed. In this portion of the report, auxiliary quench systems evaluated are documented. In order to obtain quantitative insight into this phenomenon, temperature measurements were taken on the opposite flank of gear teeth that were undergoing laser heat-treat cycling. In addition, identical measurements were taken on heat-treated teeth while employing various auxiliary quench methods, such as directional helium blasts and copper chills. In this way, the most effective quench method, that provided the lowest opposite flank temperature, could be chosen. The static ("shot") heat treatment used in this program (as opposed to beam scanning over the workpiece) does not allow the use of a water spray quench. Undoubtedly, spraying water onto a heated surface just behind a scanning beam is the best method to hinder extensive heat transfer into the workpiece. However, steam would form and, if the beam and workpiece were stationary, would cause beam attenuation above the work. Thus, water quenching was not considered here.

In these tests a 0.003-inch-diameter type K thermocouple was percussion-welded on a tooth face as close to the pitchline as possible. The thermocouple was then connected to a strip chart recorder and calibrated with known temperature sources. Since the type K thermocouple exhibits linear voltage-temperature behavior in the temperature range of interest, a linear equation could be obtained that described temperature as a function of pen deflection. This temperature measurement system was then subjected to typical laser cycles. The results are given in Table 10. The peak temperatures that were measured during these tests would be sufficient to explain the temper softening effects cited earlier. Instrumentation sensitivity limits suggest that higher peaks may have been present but not detected.

As shown in Table 10, helium blasts impinging directly on all heated areas and the opposite flank provided the lowest recorded peak temperature. Copper chills were found to provide little suppression of the temperature rise on the opposite face. Thus, the gas jet configuration employed for the limited production trials is shown in Figure 28. The three flat nozzles are directed at the root center and the flanks being

heat treated. The thin syringe nozzle is directed at the "left" flank of the adjoining tooth gap that has already been hardened.

During these tests, it was noted that the temperature measurements given in Table 10 do not relate to their corresponding beam parameters. Earlier calibration tests of the calorimeters with the cone power demonstrated the reliability of these devices as a relative measurement tool. The possible source of error was the beams not striking the same exact area on the gears from run to run. As will be seen later, this variation in beam position was attributed to a positioning error in the gear-locating spindle and was corrected for the subsequent production trials.

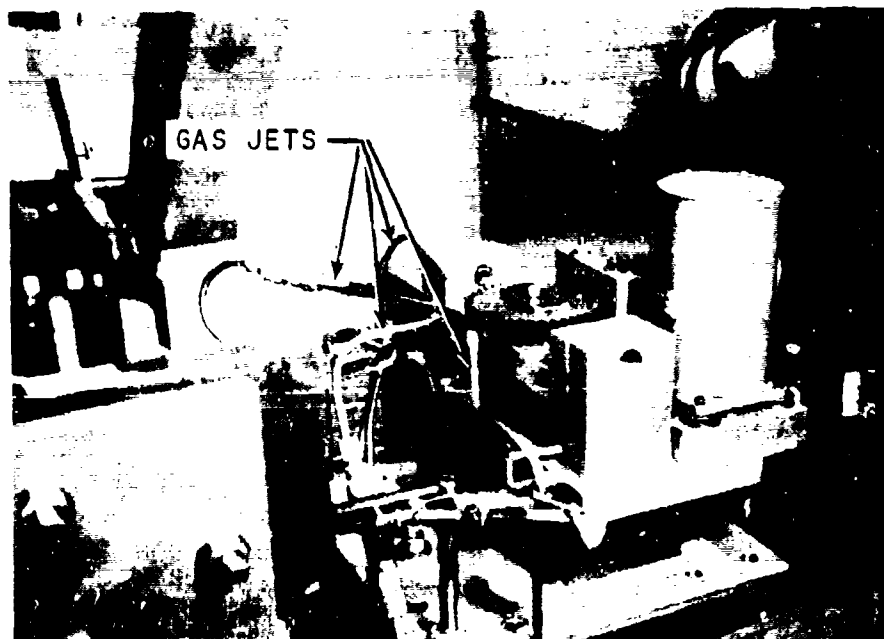


Figure 28. Final gas jet configuration.

8.4 EFFECTS OF BEAM PARAMETERS ON HARDENING OF GEAR TEETH

The very uniform response of the simple paint specimens compared to gears also suggested that heat from the initial exposure of the root might have found its way up to the flank region before the flank beams were turned up. This would have caused a preheating of the flank that would have resulted in increased flank beam absorption and deeper than expected case

TABLE 10. TEMPERATURE MEASUREMENT TESTS

Test No.	Auxiliary Quench Methods	Thermocouple Position ^a	Power in Each Leg, W				Highest Recorded Temp. ^b of
			Flanks		Roots		
			Right	Left	Right	Left	
Series 1							
1.1	None	Behind left flank at pitchline	1743	1743	1461	1640	780
1.2	None	Behind left flank at pitchline	1794	2005	1689	1425	917
1.3	Helium gas blowing on root and heated face; 100 cfm preflow; 80 psi tank pressure. Gas blast came on simultaneously with face beams.	Behind left flank at pitchline	1900	1847	1530	1794	514
Series 2 ^c							
2.1	Copper chills clamped on either edge. Chills were ground to same contour as gear profile.	Behind right flank at pitchline	1794	1768	1794	1372	958
2.2	None	Behind right flank at pitchline	1689	1741	1691	1372	1000
2.3	Same as 1.3, only a gas jet blew behind right flank as well.	Behind right flank at pitchline	1820	1741	1667	1266	622
2.4	Same as 1.3	Behind right flank at pitchline	1793	1742	1667	1398	776

Exposure times: flanks 0.175 sec; root 0.815 sec.

^aThe flank orientation corresponds to Figure 31.

^bCalibration tests had some lag in response so that these values may not represent true peak temperatures.

^cDesigned separate series because a different couple was used. Also couple in Series 1 was nearer root than Series 2.

depths. Thus, case depths on the flanks were expected to be a subfunction of the root cycle parameters. In an attempt to quantify this interactive behavior, 36 separate runs were performed using a single test gear. Root cycle parameters were held constant and face cycle parameters were varied, and vice versa. Beam power drift obscured most evidence of cycle interdependence. However, some useful data were obtained and are presented in Tables 11 and 12. Many of the runs could not be analyzed due to nonuniformity of the hardened zones on the teeth (see Figures 30, 32, 33 and 34). The aforementioned inaccuracy in the gear positioning was suspected as the source of error resulting in the shift of the hardened zone up or down the tooth flank (see Figure 30). The nonuniformity of hardened zones shown in Figures 32, 33, and 34 is due to inadequate size of the focused laser beams and is discussed later in Section 8.5. While latent heat remaining in a tooth after laser cycling could also cause nonuniformity in hardened zones, the time between cycles was so great that this source of error was not operative in these trials.

TABLE 11. PARAMETER SERIES RESULTS

Tooth Gap No.	Power in Each Leg, W		(b) Roots	Exposure Times, sec		Visual Case Depth, inch		Pitchline Root(c)	Comments
	Right	Left		Flanks	Root	Right Flank	Left Flank		
10 ^a	1794	1794	2900	0.195	0.835	.033	.035	.026	Power set at 8.5 kW
11 ^a	1688	1636	2507	0.210	0.850	.031	.037	.024	Power set at 8.5 kW
12 ^a	1674	1674	2550	0.330	0.970	.059	.055	.029	Power set at 8.5 kW
12 ^a	1688	1768	2586	0.250	0.890	.040	.047	.027	Power set at 8.5 kW
14	1900	2005	3193	0.175	0.605	.026	.031	.022	Power set at 8.5 kW
15	1847	1900	3167	0.210	0.640	.031	.039	.025	Power set at 8.5 kW
16	1647	1752	2744	0.250	0.670	.030	.031	.021	Power set at 8.5 kW
17 ^a	1794	1820	3008	0.330	0.760	.055	.060	.031	Power set at 8.5 kW
18 ^a	1688	1820	2876	0.330	0.660	.047	.055	.026	Power set at 8.5 kW
19	1900	2034	3114	0.175	0.815	.036	.041	.029	Power set at 9.0 kW
20 ^a	1847	1874	2850	0.210	0.850	.049	.049	.028	Power set at 9.0 kW
21	1900	1874	2823	0.175	0.605	.028	.031	.020	Power set at 9.0 kW
22 ^a	1900	1979	2956	0.210	0.640	.031	.039	.022	Power set at 9.0 kW
25 ^a	2085	2137	3144	0.175	0.815	.037	.039	.027	Power set at 9.5 kW
26 ^a	2032	2085	2987	0.210	0.850	.051	.051	.028	Power set at 9.5 kW
27 ^a	2058	2111	3238	0.175	0.605	.028	.031	.022	Power set at 9.5 kW
28 ^a	2005	2034	3066	0.210	0.640	.033	.036	.021	Power set at 9.5 kW
31 ^a	2216	2190	3824	0.175	0.815	.038	.043	.031	Power set at 10.5 kW

Note: Quench on front faces only; the blasts were energized simultaneously with face beams;
100 cfh preflow, 80 psi tank pressure.

^aMelt noted.

^bTotal of two root beams is presented.

^cTaken at root centerline.

TABLE 12. PARAMETER SERIES ANALYSIS

Run No.	Avg. Flank Power, W	Root Power, W	Exposure, sec		Avg. Flank Case, inch	Root Case, inch
			Flank	Root		
<u>Set No. 1: Constant High Power/Varied Exposure</u>						
14	1953	3193	0.175	0.605	.0285	.022
15	1875	3167	0.21	0.64	.035	.025
	(-4) ^a	(-1) ^a	(+20) ^a	(+6) ^a	(+23) ^a	(+14) ^a
19	1967	3114	0.175	0.815	.0385	.029
	(+1) ^a	(-2.5) ^a	(0) ^a	(+35) ^a	(+35) ^a	(+32) ^a
<u>Set No. 2: Constant Low Power/Varied Exposure</u>						
11	1674	2507	0.21	0.85	.034	.024
12	1674	2550	0.33	0.97	.057	.029
	(+1) ^b	(+2) ^b	(+57) ^b	(+14) ^b	(+68) ^b	(+21) ^b
13	1728	2586	0.25	0.89	.0435	.027
	(+4) ^b	(+3) ^b	(+19) ^b	(+5) ^b	(+28) ^b	(+13) ^b
<u>Set No. 3: Constant Exposure/Varied Power</u>						
11	1662	2507	0.21	0.85	.034	.024
20	1860	2850	0.21	0.85	.049	.028
	(+12) ^b	(+14) ^b	(--)	(--)	(+44) ^b	(+17) ^b
26	2058	2987	0.21	0.85	.051	.028
	(+24) ^b	(+19) ^b	(--)	(--)	(+50) ^b	(+18) ^b

^aAverage variance, in percent, based on Run No. 14 values.

^bAverage variance, in percent, based on Run No. 11 values.

8.5 PROTOTYPE PRODUCTION TRIALS

Prior to hardening the prototype gears, an analysis of the workpiece positioner indicated a slight inaccuracy in the maintenance of initial gear alignment. Once these positional inaccuracies were observed and before an entire gear was laser hardened, a means for establishing an accurate position had to be devised. A dial indicator was placed to track the position of tooth tips 90 degrees away from the point of beam impingement. Once the gear was placed in such a way as to obtain good hardened case balance, the indicator was set at zero. During the prototype trial runs, an indicator reading was always checked after heat treating two tooth gaps. When required, the gear position was readjusted to again obtain a zero reading on the indicator by pulsing the stepping motor controlling gear rotational position.

Independent adjustment of the root and flank beam power levels was necessary during the prototype trial hardening operations. The goal was to expose each tooth flank for .175 second at 2000 watts, and each root .65 second at 1800 watts and .825 second at 1800 watts, while keeping the flank beam power (beams directed at the tooth faces) relatively consistent. At constant flank power the total root beam power varied up to 20 percent. The pressure of helium blasts during the prototype trials was increased to minimize the chances of surface melting. It is possible that increasing the blast pressure resulted in the increased surface burning that was noted because of air entrapment.

Two gears, manufactured in accordance with Appendix A, were laser hardened during the prototype production trial runs. For the most part, two adjoining tooth gaps were hardened in succession and then the gear position was checked with dial indicator. The power setting was adjusted up or down based on the calorimeter readings in each of the four legs of the system. The two gears hardened are referred to as test gear 1 and test gear 2 respectively in their order of hardening. Each tooth gap or root on the two gears was numbered 1 through 40. The laser hardening parameters for the two gears are summarized in Table 13. The power setting used is shown as a range because it was not the same for each tooth gap; changes were made during the hardening operation based on calorimeter readings. The sequence of steps used in the hardening process was the same as described in Section 7.

Table 13. LASER HARDENING PARAMETERS USED
IN PROTOTYPE PRODUCTION TRIALS

Laser Hardening Parameter	Test Gear 1	Test Gear 2
Power setting (undivided beam), kilowatt	7.8 - 8.2	7.3 - 8.3
Root Beam No. 1 - F-setting	0.1	0.1
Time, seconds	0.65	0.65
Root Beam No. 2 - F-setting	0.1	0.1
Time, seconds	0.825	0.825
Face Beams (2) - F-setting	4.0	4.0
Time, seconds	0.175	0.175
Helium Gas - Prewflow, CFH	120	120
Blast, PSI	100	100

The test gears were tempered at 300°F for 4 hours after laser hardening. The gears were then abrasively cleaned with a fine mesh garnet blast and nital etch inspected. Nital etch inspection was found to be an effective product assurance tool in determining that each gear tooth had been laser hardened. The gears were next subjected to magnetic particle inspection. Both test gears were found to be acceptable in the nital etch and magnetic particle inspections.

8.5.1 Test Gear No. 1

Test gear 1 was surface ground to remove .113 inch of thickness (approximately one third of the gear thickness) from one end face. Surface grinding was accomplished at a slow down-feed rate under flooded coolant conditions to assure that no burning or overheating of the gear would occur. The ground end face was metallographically etched with 2 percent nital solution to reveal the laser hardened case depths on the profile of all the gear teeth. Figure 29 shows the etched case depth profiles for test gear 1. A close-up of the gear is shown in Figure 30. The gear tooth roots are numbered sequentially in the order they were hardened.

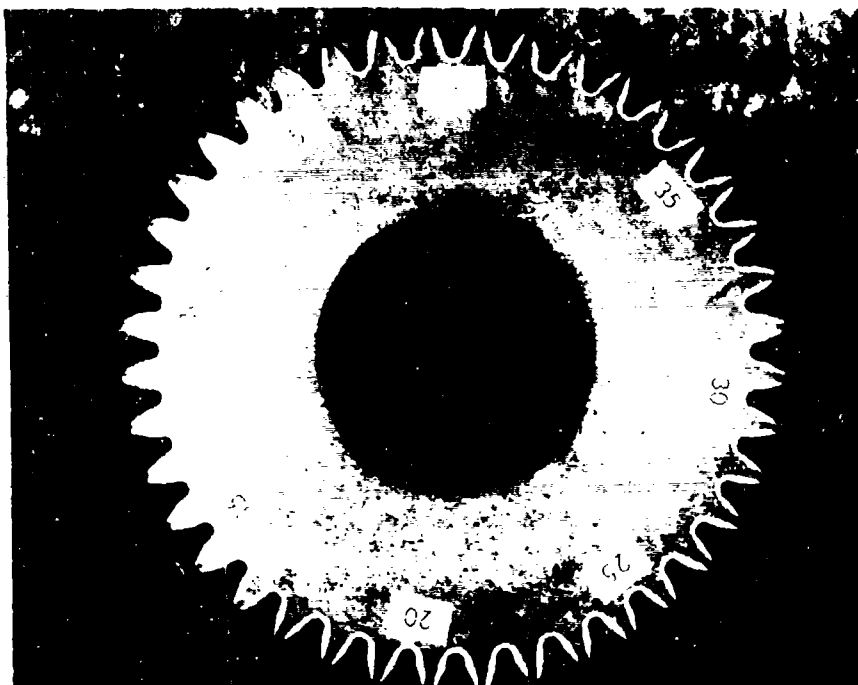


Figure 29. Test Gear 1 laser hardened case profile. .113 inch of material ground from one end face and etched in 2% nital to reveal the case.

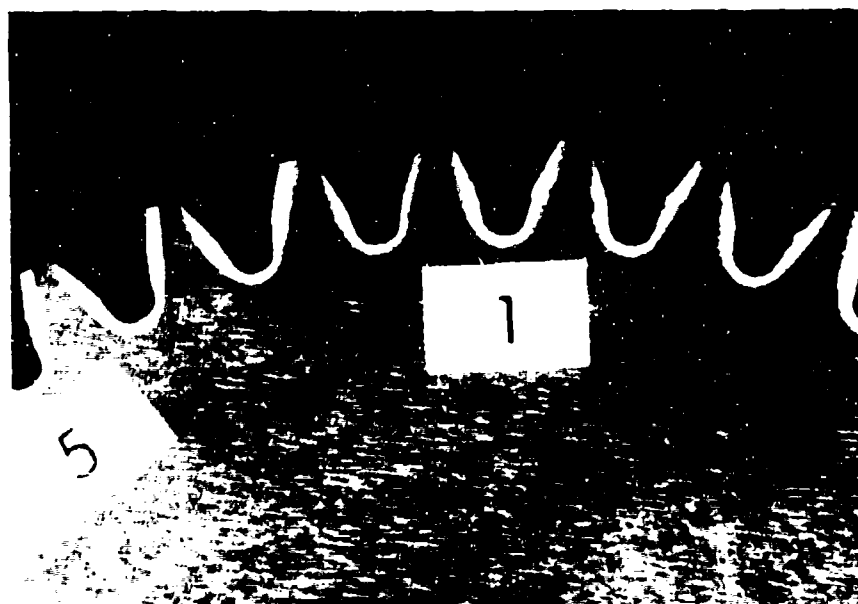


Figure 30. Close-up of Test Gear 1.

The visual case depths on each tooth and root were measured and are reported in Table 14. The case depths were measured at the approximate pitch diameter on the flanks and root center. Figure 31 shows the root/flank location terminology used in the evaluation of the two test gears.

Three segments, approximately equally spaced, from the gear were removed for metallurgical and microhardness evaluation. The effective case depths at approximate pitch diameters and root centers were measured at nine locations and the results are presented in Table 15. The gear teeth selected for microhardness testing also represented shallow, intermediate and deep east flank visual case depths (see Table 14). The case depth at east flank is significant because in the laser hardening cycle it is the laser exposure of the east flank that tends to temper the west flank of the previously hardened tooth gap. Some incidence of melting was noted on test gear 1. The depth of melting noted is shown in Table 15. In general, the flanks of the gear teeth were overcased while the case depths at the root were within the desired tolerance of .026 - .034 inch. While the flank case depths show significant variation, the root center case depths are quite consistent.

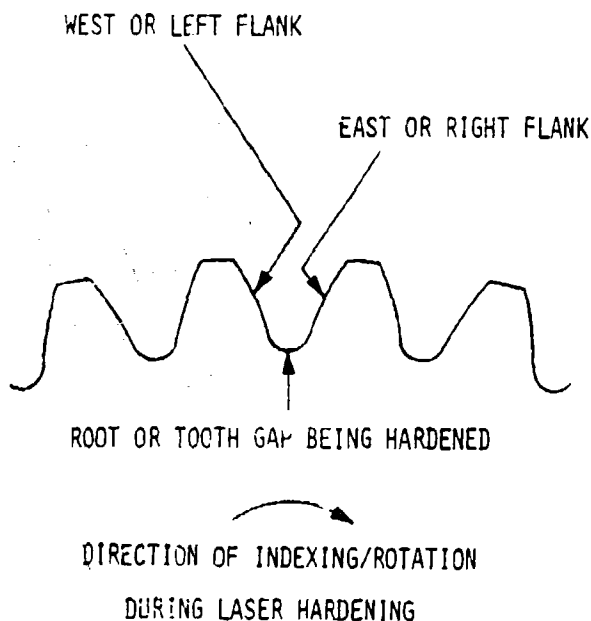


Figure 31. Root and flank location and terminology used during evaluation of Test Gears 1 and 2.

Table 15 quite vividly shows the problem of tempering of the west flank during hardening of the east flank of the next tooth gap. (See Figure 30.) Also, it is clear from Table 15 that the tooth gap identified as 1 had both its flanks tempered while both flanks of tooth gap 40 had surface hardness of Rc 60. This is because tooth gap 1 is the only location on gear where both adjacent involutes are subsequently laser hardened and because tooth gap 40 is the last tooth gap to be hardened and thereby has good surface hardness on both its flanks.

A comparison of visual case depth with the effective case depth (from microhardness testing) is shown in Table 16. The discrepancies in case depth measurements made by both methods on the tooth flanks are due to some variability in case depth and to the "eyeball" selection of the pitch diameter on the tooth involute profile (see Figure 30). The root case depths correlate very well.

8.5.2 Test Gear No. 2

Test gear 2 was subjected to a slightly different evaluation than test gear 1. Three teeth, equally spaced at 120 degrees were sectioned and removed from the gear first. These teeth were sectioned at approximately the pitch diameter to determine the uniformity of the laser hardened case from end face to end face. Figures 32, 33, and 34 show these gear teeth after metallographic polish and etch. These photographs show a great difference in case depth from end face to end face. The case depth varies from practically nothing at the end face edgebreak to .057 inch maximum at the center of one of the teeth. Table 17 shows the maximum surface hardness (converted from DPH), Rc 50 depth, and depth of melting noted on the three teeth sections at the center or maximum case depth location.

TABLE 14. VISUAL CASE DEPTHS - TEST GEAR 1

Root No.	Visual Case Depth (in.)		
	West Flank	Root Center	East Flank
1	.042	.032	.045*
2	.035	.030	.040
3	.035	.030	.042
4	.037	.030	.043
5	.035	.030	.040*
6	.031	.030	.040*
7	.040	.030	.042*
8	.040	.030	.040
9	.040	.030	.040
10	.040	.030	.042
11	.040	.030	.042
12	.035	.030	.042
13	.035	.030	.040
14	.035	.030	.042
15	.035	.027	.040
16	.035	.030	.042
17	.035	.030	.040
18	.040	.030	.042
19	.035	.030	.040
20	.037	.030	.040
21	.037	.032	.040
22	.037	.030	.042
23	.035	.030	.042
24	.035	.027	.040
25	.033	.027	.040
26	.040	.030	.042
27	.040	.027	.040*
28	.042	.027	.040*
29	.035	.027	.040*
30	.042	.030	.040
31	.037	.027	.040
32	.037	.027	.040
33	.035	.027	.040
34	.037	.026	.040
35	.037	.026	.040
36	.035	.027	.040
37	.037	.027	.035
38	.035	.026	.037
39	.042	.027	.040*
40	.035	.027	.037*

*Teeth chosen for microhardness evaluation

TABLE 15. MICROHARDNESS TEST RESULTS - TEST GEAR 1

Tooth or Gap No.	West Flank				Root Center				East Flank			
	Max Hardness (Rc)	Rc 50 Depth (inch)	Depth of Melting (inch)	Max Hardness (Rc)	Rc 50 Depth (inch)	Depth of Melting (inch)	Max Hardness (Rc)	Rc 50 Depth (inch)	Max Hardness (Rc)	Rc 50 Depth (inch)	Depth of Melting (inch)	
1	53.5	.028	None	59.3	.024	None	54.1	.038			.001	
5	55.8	.043	.002	60.0	.029	None	60.6	.034			.003	
6	56.3	.039	None	59.3	.029	None	60.0	.039			None	
7	56.9	.040	None	60.0	.028	None	60.0	.037			.022	
27	55.2	.035	None	60.0	.026	None	60.0	.037			.001	
28	55.2	.036	None	60.0	.026	None	60.6	.040			.005	
29	54.6	.034	None	60.0	.025	None	59.3	.035			None	
39	55.2	.038	None	60.6	.025	None	60.0	.045			.002	
40	60.0	.035	None	61.6	.029	None	60.0	.040			.002	

Note: Maximum hardness values are converted from DPH.

TABLE 16. LASER HARDENED CASE DEPTH COMPARISON
(VISUAL MEASUREMENT VS. Rc 50 MEASUREMENT)
TEST GEAR 1

Root No.	West P.D. (in.)		East P.D. (in.)		Root (in.)	
	Visual	Rc 50	Visual	Rc 50	Visual	Rc 50
1	.042	.028	.045	.038	.032*	.024*
5	.035	.043	.040	.034	.030	.029
6	.031	.039	.040	.039	.030	.029
7	.040	.040	.042	.037	.030	.028
27	.040	.035	.040	.037	.027	.026
28	.042	.036	.040	.040	.027	.026
29	.035	.034	.040	.035	.027	.025
39	.042	.038	.040	.045	.027	.025
40	.035	.035	.037	.040	.027	.029

*Root discrepancy felt to be due to tempering of this root by laser hardening of both adjacent teeth.

TABLE 17. MAXIMUM CASE DEPTH AT PITCH DIAMETER
TEST GEAR 2

Tooth Location (Centerline)	Max. Hardness (Rc)	Rc 50 Depth (in.)	Depth of Melting (in.)
0° East P.D.	60.0	.048	.003
0° West P.D.	53.5	.037	.004
120° East P.D.	60.6	.039	.003
120° West P.D.	58.8	.057	.003
240° East P.D.	60.0	.037	.002
240° West P.D.	58.8	.054	.003

END
FACE →

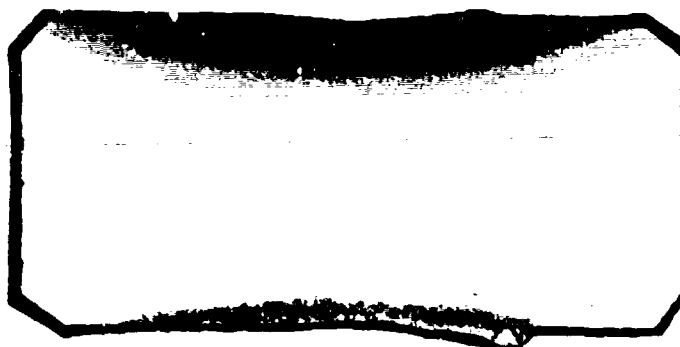


Figure 32. Test gear 2 - a cross section taken through the 0° tooth at approximately the pitch diameter and etched in 2% nital to reveal the laser hardened case depth.

END
FACE →

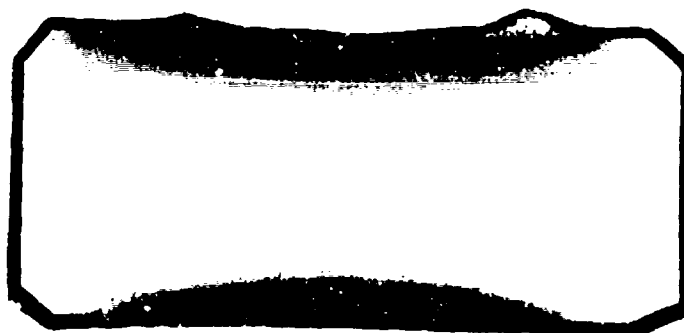


Figure 33. Test gear 2 - a cross section taken through the 120° tooth at approximately the pitch diameter and etched in 2% nital to reveal the laser hardened case depth.

END
FACE →

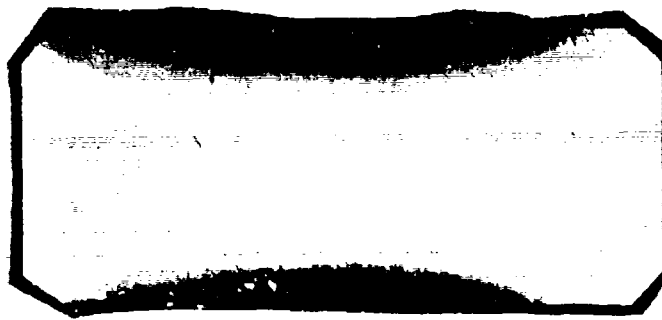


Figure 34. Test gear 2 - a cross section taken through the 240° tooth at approximately the pitch diameter and etched in 2% nital to reveal the laser hardened case.

Microhardness tests were also made from end face to end face at a depth of about .005 inch below surface on the specimens shown in Figures 32, 33, and 34. These tests showed the hardness to be uniform within ± 1 Rc from one end face to the other inside the laser hardened area (the darker etching areas of Figures 32, 33, and 34).

After discovering the problem of lack of full laser coverage from end face to end face, an additional specimen was prepared which showed the laser hardened case from end face to end face at the root. This specimen showed a uniform laser hardened case depth. It is believed that the root case depth uniformity was due to the fact that two laser beams were used to harden the tooth root.

After the three teeth shown in Figures 32, 33, and 34 were removed, test gear 2 was surface ground from one end face, similar to test gear 1. Test gear 2 was then etched in 2 percent nital solution and the laser hardened visual case depths were measured and are presented in Table 18. Figure 35 is a photograph of test gear 2 after grinding and etching. Close comparison of Figures 29 and 35 will show that on test gear 2 the side from which .113 inch of material was removed was actually facing down during laser hardening. Therefore, the flanks on the right side of each root in gear 2 are the same as the west flank of Figure 29.

Tooth roots 3, 4, 5, 19, 20 and 21 were subjected to microhardness and metallographic evaluation and the results are shown in Table 19. As in test gear 1, the west flanks were tempered in all instances.

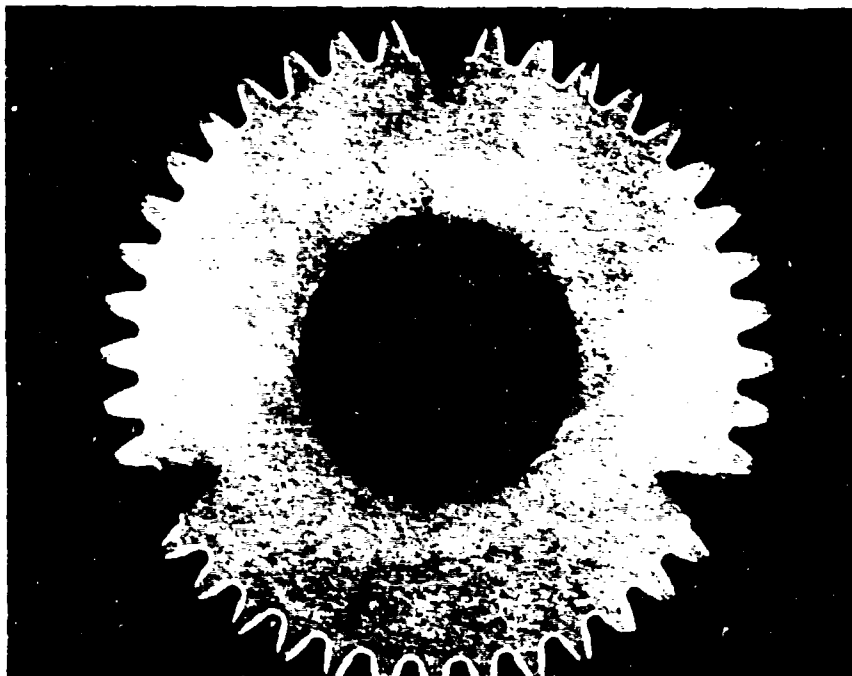


Figure 35. Test gear 2 laser hardened case profile.
.113 inch of material ground from one end
face and etched in 2% nital to reveal the
case.

TABLE 18. VISUAL CASE DEPTHS - TEST GEAR 2

Root No.	Visual Case Depth (in.)		
	West Flank	Root Center	East Flank
1	(a)	(a)	.040
2	.035	(a)	-
3	.036	.028	.037*
4	.036	.028	.037*
5	.036	.025	.037*
6	.036	.025	.037
7	.036	.026	.041
8	.036	.025	.040
9	.036	.030	.040
10	.036	.030	.041
11	.036	.028	.036
12	.036	.028	.036
13	.040	.030	.038
14	(a)	(a)	.030
15	.040	(a)	(a)
16	.036	.030	.042
17	.036	.032	.045
18	.036	.030	.045
19	.038	.032	.048*
20	.038	.030	.048*
21	.040	.032	.048*
22	.040	.032	.048
23	.040	.032	.048
24	.040	.029	.048
25	.036	.029	.048
26	.036	.034	.048
27	.036	.032	.048
28	(a)	(a)	.032
29	.038	(a)	(a)
30	.036	.030	.035
31	.036	.032	.043
32	.040	.032	.038
33	.036	.030	.038
34	.036	.026	.036
35	.036	.028	.040
36	.036	.028	.040
37	.036	.028	.041
38	.036	.028	.040
39	.034	.028	.040
40	.034	.030	.040

*Teeth chosen for microhardness evaluation

(a) Not evaluated because teeth were removed for evaluation of case depth across the width of tooth.

TABLE 19. MICROHARDNESS TEST RESULTS - TEST GEAR 2

Root or Tooth Gap No.	West Flank			Root Center			East Flank		
	Max Hardness (Rc)	Rc 50 Depth (inch)	Depth of Melting (inch)	Max Hardness (Rc)	Rc 50 Depth (inch)	Depth of Melting (inch)	Max Hardness (Rc)	Rc 50 Depth (inch)	Depth of Melting (inch)
3	55.2	.034	None	60.6	.025	None	60.6	.035	None
4	55.2	.033	None	60.0	.025	None	59.3	.035	.006
5	55.2	.038	None	60.0	.026	None	60.0	.030	.008
19	56.9	.044	.0011	60.6	.030	.0013	60.0	.030	.0002
20	55.8	.043	.0007	60.0	.029	None	60.0	.030	.0005
21	55.8	.042	.0004	60.0	.031	.0008	60.0	.035	.0003

Note: Maximum hardness values are converted from BPH.

8.5.3 DISCUSSION

The results of evaluation of test gears 1 and 2 showed that the problems of tempering of the west flank exists when the east flank is overcased (test gear 1, root no. 39) as well as when the east flank is within the desired case depth range (test gear 1, root no. 5 and test gear 2, root nos. 5, 19 and 20). This further indicates that an auxiliary means of cooling the gears is necessary to obtain Rc 60 minimum surface hardness on the west flank.

The repeatability of the laser hardening process used in this program was not adequate to consistently produce a case depth in a tolerance band of .008 to .010 inch, which is typical of the requirement for aircraft quality accessory drive gears.

The presence of recast layer on several teeth of the prototype gears dictates that in a production mode laser hardened gears will have to be finish ground if used in aircraft application.

The lack of case depth uniformity from end face to end face was a problem that was not discovered until quite late in the program. The program was terminated due to funding limitations before this problem could be overcome.

Comparative cost analysis of laser hardening and carburizing processes was conducted using four baseline accessory gears and is presented in Appendix D. For the four gear configurations considered, laser hardening cost was approximately 38 percent of the cost of carburizing for a production lot of 100 pieces. (This is after an investment of an estimated \$44,250 in tooling for laser hardening.) The cost benefit of laser hardening is primarily due to the elimination of labor intensive operations required in carburizing (such as masking, copper plating, and blast cleaning) and the reduction of costly furnace time. Reduced energy usage in laser hardening, when compared to carburizing, is another advantage of the process that will become even more important in future years.

9. CONCLUSIONS

In spite of termination of this program prior to a successful completion, several important conclusions were reached based on which future efforts may be formulated:

1. Laser hardening of D6AC provides a surface hardness that is higher than that achieved through conventional hardening followed by oil or water quench.
2. Although surface hardening of gears is technically feasible, its applicability to helicopter gears was not demonstrated during this program because:
 - a. Gears were held in a fixed position during exposure rather than scanned across the laser beams. This caused nonuniform heating across the tooth face and limited the means of auxiliary cooling needed.
 - b. The large optical distance from laser unit to the workpiece contributed to drift problems in both power density and beam location.
 - c. The contract was concluded because of funding limitations before these conditions were corrected.
3. The convex beam integrator was shown to be a workable optic. Additional work is needed to optimize fabrication techniques to enhance its imaging ability.
4. The flank-root-flank (FRF) method of laser hardening a gear tooth has the disadvantage of back side tempering, specially for gears of diametral pitch of 10 or finer with effective case depths in the range of those generally used for carburized gears.
5. The problems of spatial drift (or beam displacement) and total power drift in the primary beam could be detected and often compensated for by the operator on a tooth-by-tooth basis. In a production environment, this could be automated with an adequate feedback system and a microprocessor.
6. Independent power drift in individual beams in the multibeam system used here was very difficult to control. This power drift arises from the variation in power along the annular form of the incoming laser beam. This problem may be overcome by integrating the incoming beam before splitting it or by providing a separate source for each beam thus rendering all beams independently controllable.

7. In-line calorimeters provide an effective means for monitoring the power drift in each leg of a multi-beam system.
8. The accuracy with which each tooth is positioned for laser hardening is extremely important. For production applications, a highly precise indexing mechanism will be required.
9. Spot hardening (no relative motion between the laser beams and workpiece) of the gear teeth, with the optics used in this program, had the disadvantage of incomplete coverage from end face to end face for the .375-inch-wide gears. A more generic approach would be to move the gear teeth across the laser beam. This would also allow hardening of several gears at a time.
10. The inconsistencies in laser hardening observed in this program (e.g., changes in power in each beam, spatial drift, and positioning error) indicate that in a production mode this process will require some special quality assurance provisions. It may be necessary to destructively test the first and last parts of each run to assure that the process is under adequate control. It must be noted here that even induction hardening, for aircraft applications, often requires evaluation of first and last parts from each setup to guarantee optimum control. Advanced techniques, like closed loop monitoring for laser power and location adjustments could significantly improve reliability and repeatability of the laser hardening process in the future.

10. RECOMMENDATIONS

Based on the findings of this program, the following recommendations are made for future efforts in the field of laser hardening of gears:

1. A preliminary economic analysis conducted as a part of this program had demonstrated that laser hardening of aircraft quality accessory drive type spur gears has a distinct cost benefit over the conventional case hardening method of carburizing. Additional work in this field is certainly warranted, particularly in light of the fact that a viable approach to laser harden a spur gear configuration, namely the multibeam approach, has been identified and developed.
2. In any future effort, more emphasis should be placed on gear steel selection. A more highly alloyed temper-resistant steel would be very desirable since it would minimize and under certain conditions would completely eliminate the problem of tempering of adjoining previously hardened areas.

In this program, the material choice was restricted to a low alloy steel that would yield Rc 60 minimum surface hardness and yet have a Rc 33-41 core (comparable to carburized AMS 6265 gear steel).

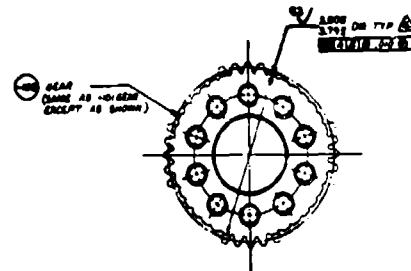
3. During gear steel selection, laser hardening tests should be conducted on flat specimens of varying thicknesses. Laser hardening both faces of such specimens would allow the empirical determination of minimum section thickness at which the problem of tempering could be avoided. Candidate gear steels can then be graded according to this minimum section thickness. The minimum section thickness thus arrived would also indicate the selection of gear pitch and case depth that can be produced by laser hardening.
4. Any future attempt should certainly contain provisions for traversing or scanning of the tooth face across the laser beams. This is a more generic approach since it is independent of gear thickness. It would allow simultaneous hardening of several gears and would assure uniform end face to end face case depth. Scanning could also allow the incorporation of a liquid quench that may significantly reduce or eliminate the problem of tempering of previously hardened areas.

5. The complexity of the prototype optical system used in this program could be significantly decreased. For instance, the convex beam integrators could be replicated to form concave integrators, thereby eliminating the need for spherical reimaging mirrors. The less mirrors employed, the less process variations realized. A shorter, less complex beam transfer path would also minimize the number of optics involved.
6. Many improvements could be made on the primary beam splitting techniques used here. For example, the primary incoming beam could be integrated prior to striking the pyramidal divider. Hence, the power variations within the primary beam would not promote power drift in the split-off beams. Spatial drift of the incoming beam could be controlled by employing water-cooled transfer optics. Closed loop control between the calorimeters and the feeder mirror could be employed to compensate for any remaining spatial drift due to atmospheric effects.
7. Calorimetric control of the beam splitting process could be upgraded to include calibration heaters and more stable absorptive coatings (e.g., an Al_2O_3 layer on an anodized aluminum beam shutter).
8. A totally different multibeam technique could be attempted. This could involve the use of three smaller lasers in lieu of the splitting of one more powerful laser beam. One laser could be dedicated to the root area with the remaining two dedicated to the flanks. Whether one approach is more cost effective than the other could only be assessed for a particular manufacturing environment. Other possible laser applications within the plant, burdening of the machine, initial investment, etc., would have to be considered for each specific case.

LIST OF REFERENCES

1. F. D. Seaman, D. S. Ganamuthy, "Using the Industrial Laser to Surface Harden and Alloy," Metal Progress, Aug. 1975.
2. L. Bonello and M. A. Howes, "Some Factors Affecting the Laser Heat Treating Process," Heat Treatment '79, May 1979.
3. Y. Arata, H. Martino and I. Miyamoto, "Heat Flow in Laser Hardening," International Institute of Welding (London) Document, IV-241-78, April 1978.
4. B. Sanders and V. Gregson, "Optical Reflectivity of Some Metals Using a Transversely Excited CO₂ Laser," Paper presented at the Electro-optics Design² Conference - 1973, New York.
5. S. L. Ream, "A Convex Beam Integrator," Laser Focus, Nov. 1979.

6



GEAR DATA

TYPE OF GEAR	_____	ABSOLUTE SPUR
NUMBER OF TEETH	_____	40
DIAMETRAL PITCH	_____	10
PRESSURE ANGLE	_____	20°
PITCH DIAMETER	_____	4.0000
CIRCULAR PITCH	_____	3.142
BASE CIRCLE DIAMETER	_____	5.79870483

INVOLUTE DATA		WALL	MEMBER
BASE LINE DIA		10	
IN ROUNDED RAIL		75.50	
IN ROUNDED OF CURVATURE			0.750
S.R	11.91" - 12.83"		2.900 - 4.010
S.R.	23.78" - 24.71"		7.800 - 8.100
S.R.	27.90"		9.617
START OF TOP (EDGE BREAK) REF	27.90" - 28.36"		9.617 - 10.000
TOP RAIL OF TRAVEL	1.24"		0.000
START OF RAIL (EDGE OF TIE) REF	9.60"		0.000
MIN. SLOPE OF			
MINUTE SLOPE LINE	0		
TOP PROJECTION LINE	- .0000		

MINIMUM SLOPE OF TROUGH SLOPE LINE _____ 0
SURFACE AT HIGHEST E.C. & HIGHEST _____ 0.0
CURVE OF END INFLAT _____ 0.0

DEPTH TO TIGHT SANDS	0000
ACCUMULATED SANDS	0000
SLOPE OF PROFILE GRADE LINE	+ 0000/0
SLOPE OF TOP ROAD GRADE	0000
PROFILE FALLSIES OF FALLOW	000
PROFILE REMAINS	0000070
PROFILE UNDERCUT	0000
LEAK FALLNESS	0000
LEAK FALLOW	000000
LEAK REMAINS	000070
LEAK UNDERCUT	0000
SLOPE OF PROFILE GRADE LINE	+ 0000/0
GRIP	0000

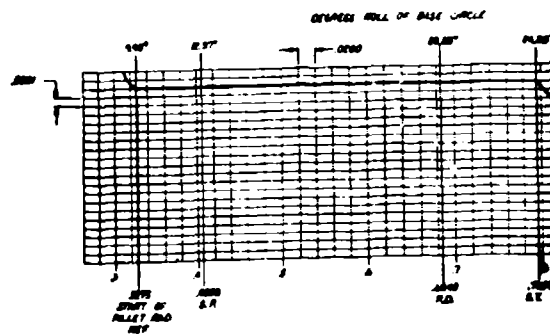
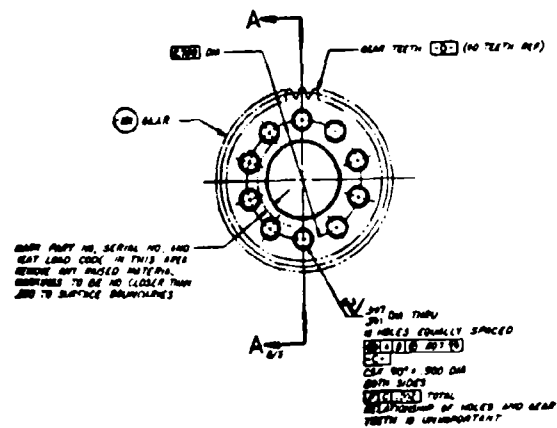
REPORT OF _____

DATE _____

CLASSIFICATION _____
REPORT NUMBER _____

CLASSIFICATION _____

DISTANCE WITH MAINS BEAM _____ 100-000
 AT SAME CORRECT DISTANCE _____ 10000



SERIES OF CURVES IN INCHES
 INVOLUTE CHART FOR GEAR TEETH
 MINIMUM THROATINGS AND MODIFICATIONS SHOWN FOR

APPENDIX B D6AC RAW MATERIAL EVALUATION RESULTS

TABLE B-1. D6AC CHEMICAL ANALYSIS

Crucible Heat No.	Bar Diameter	Analysis By	C	Mn	P	S	ANALYSIS (% wL)					V
							Si	Ni	Cr	No		
7153726	5.25	Mill	.48	.81	.008	.004	.24	.59	1.04	.95		.11
7153726	5.25	BHT	.50	.80	.007	.007	.24	.62	1.09	1.07		.12
7147355	7.0	Mill	.46	.79	.005	.004	.30	.57	1.11	.98		.12
7147356	7.0	BHT	.47	.80	.005	.005	.28	.60	1.15	1.05		.11
AMS 6431 Requirement			.45/.50	.60/.90	.015 max	.015 max	.15/.30	.40/.70	.90/1.20	.90/1.10		.08/.15

TABLE B-2. D6AC MACROSTRUCTURE TESTS (MIL-STD-430)
Test Results

Crucible Heat No.	Bar Diameter	Test Results			
		A (Center Defect)	B (Sub-Surf. Defect)	C (Ring Defect)	D (Misc. Defect)
7153726	5.25	1	1	1	0
7117356	7.0	2	1	1	1

TABLE B-3. D6AC GRAIN SIZE DETERMINATION

Crucible Heat No.	Bar Diameter	ASTM GRAIN SIZE
7153726	5.25	8
7147356	7.0	6

TABLE B-4. D6AC MICROCLEANLINESS RATING (J-K)

Crucible Heat No.	Bar Diameter	Location	Type	A (Sulfide)						B (Alumina)						C (Silicate)						D (Globular)					
				Thin		Heavy		Thin		Heavy		Thin		Heavy		Thin		Heavy		Thin		Thin		Heavy		Thin	
				Edge	Center	Edge	Center	Edge	Center	Edge	Center	Edge	Center	Edge	Center	Edge	Center	Edge	Center	Edge	Center	Edge	Center	Edge	Center	Edge	Center
7153726	5.25			.5	1.0	0	.5	0	.5	0	0	0	0	0	0	0	0	0	0	0	0	1.0	1.0	.5	.5	.5	.5
7147356	7.0			1.0	1.5	.5	1.0	.5	1.0	.5	1.0	.5	1.0	.5	1.0	.5	1.0	.5	1.0	.5	1.0	.5	1.0	1.0	.5	.5	.5

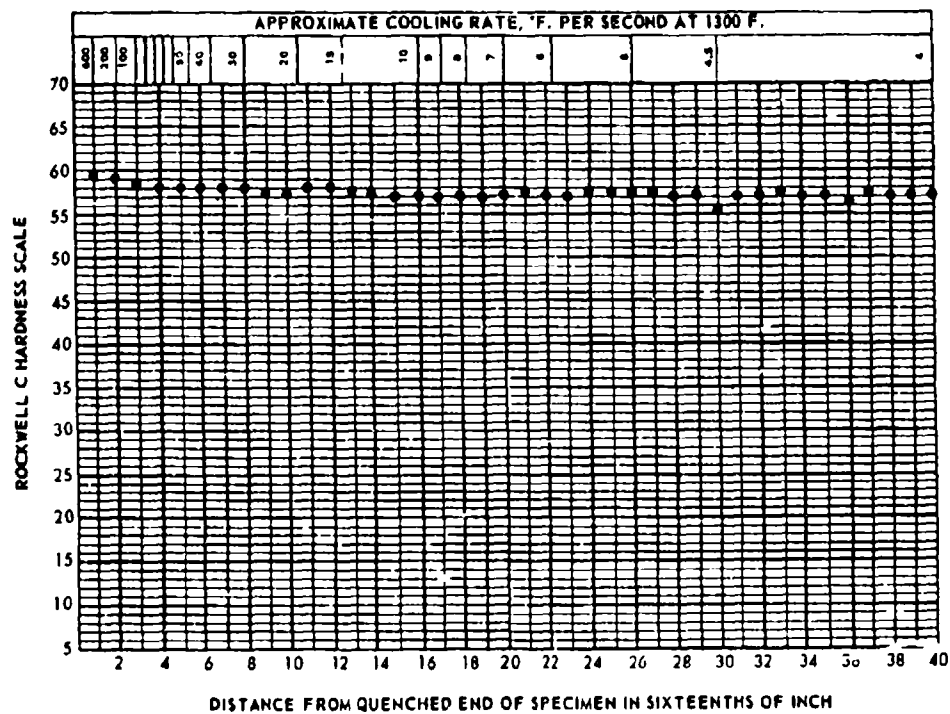


Figure B-1. Jominy hardenability curve for 5.25-inch-diameter bar of D6AC (Heat No. 7153726).

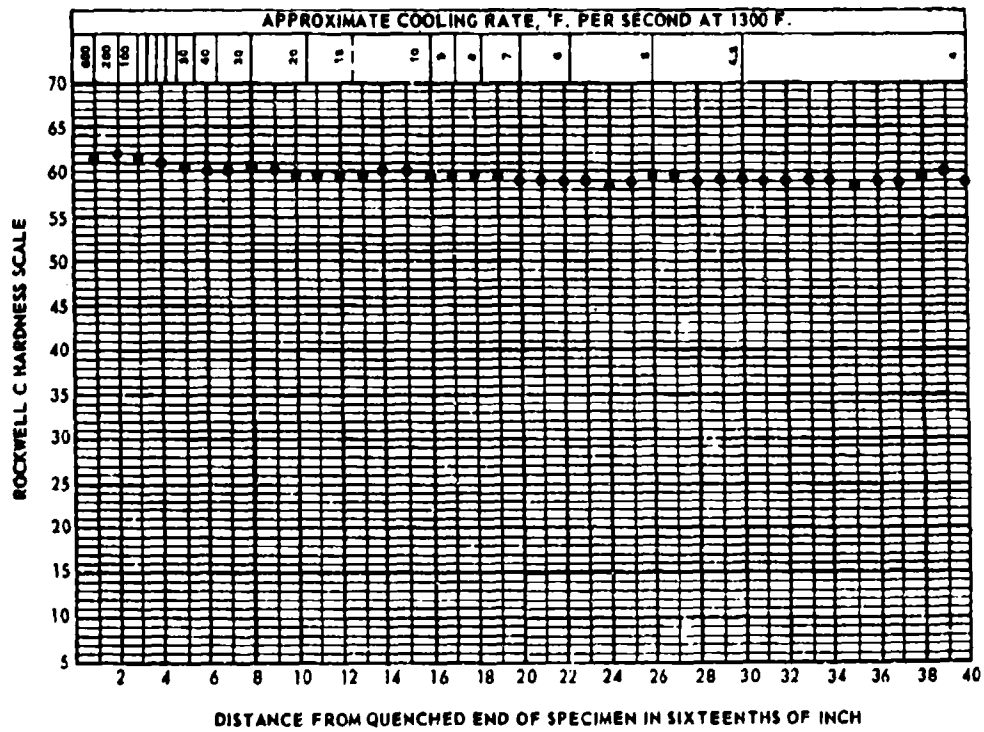


Figure B-2. Jominy hardenability curve for 7.0-inch-diameter bar of D6AC (Heat No. 7147356).

APPENDIX C

SUMMARY OF CHARACTERISTICS OF IITRI LASER FACILITY

Characteristic	Specification
Type	Closed cycle gas laser with electron beam ionizer.
Operating Mode	Continuous wave output, steady-state operation; manual, automatic and jog capabilities built-in.
Output Wavelength	10.6 micron (far infrared)
Output Power	Continuously adjustable over the range of 1 to 15 kilowatts with closed-loop power control and direct-reading power monitor.
Output Power Stability	$\pm 3\%$ of set-point; 1/4 second response time.
Construction	Complies with Joint Industrial Council National Electrical Manufacturer Association Standards. Complies with U. S. Government standards for noise level and X-radiation.
Optics	All optical surfaces are reflecting.
Output Window	Aerodynamic window.
Output Beam	Approximately F/25 diverging beam beyond aerodynamic window.
Mode Structure	Radially symmetrical focal spot with approximately Gaussian distribution about center of spot.
Spot Size	Approximately 0.006 times the F-number of a telescope used to generate the spot.

APPENDIX D

COMPARATIVE COST ESTIMATES (LASER HARDENING VERSUS CARBURIZING)

GENERAL

A cost analysis was performed using four baseline accessory gears to compare laser hardening with the conventional case hardening process of gas carburizing. As in any analysis that is based on estimates, certain assumptions were made. These assumptions are listed below.

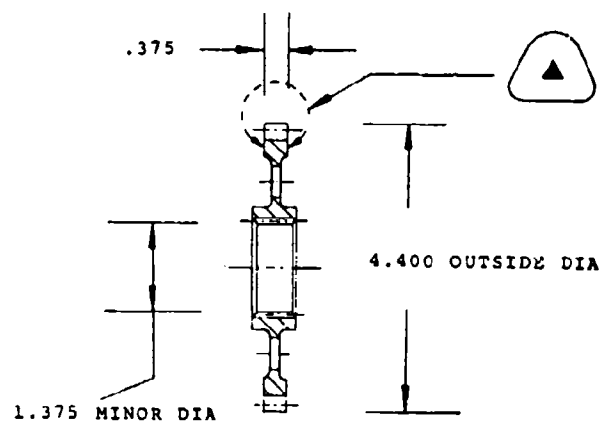
1. Technical success. It is assumed that the program will be a technical success as measured by the fatigue testing of laser-hardened accessory drive spur gear specimens in comparison with carburized 9310 specimens.
2. Qualification program. It is assumed that the technology developed here will be used on new designs and, therefore, will not entail a separate qualification program. Alternately, it may be stated that if used on existing designs, the qualification effort will be funded separately, independent of this program.
3. Laser hardening as a subcontracted task. It is assumed that the volume of accessory drive gear production using the newly developed technology of laser hardening will not justify procurement and installation of a laser heat treating station at BHT. The present analysis, therefore, treats laser hardening as a subcontracted task.

BASELINE ACCESSORY DRIVE GEARS

The analysis is based on the cost of case hardening of four accessory drive gear configurations. These gear configurations are shown in Figures D-1 through D-4. These configurations are similar to the accessory drive gears used in the 30 KVA alternator drive quill of UH-1H helicopters.

CASE HARDENING COST ESTIMATES

The carburizing costs were obtained by estimating total manufacturing hours required for carburizing, including pre-carburize and postcarburize processing for each configuration and converting these to dollars using 1981 composite labor rates at BHT. The costs of laser hardening the same four parts were obtained from IITRI. The cost estimates provided by IITRI are also based on 1981 labor rates. The laser hardening setup

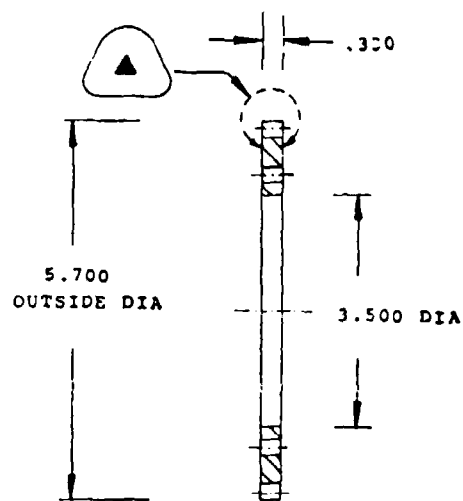


NUMBER OF TEETH: 42
 DIAMETRAL PITCH: 10
 DIMENSIONS IN INCHES



THIS AREA TO BE CASE HARDENED TO AN EFFECTIVE
 CASE DEPTH OF $.026-.034$ INCH.

Figure D-1. Gear configuration A.

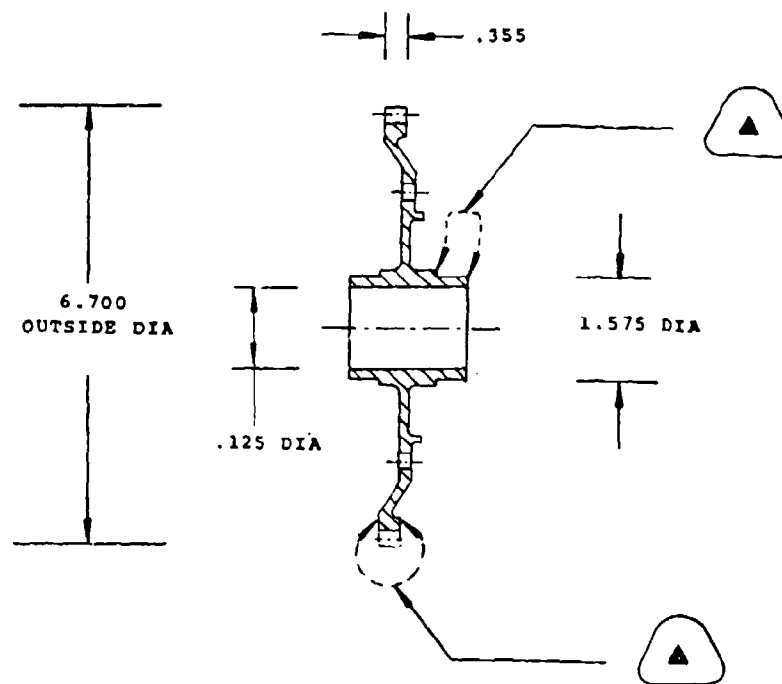


NUMBER OF TEETH: 35
 DIAMETRAL PITCH: 10
 DIMENSIONS IN INCHES



THIS AREA TO BE CASE HARDENED TO AN EFFECTIVE
 CASE DEPTH OF .026-.034 INCH.

Figure D-2. Gear configuration B.

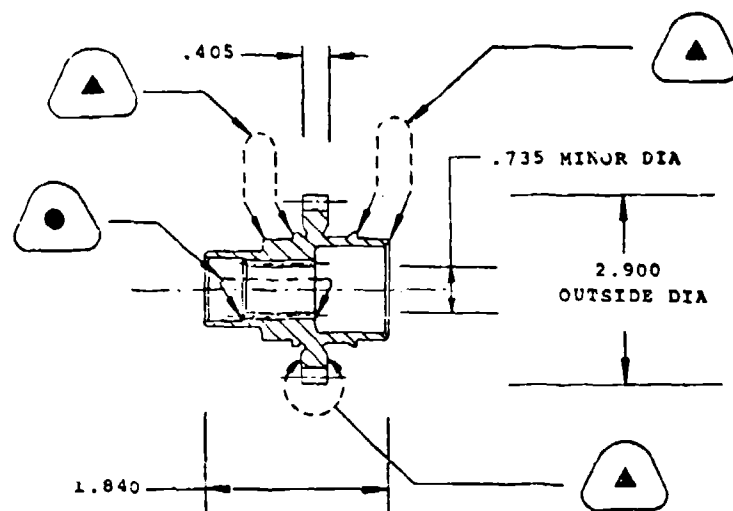


NUMBER OF TEETH: 65
DIAMETRAL PITCH: 10
DIMENSIONS IN INCHES



THESE AREAS TO BE CASE HARDENED TO AN EFFECTIVE
CASE DEPTH OF .026-.034 INCH.

Figure D-3. Gear configuration C.



NUMBER OF TEETH: 27
 DIAMETRAL PITCH: 10
 DIMENSIONS IN INCHES



THESE AREAS TO BE CASE HARDENED TO AN EFFECTIVE
 CASE DEPTH OF .026-.034 INCH.



THIS AREA TO BE CASE HARDENED TO AN EFFECTIVE
 CASE DEPTH OF .010-.020 INCH.

Figure D-4. Gear configuration D.

costs have been amortized over the quantity of parts in each list. Production lot sizes of 25, 100 and 200 are used in the analysis. The cost comparisons of the two case hardening processes for the four gear configurations are shown in Tables D-1 through D-4. Table D-5 summarizes the comparative case hardening costs for the four gears for a production lot size of 100 units.

TABLE D-1. CASE HARDENING COST ESTIMATES

Gear Configuration: A

Hardening Method	Lot Size (a)	Hardening *Cost for the Lot (b)	Quality Assurance *Cost Per Lot (c)	Total Hardening *Cost Per Lot (b) + (c)	Total Hardening *Cost Per Piece $\frac{(b) + (c)}{(a)}$
Carburizing	25	2159.08	141.84	2300.92	92.04
	100	5456.95	141.84	5598.79	55.99
	200	9854.11	141.84	9995.95	49.98
Laser	25	1000.75	212.76	1213.51	48.54
	100	2109.00	212.76	2321.76	23.22
	200	3664.00	212.76	3876.76	19.28

* In 1981 dollars

TABLE D-2. CASE HARDENING COST ESTIMATES

Gear Configuration: B

Hardening Method	Lot Size (a)	Hardening *Cost for the Lot (b)	Quality Assurance *Cost Per Lot (c)	Total Hardening *Cost Per Lot (b) + (c)	Total Hardening *Cost Per Piece $\frac{(b) + (c)}{(a)}$
Carburizing	25	2159.08	141.84	2300.92	92.04
	100	5456.95	141.84	5598.79	55.99
	200	9854.11	141.84	9995.95	49.98
Laser	25	1075.75	212.76	1288.51	51.54
	100	2413.00	212.76	2625.76	26.26
	200	4276.00	212.76	4488.76	22.44

* In 1981 dollars

TABLE D-3. CASE HARDENING COST ESTIMATES

Gear Configuration: C

Hardening Method	Lot Size (a)	Hardening *Cost for the Lot (b)	Quality Assurance *Cost Per Lot (c)	Total Hardening *Cost Per Lot (b) + (c)	Total Hardening *Cost Per Piece (b) + (c) (a)
Carburizing	25	2829.47	141.84	2971.31	118.85
	100	7078.74	141.84	7220.58	72.21
	200	12744.44	141.84	12886.28	64.43
Laser	25	1622.25	248.22	1870.47	74.82
	100	3757.00	248.22	4005.22	40.05
	200	6712.00	248.22	6960.22	34.80

* In 1981 dollars

TABLE D-4. CASE HARDENING COST ESTIMATES

Gear Configuration: D

Hardening Method	Lot Size (a)	Hardening *Cost for the Lot (b)	Quality Assurance *Cost Per Lot (c)	Total Hardening *Cost Per Lot (b) + (c)	Total Hardening *Cost Per Piece (b) + (c) (a)
Carburizing	25	5016.49	177.30	5193.79	207.75
	100	15923.16	177.30	16100.46	161.00
	200	30465.38	177.30	30642.68	153.21
Laser	25	1827.25	319.13	2146.38	85.86
	100	3757.00	319.13	4076.22	40.76
	200	6412.00	319.13	6731.13	33.66

* In 1981 dollars

TABLE D-5. CASE HARDENING COST ESTIMATES
CARBURIZING VS LASER HARDENING

Production Lot Size: 100 Units

Gear Configuration	Carburizing		Laser Hardening		Laser Hardening Cost Benefit Per Unit
	Tooling \$	Unit Cost \$	Tooling \$	Unit Cost \$	
A	None	55.99	10,500.00	23.22	32.77
B	None	55.99	10,500.00	26.26	29.73
C	3,500.00	72.21	11,000.00	40.05	32.16
D	None	161.00	12,250.00	40.76	120.24
Total for the Quill		345.19		130.29	